Hybrid UAV

Design Synthesis Exercise: Final Report

Group 14

June 30th, 2017

TU Delft

This page is intentionally left blank.

Delft University of Technology

AE3200 - Design Synthesis Exercise

Final Report

Version 1.2

Authors:
4384385 Jong, C.P.L. de
4221699 Kim, M.
4376161 Lee, J.J. van de
4371321 Lovell-Prescod, G.H.
4308220 Ruland, O.L.
4344499 Sokolowski, P.M.
4279832 Steiner, L.F.
4364228 Wellens, L.
4280806 Wheeler, K.
4381726 Wiechers, S.M.G.

Supervisors:
Jos Sinke
Sebastian Rapp
Erik-Jan van Kampen

Cover Image: Pexels
https://static.pexels.com/photos/107989/pexels-photo-107989.jpeg

This page is intentionally left blank.

Preface

This report is the fourth and final document in a series of reports on the design of a Hybrid Unmanned Aerial Vehicle (UAV). The project is executed by 10 students in 11 weeks for the design synthesis exercise. The first document presents the project plan. In this document, the organisation and planning of the project were described and first steps were taken into the design process. The second dealt with the baseline of the project, including twenty ideas and five concepts that would be investigated further. Also, a market analysis was made. This was followed by the midterm report, which presented an analysis and a trade-off in which one final concept was selected. In this report, the preliminary design of the chosen concept will be discussed. The report will be followed by an executive summary and a poster. Both will give an overview of the project.

Group 14 would like to thank Ir. J. Sinke, Dr. Ir. E. van Kampen and Ir. S. Rapp for their advise, professional assistance and feedback. The group also sends special thanks to Hybrid UAV companies Avy and Atmos for their advice and specialist feedback.

Executive Summary

The Unmanned Aerial Vehicle (UAV) market is growing, as the field of application becomes increasingly diverse. Various missions performed by UAVs such as transport, surveillance and monitoring missions can be less challenging and more efficient compared to missions carried out by manned aircraft. The new design principle of combining a helicopter and a conventional aircraft has been proven to be prominent, as it allows a UAV to be versatile and have capability of being retrofitted to different mission profiles; these Hybrid UAVs are able to operate at broader conditions, as they can take-off and land without a runway and have a horizontal flight performance of a conventional aircraft.

Due to the above mentioned advantages, a project has been set up aiming to culminate with the documentation and presentation of an efficient Hybrid UAV design which can be controlled remotely within visual line of sight with the capability of possible beyond visual line of sight control. The necessary requirements to be complied with were based on the mission need statement characterised as follows.

> *Carry out both supervised and autonomous monitoring and transport missions, comprising vertical take-off and landing, and sustained high-velocity horizontal flight.*

Requirements

This section gives a list of the most important requirements derived from the mission need statement.

SYS-C-1:	The production and distributed development cost per unit shall be limited to an amount of 30k EUR.
SYS-PH-2:	The UAV shall have a MTOW of maximum 25 kg.
SYS-OP-1.1:	The UAV shall be able to airdrop its payload during operation.
SYS-PF-1.1:	The UAV shall be able to carry a payload of at least 10 kg.
SYS-PF-1.2:	The UAV shall be able to fly at a horizontal velocity of at least 200 km/h at cruise altitude carrying 10 kg of payload.
SYS-PF-1.3:	The UAV shall have a minimum range of 200 km carrying 10 kg of payload.
SYS-PF-1.4:	The UAV shall have a minimum endurance of 1 hour carrying 10 kg of payload.

It is determined that not all requirements can be met simultaneously due to the EASA A3 regulation stating that the mass cannot exceed 25 kg. To solve this problem, the payload will be interchangeable with extra batteries. This modular payload will give the operator the freedom to operate various missions at full performance.

Trade-off

In a previous phase, five concepts were chosen to be analysed further in order to obtain one concept on which the final design is based. The five concepts are: a tailsitter, a tiltable wing in tandem configuration, a prandtl-boxed wing with tiltable propellers, a 'tiltrotor' configuration where the propellers (located at the wing tips) can rotate, and a winged quadcopter layout. Detailed information about these concepts can be found in the baseline report [1].

This section is a summary of the trade-off process performed in the midterm report [2]. The criteria chosen for the trade-off are performance, manoeuvrability & stability, ground handling, development risk, production cost, sustainability and reliability. Detailed explanation of the separate criteria scores are the result of extensive research on each criterion. The reasoning behind these scores can be found in the midterm report [2]. According to this trade-off, the best concept layout is a winged quadcopter. It consists of a fuselage with one wing and a tail. On both sides, tiltable propeller engines are installed on the front and aft sides of the wing. This allows the UAV to fly both like a quadcopter and like an airplane.

Design Approach

Now that the concept has been chosen, detailed design can be performed. To steer the design phase in the right direction, some preparation work needs to be done. The first step taken is to divide the system into subsystems which cover all aspects of the aircraft. When the subsystems are known, the work needed to be done can be split up into different departments. Each department will focus on one aspect for the several subsystems. Table 1 shows which department focuses on which subsystem, and also which department is leading for each subsystem. With the division of tasks and subsystem done, some tools will be implemented to aid the designing.

Table 1: Departments and Responsibilities

Department	**Leading on**	**Working on**
Aerodynamics	Wing	Wing, Tail, Fuselage and Propulsion Unit
Command & Data Handling	Avionics and Ground Control	Payload, Avionics and Ground Station
Power & Propulsion	Propulsion Unit and Power Unit	Propulsion Unit and Power Unit
Stability & Control	Tail	Wing and Tail
Structures	Fuselage	Payload, Wing, Tail and Fuselage

Tools There are several tools that can be used to ensure that the communication between departments goes as planned and that there are no major mistakes made during designing. This paragraph will shortly discuss the tools implemented in the design phase. The first tool is an N^2 chart which shows the interrelations between the subsystem and departments. This way, it is possible to see which inputs affect the subsystem that is being worked on, and from which department this input can be expected. The next tool is a work flow diagram, which each department will make to guide them through the process. The work flow diagram will be made to have a clear overview of the work that needs to be done, and in which order. Next up is the 'Master Set', which contains all the up-to-date values used for designing. This Master Set is automatically imported into Python to ensure good use of values during the iterations made. The next tool is used for the task division. It is an excel sheet which contains all the work that needs to be done (designing and writing). This sheet is a living document and updated regularly, giving an overview of all the work that has been done and still needs to be done. The last tool is used to control the designing departments. Budgets have been assigned to the mass, the cost and the power used of the aircraft. These budgets have been put in place so that the design does not exceed certain values which can threaten the goal of meeting the requirements.

Design Process Before the designing can start, values need to be estimated to start-off the design phase. These initial values will be replaced with actual values when they are known. With the initial values, each department will start designing according to the work flow diagram, this means not all the departments will start on the subsystem. Due to this, the values used for the first iteration do not correspond with the latest values, hence more iterations are needed. To iterate easily, most departments make use of a python code to simplify the calculations and calculate the new values in a short amount of time. Once all design aspects have been evaluated, all variables will near their end-value as more iterations are being made. During the designing, various analyses are done to see if the system complies with the given constraints and requirements.

To make sure that the method of designing is correct, or implemented correctly, verification and validation will be done throughout the design process. Calculations and code will need to be verified while models and programs will need to be validated. This ensures that the method used was correct and the values achieved are realistic.

Design Analysis

Power & Propulsion The propulsion department primarily focuses on designing a versatile propulsion unit capable of both VTOL (Vertical Take-Off and Landing) and high-speed horizontal flight, while the power department designs a battery system that can provide enough power for the propulsion system as well as avionics. Off-the-shelf components are chosen for the power and propulsion subsystems.

As a first step of designing a power subsystem, a propulsion configuration was chosen in terms of motor location and the number of motors, based on constraints generated by stability & control and aerodynamics department. A wing-mounted motor configuration with four motors was selected, with each motor capable of rotating for VTOL and horizontal flight. The following variables for the propulsion unit had to be gathered and iterated in order to obtain an optimal configuration: propeller diameter & pitch, motor Revolutions Per Minute (RPM), required thrust and required power. By using a self-developed tool and an online tool that utilises the variables, motor & propeller combinations for the front and aft motors were obtained. It was decided that front motors and propellers would be fully dedicated for VTOL, while the aft motors and propellers would primarily propel the UAV for horizontal flight and assist front motors for VTOL and control. The chosen propulsion components can be seen in Table 2.

Table 2: Off-the-shelf Component Selection propulsion unit Subsystems

Component	**Product Name**	**Q.**	**Unit Mass [g]**	**Unit Cost[€]**
Front Motor	Hacker Q60-7M (10S)	2	520	410
Front Propeller	AC Carbon 16x10	2	25	11.8
Front Speed Controller	MasterSPIN 99 Pro	2	105	229
Front spinner	Spinner RFM 40x6	2	n.a	30.9
Aft Motor	Hacker A50-12L (8S)	2	445	184
Aft Propeller	APC 11x14	2	40	3.50
Aft Speed Controller	X-70-SB	2	54	99.0
Aft spinner	Ae-spinner A/K 45	2	n.a	8.65
Total			2387	1950

In order to calculate a required battery capacity, the most extreme mission had to be defined. It consists of one minute of VTOL, 5 minutes of hovering and maximum range flight. Based on the total required power for the most extreme mission, a required battery capacity of 24190mAh was obtained. Motor specifications such as voltage put an extra constraint on battery selection. A DC-DC converter is chosen to manage different volts, since the voltage of the front motors and aft motors are 37V and 30V respectively. After the battery was chosen, miscellaneous components such as battery cable, servo with extended cable and connectors were selected. The complete power subsystem components including the rotating mechanism can be seen in Table 3.

Table 3: Off-The-Shelf Component Choice Power Subsystem Including Rotating Mechanism

Component	**Product Name**	**Q.**	**Unit Mass [g]**	**Unit Cost[€]**
DC-DC Converter	LM2596 DC 3.2-40V to 1.25-37V	2	n.a	2.70
Rotating Mechanism	Tricopter Tilt Mechanism	4	10.6	8.50
Servo	BMS-210DMH	4	17.5	24.2
Servo wire	DITEX Servowire Extension	4	n.a	7.30
Battery	Zippy Compact 5800mAh 10S Lipo	5	1268	135
Power cabling	Turnigy HQ 8 AWG Silicon wire	4	120/m	3.50/m
Connector	Nylon XT90 Connectors	5	78.0	8.40
Total			7010	860

Aerodynamics Analysis The aerodynamics department has its focus on the aerodynamic forces created by the aircraft. The aircraft will need to generate enough lift while minimising the amount of drag. There are four subsystems needing to be designed by the aerodynamics group: the wing, the tail, the fuselage and the pylon from the propulsion subsystem. The wing and the horizontal tail have a similar design process. An optimal planform had to be found which will create the least amount of drag, this turned out to be an elliptical planform. This would be possible for the horizontal tail but not for the wing due to a cost constraint during manufacturing. To find a suitable solution for the wing, an optimisation code has been written in Python which would iterate through all possible variables. There was one limit set, that there would be a maximum of two tapers across the wing (to restrain the manufacturing costs). The horizontal tailplane and vertical tailplane have been sized by using a conventional aspect ratio and a conventional taper ratio. The last variable needed to size the empennage was the surface area of the tailplanes, which was calculated by the stability & control department. The planforms of the wing, horizontal tailplane and vertical tailplane can be seen in figs. 1 to 3, respectively.

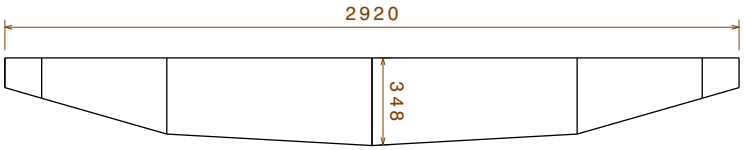

Figure 1: Planform of the Wing, Dimensions in mm

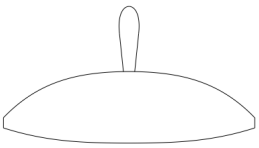

Figure 2: Top View of the Horizontal Tailplane, On Top Of The Vertical Tailplane

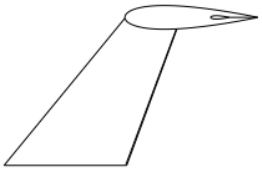

Figure 3: Side View of the Vertical Tailplane

The aim of the aerodynamic design of the fuselage is to minimise the drag it produces. Therefore the starting point of the design process was to find how the geometry of the fuselage affects the drag. Using the Roskam parametric equations for the drag of a fuselage, it was found that there are two independent variables which directly influence the amount of produced drag, namely the length of the fuselage and the maximal cross sectional frontal area. In most cases, the smaller the maximal cross sectional frontal area, the lower the drag. Furthermore, for each cross sectional area there exists an optimal fuselage length which results in the lowest possible drag for that cross sectional area. Due to the constraints set by the payload subsystem, the smallest achievable maximal cross sectional frontal area was set at 0.053 m^2. The fuselage length was set to 1.7 meters. Unfortunately this is not the optimal length due to the constraints set by the structures department.

The design of the engine pylons was carried out in the same manner as the fuselage. In this case the independent variables were the pylon diameter and length. These were set to 2 cm and 90 cm respectively. Again, it was not possible to design the pylon for the optimal length.

Stability & Control Throughout the design phase, the stability and control department was responsible for investigating what was required to ensure that the UAV was both stable and controllable. Both longitudinal and lateral static stability were investigated during horizontal flight and what series of steps must be taken to pitch, roll and yaw during vertical flight. Transition between vertical and horizontal flight was also explored.

The ratio between the surface area of the horizontal tailplane to the main wing as well as the location of the leading edge of the main wing were found by overlaying the scissor plot with the minimum and maximum c.g. location (as a function of the leading edge location). By simply multiplying the ratio with the surface area of the main wing, which is defined by the required lift, the surface area of the horizontal tailplane is seen to be 0.106 m^2.

The vertical tailplane was sized assuming a worst case scenario of one engine inoperative with a side slip angle of 5°. The surface area of the vertical tailplane can be obtained by calculating the force required to counter the moment created as a result of one engine being inoperative. This surface was chosen to be 0.03 m^2.

Then, for horizontal control, control surfaces needed to be sized. Using newtons seconds law, it was possible to obtain the yaw moments necessary in order to create a specific angular acceleration. With the maximum deflection angles, the surface area and location of each control surface is now obtained. From this, worst case scenario is assumed in order to calculate the hinge moments that the actuators have to carry. A suitable servo is then chosen.

In order to get a proper understanding of the power required of the batteries and motors during vertical flight, the manoeuvres and required power splits must be characterised. The angular acceleration that the UAV must be capable of delivering are stipulated in the requirements. For the most part the combined power delivered by the four motors is kept constant however it was important to characterise the power splits as they are driving in the choice of motors selected. The motors are set up as depicted in Figure 4

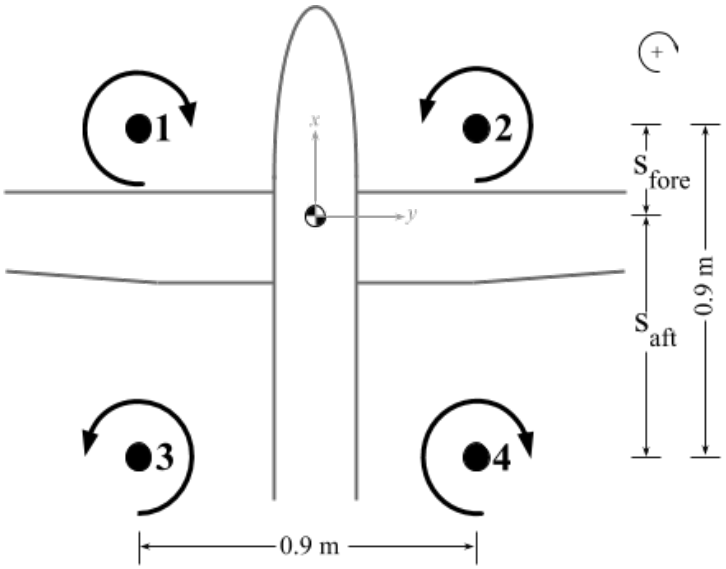

Figure 4: Configuration with respect to the Centre of Gravity

For pitch motors 1 & 2 and 3 & 4 work in pairs, for roll motors 1 & 3 and 2 & 4 work in pairs and for yaw motors 1 & 4 and motors 2 & 3 work in pairs.

Structural Analysis The structural department is involved in the design of the majority of the subsystems. However, the main focus is put on the wing and fuselage subsystems as to these designs the structural considerations are a top priority. The first step in the design process of any structure is to investigate the loading cases to which the structure is expected to be subjected. It is found that the most severe loading cases follow from gust loads. The combination of the relatively large surface area of the wing with the low weight of the UAV makes it very susceptible to gust loads. The maximum load factors resulting from these gusts are -6.7 and 8.7.

Based on these loads combined with a safety factor of 1.5, the internal forces and moments are evaluated and the locations of their maximums are found. Then, the geometry and the materials of the structural members in the wing and fuselage are selected in tandem and the structure is analysed for internal stresses and checked for failure. In the case of failure or large margins from failure, changes in material or geometry are made and the process is repeated. Next the designs weight and material cost are estimated and checked for budget compliance. If the design is within the budgetary constraints, then the design is also checked against the specific subsystem requirements. After a number of iterations on this process, the resulting design was modelled in Catia. Figure 5 depicts an isometric view of the internal structure of the vehicle.

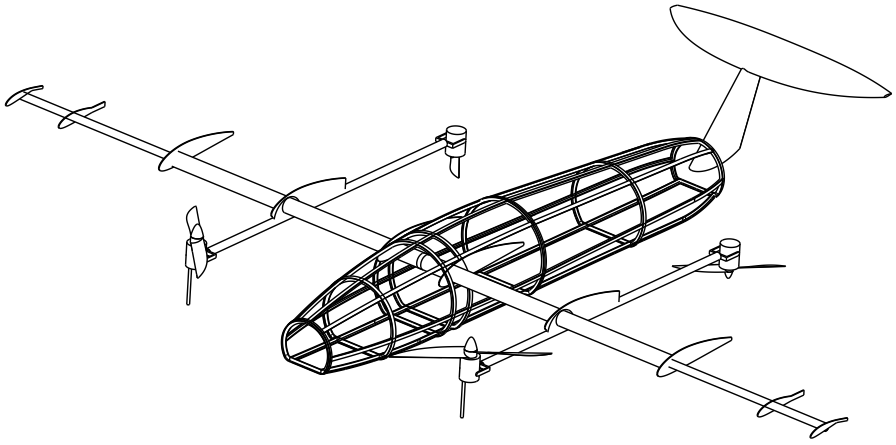

Figure 5: Internal structure of the UAV

The wing structure consists of a carbon fibre composite tube that act as the main load carrying member that transfers loads into the fuselage. Attached to this tube are carbon fibre spars that transfer loads from the foam skin. The fuselage structure comprises frames, stringers and a load carrying skin. These components are all made from a glass fibre epoxy composite. There are seven frames spaced along the fuselage at important locations of load introduction into the fuselage. Furthermore, seven stringers run between the frames in the longitudinal direction. The inner structure of the horizontal and vertical tail planes are similar to the design of the main wing. However, these are not visible in Figure 5. Finally, the propulsion units are attached to carbon fibre pylons which are suspended under the wings.

Command & Data Handling The command and data handling subsystem is mainly responsible for the design of the ground station and the design of the avionics subsystem. This also includes the necessary hardware required in order to be able to fly autonomously as well as the data link between the UAV and the ground station.

The design of the avionics system started by performing a trade-off regarding the flight controller used to process all the necessary data. It was concluded, that a combination of a Pixhawk 2.1 flight controller together with the open source paparazzi software performed best. Using open source software on an off-the-shelf flight controller makes it possible to adapt required functions accordingly. The pixhawk flight controller uses redundant attitude sensors, however in order to obtain flight speed data, two airdata sensors are added and a GPS module is used to determine the position. Then, two laser sensors will constantly detect ground distance and scan for possible obstacles in the drones flight path. Table 4 gives an overview of the different avionics components.

As radio communication can not achieve the required ranges of at least 200 km, the telemetry system will rely on a main cellular network connection in order to transfer data to the ground station and receive different commands from the operator. Message authentication codes are used to ensure that no third party can interfere with the dataflow. Next to this, a radio control link is added to make it possible to control the drone directly in close distance if no cellular link is available. In case the link to the ground station is lost for more than 10 seconds, the UAV will return back to it‘s starting position.

Finally, the ground station is designed based on a software package. As the UAVs main communication link uses an internet connection, control of the drone is then possible using a device connected to the internet. These can be for example smartphones, laptops or tablets.

Table 4: List of Avionics Subsystem Components

System type	**Selected system**
Flight control module	Pixhawk 2.1
Flight control software	Paparazzi
Ground avoidance system	SF30-C Laser Rangefinder
Object avoidance system	Jenoptik DLEM 20
GPS	Here GNSS for Pixhawk
2x Airdata sensors	Digital Airspeed sensor
Radio Control	Frsky V8FR-II receiver
	FrSky 2.4GHz Accst Taranis X9D PLUS
Telemetry	u-Blox TOBY L2-series
Payload link	USB or other cable

Conclusion

In conclusion, the UAV was designed using five specialist teams of two members. These teams are aerodynamics, structure, command & data handling, power & propulsion and stability & control. After a trade-off, a winged quadcopter layout performed best.

During the preliminary analysis, it was found out that it will not be possible to comply with both the requirements set by the stakeholders and the regulations imposed by EASA. To solve this problem, it was decided that the payload weight can be converted to battery mass in order to improve endurance and range. This modular payload will makes it possible to obtain an endurance of one hour or a range of 200 km, however with the price of not being able to carry a payload of 10 kg.

The final design consists of a winged quadcopter layout. It uses four motors for VTOL and horizontal flight. The front propellers are designed for vertical flight and will be fully dedicated for this. In horizontal flight they can be used as redundancy in case the control surfaces fail or in case of engine failure. The aft propellers are primarily used to propel the aircraft in horizontal flight and are rotatable to assist in vertical flight.

The wing, fuselage and tailplane are designed for minimum drag while still being able to carry the necessary loads. The wing uses a quasi elliptical distribution in order to decrease the lift-induced drag. The control surfaces were designed to support the necessary moments for yaw, roll and pitch control. In vertical flight, mainly a change in either propeller pitch or speed is used to control the attitude of the UAV. Using a scissors plot the optimal wing location and necessary horizontal tail surface is found for longitudinal stability and control.

The avionics of the UAV consist of an autonomous flight controller performing its mission using a set of waypoints. A cellular connection is used to transfer data (like waypoints or sensor data) from the UAV to the ground station. In case of closer proximity a radio control link can be used to directly control the UAV in line of sight. The ground station consists of a controller for radio control and a tablet/laptop connected to the internet. The necessary ground station software is the open source paparazzi.

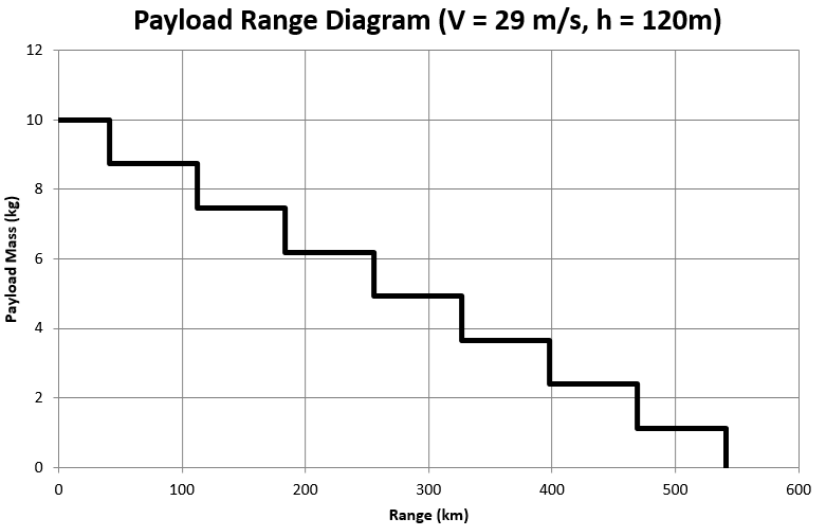

Figure 6: Payload range diagram

Figure 6 shows the payload range diagram for the modular payload that needs to be used to fulfil the requirements. The maximum range with full payload is 40km, while the range will increase till 600km with no payload.

The design meets all requirements except three. The first two are the requirements stating that it needs a top speed of 200 km/h with a payload of 10 kg and an endurance of 1 hour with a payload of 10 kg; these problems have been solved with the aforementioned solution of having a modular payload. The last requirement not met is that the UAV cannot communicate with other UAVs.

Table of Contents

List of Symbols

Abbreviations

BVLOS	Beyond Visual Line Of Sight
CED	Cumulative Energy Demand
CFD	Computational Fluid Dynamics
CP	Centre of Pressure
DSE	Design Synthesis Exercise
EASA	European Aviation Safety Agency
EBS	Empennage Base Structure
EPP	Expanded Polypropylene
FBS	Fuselage Base Structure
GPS	Global Positioning System
GSM	Global System for Mobile communications
HMAC	Hash-based Message Authentication Code
HS	Horizontal Stabiliser
LCA	Life Cycle Assessment
LCI	Life Cycle Inventory
LTE	Long Term Evolution
MAC	Message Authentication Code
MAVLink	Micro Air Vehicle communication Link
MEW	Manufacturing Empty Weight
MNS	Mission Need Statement
MOI	Moment Of Inertia
MTOW	Maximum Take Off Weight
OEI	One Engine Inoperative
PB	Payload Bay
PDC	Python Drag Calculator
POS	Project Objective Statement
PWM	Pulse Width Modulation
RAMS	Reliability, Availability, Maintainability and Safety
RC	Radio Control
RPM	Revolution Per Minute
SM	Safety Margin
STC	Static Thrust Calculator
UAS	Unmanned Aerial System
VLM	Vortex Lattice Method
VLOS	Visual Line Of Sight
VS	Vertical Stabiliser
VTOL	Vertical Take-Off and Landing
WMS	Wing Main Structure

Roman Symbols

A	Enclosed area	[m^2]
A_{fore}	Front propeller area	[m^2]
$A_{frontal}$	Frontal area of fuselage cross section	[m^2]
A_{prop}	Propeller area	[m^2]
AR	Aspect ratio	[-]
AR_h	Aspect ratio of horizontal tail	[-]
AR_v	Aspect ratio of vertical tail	[-]
AR_w	Aspect Ratio of wing	[-]
B	Boom area	[m^2]
b_h	Span of horizontal tail	[m]
b_v	Span of vertical tail	[m]
b_w	Span of wing	[m]
c	Airfoil chord	[m]
C_d	Drag coefficient of airfoil	[-]
C_L	Lift coefficient	[-]
C_l	Lift coefficient of airfoil	[-]
$c_{aileron}$	Aileron chord length	[m]
$C_{D,0_{fus}}$	$C_{D,0}$ of the fuselage	[-]

$C_{D,0_h}$	Zero lift drag of horizontal tail	[-]
$C_{D,0_{pylon}}$	$C_{D,0}$ of the pylons	[-]
$C_{D,0_v}$	Zero lift drag of vertical tail	[-]
$C_{D,cr_{fus}}$	$C_{D,cr}$ of the fuselage	[-]
C_{D,cr_h}	Drag coefficient during cruise of horizontal tail	[-]
$C_{D,cr_{pylon}}$	$C_{D,cr}$ of the pylons	[-]
C_{D,cr_v}	Drag coefficient during cruise of vertical tail	[-]
$C_{d,cruise}$	Airfoil drag coefficient at cruise	[-]
$C_{D,cr}$	Cruise wing drag coefficient	[-]
$C_{D,h}$	Horizontal tail drag coefficient	[-]
$C_{d_{0,v}}$	Airfoil zero-lift drag coefficient of vertical tail	[-]
C_{D_0}	Zero lift drag coefficient	[-]
C_D	Drag coefficient	[-]
$c_{elevator}$	Chord wise length of elevator	[cm]
$C_{L,cr_{fus}}$	$C_{L,cr}$ of the fuselage	[-]
$C_{l,cruise}$	Lift coefficient of airfoil during cruise	[-]
$C_{L,cr}$	Cruise wing lift coefficient	[-]
$C_{L,h}$	Horizontal tail lift coefficient	[-]
$C_{l,max}$	Airfoil maximum lift coefficient	[-]
C_{l_h}	Horizontal tailplane airfoil lift coefficient	[-]
$C_{L_{\alpha_h}}$	Lift slope coefficient of the tail	[-]
$C_{L_{\alpha_{A-h}}}$	Lift slope coefficient of the aircraft minus tail	[-]
$C_{L_{\alpha_v}}$	Lift slope coefficient the vertical tail	[-]
$C_{L_{\beta_v}}$	Vertical tailplane lift coefficient slope	[-]
C_{l_h}	Airfoil lift coefficient of horizontal tail	[-]
C_{L_v}	Vertical tail lift coefficient	[-]
$C_{M,ac}$	Pitching moment coefficient around the aerodynamic center of the wing	[-]
C_{n_δ}	Normal force gradient	[-]
c_{r_h}	Root chord of horizontal tail	[m]
c_{r_v}	Root chord of vertical tail	[m]
c_{r_w}	Root chord of wing	[m]
$C_{req,efp}$	Required battery capacity for essential flight phases	[mAh]
$C_{req,efs}$	Required battery capacity for extreme flight scenario	[mAh]
C_{req}	Required battery capacity	[mAh]
c_{rudder}	Chord wise length of rudder	[cm]
c_{t_h}	Tip chord of horizontal tail	[m]
c_{t_v}	Tip chord of vertical tail	[m]
c_{t_w}	Tip chord of wing	[m]
c_{vt}	Tail volume coefficient	[-]
$\bar{c}_w$	Mean aerodynamic chord of the wing	[m]
D	Drag	[N]
$d_{back_{engine}}$	Distance from wing aerodynamic center to the back engines	[m]
D_{cr}	Drag generated during cruise flight	[N]
$d_{front_{engine}}$	Distance from wing aerodynamic center to the front engines	[m]
$D_{h,cr}$	Horizontal tail drag at cruise	[N]
$D_{prop_{back}}$	Diameter of back propellers	[m]
$D_{prop_{front}}$	Diameter of frontal propellers	[m]
D_{pylon}	Pylon diameter	[m]
dz/dx	Mean camber line slope	[-]
e	Oswald factor	[-]
F	Force	[N]
h_{fus}	Fuselage height	[m]
I	Area Moment of inertia	[m^4]
I	Current	[A]

i_h	Horizontal tail incidence angle	[deg]	
i_v	Vertical tail incidence angle	[deg]	
I_{xx}	Mass Moment of Inertia around the x-axis	[kg m^2]	
I_{yy}	Mass Moment of Inertia around the y-axis	[kg m^2]	
I_{zz}	Mass Moment of Inertia around the z-axis	[kg m^2]	
l_h	Distance between the a.c. of the wing and the a.c. of the tail	[m]	
l_v	Distance between the centre of gravity and the aerodynamic centre of the vertical tailplane	[m]	
L_{cr}	Lift at cruise velocity	[N]	
L_{fus}	Fuselage length	[m]	
$L_{h,cr}$	Horizontal tail lift at cruise	[N]	
$l_{taperchange}$	Length where taper changes, as seen from the tip	[m]	
l_{twist}	Length of twist on wing (one side)	[m]	
m	Airfoil maximum camber as a fraction of the chord multiplied by 100	[-]	
M_{pitch}	Moment required for pitch manoeuvre	[Nm]	
M_{roll}	Moment required for roll manoeuvre	[Nm]	
M_{yaw}	Moment required for yaw manoeuvre	[Nm]	
N	Normal force	[N]	
p	Airfoil maximum camber position as a fraction of the chord multiplied by 10	[-]	
$P_{out,max}$	Power required	[W]	
$P_{req,aft}$	Required power for an aft motor	[W]	
$P_{req,front}$	Required power for a front motor	[W]	
P_{req}	Required power	[W]	
q	Dynamic pressure	[MPa]	
q_s	Shear flow	[N/mm]	
S	Wing surface area	[m^2]	
S_h	Horizontal tail surface area	[m^2]	
S_{aft}	Distance from maximum c.g. position	[m]	
$S_{aileron}$	Aileron surface area	[m^2]	
$S_{elevator}$	Surface area of elevator	[m^2]	
S_{fore}	Distance from minimum c.g. position	[m]	
S_{rudder}	Surface area of rudder	[m^2]	
S_v	Vertical tail surface area	[m^2]	
S_x	Shear force in x-direction	[N]	
S_y	Shear force in y-direction	[N]	
S_z	Shear force in z-direction	[N]	
T	Thrust	[N]	
T	Torque	[Nm]	
t	Skin thickness	[mm]	
t_{flight}	Flight duration	[min]	
T_{fore}	Front motor-propeller couple thrust	[N]	
$T_{max,out}$	Maximum thrust output	[N]	
T_{max}	Maximum thrust	[N]	
$T_{out,max}$	Maximum thrust output needed	[N]	
$T_{reduced,out}$	Maximum thrust output without overheating	[N]	
$T_{req,max}$	Maximum required thrust	[N]	
T_{req}	Thrust required	[N]	
V	Airspeed	[m/s]	
V_∞	Undisturbed airflow velocity	[m/s]	
V_h/V	Tail/wing speed ratio	[-]	
V_{range}	Maximum range velocity	[m/s]	
W	Weight	[N]	
w_{fus}	Fuselage width	[m]	
$w_{induced}$	Induced velocity	[m/s]	

x/c	Position along airfoil chord	[-]	
x_Γ	Position of the panel vortex as a fraction of the airfoil chord	[-]	
$x_{a.c.}$	Position of the aerodynamic centre of the wing from the nose	[m]	
x_{ac_h}	Distance from nose to the aerodynamic centre of the horizontal tail	[m]	
$x_{c.g._{max}}$	Maximum centre of gravity position from the nose	[m]	
$x_{c.g._{min}}$	Minimum centre of gravity position from the nose	[m]	
x_{cp}	Position of the panel control point as a fraction of the airfoil chord	[-]	
x_{LE}	Leading edge position of the wing from the nose	[m]	
y_{engine}	Distance between engines and centre of gravity along the wingspan	[m]	
z	Mean camber line height as a fraction of the airfoil chord	[-]	

Greek Symbols

α	Angle of attack	[deg]
α	Angular acceleration	[rad/s^2]
α_{crit}	Airfoil critical angle of attack	[deg]
$\ddot{\phi}$	Angular roll acceleration	[rad/s^2]
$\ddot{\psi}$	Angular yaw acceleration	[rad/s^2]
$\ddot{\theta}$	Angular pitching acceleration	[rad/s^2]
$\Delta\alpha_{tip}$	Maximum twist angle at tip	[deg]
$\Delta\tau$	Change in torque	[Nm]
ΔP	Change in power	[W]
ΔT	Change in thrust	[N]
δ	Control surface deflection angle	[deg]
$\delta_{aileron_{max}}$	Aileron maximum deflection angle	[deg]
$\delta_{elevator_{max}}$	Elevator maximum deflection angle	[deg]
$\delta_{rudder_{max}}$	Rudder maximum deflection angle	[deg]
$d\epsilon/d\alpha$	Downwash	[-]
Γ	Vortex strength	$[m^2/s]$
λ_h	Taper ratio of horizontal tail	[-]
Λ_v	Sweep angle of the vertical tailplane	[deg]
λ_v	Taper ratio of vertical tail	[-]
λ_{root}	Taper ratio at root of wing	[-]
λ_{tip}	Taper ratio at tip of wing	[-]
ω	Angular velocity	[RPM]
ρ	Air density at sea level	$[kg/m^3]$
σ	Normal stress	$[N/m^2]$
σ_x	Normal stress in x-direction	[MPa]
τ	Shear stress	$[N/m^2]$
τ	Torque	[Nm]
θ	Independent variable of the circular description of an airfoil geometry	[rad]

1 Introduction

In recent years, significant advances have been made in both the capabilities of automated control systems and the miniaturisation of technological components, both of which have been attributed to the exponential growth in the Unmanned Aerial Vehicle market over the last decade. Tasks that traditionally required constant human supervision, control and even physical effort are steadily being replaced by UAVs, which signals the rise of UAVs being used in commercial applications.

Despite significant advances being made in the UAV market, what has proven to be challenging is combining the high velocity horizontal flight capabilities of fixed wing aircraft with the vertical take-off and landing and hovering capabilities typical of rotor aircraft. Hybrid UAVs aim to seamlessly combine the two and this challenge is what necessitates the research, calculations, and design documented in this report.

The project of which this report is the outcome, aims to document and present an efficient Hybrid UAV design which can be controlled remotely within Visual Line Of Sight (VLOS), with the capability of Beyond Visual Line Of Sight (BVLOS) control in the future. Derived from the aforementioned goal is the Project Objective Statement (POS) which summarises the goal of the project and the steps required to achieve it, and is characterised as follows:

> *Design and optimise a Hybrid UAV that meets requirements and constraints by using project management and systems engineering tools, by a team of 10 students within 11 weeks.*

The required functions of the Hybrid UAV identified and defined in the baseline report form the foundation upon which the requirements and constraints are determined [1]. These functions and requirements follow indirectly from the Mission Need Statement (MNS) which concisely defines what the goal of the design is and is characterised as follows:

> *Carry out both remotely controlled and supervised autonomous monitoring and transport missions, comprising vertical take-off and landing, and sustained high-velocity horizontal flight.*

Chapter 2 characterises the required functions of the UAV and as a result defines what the product of the design process should be. Chapter 3 defines the approach to be taken to get to the desired result by outlining what preparation, tools, and verification & validation procedures are necessary. Chapter 4 analyses both the market and the direct stakeholders, and Chapter 5 defines the general system requirements. Chapter 6 briefly discusses the basis of the baseline report (such as the trade-off) and reveals the winning concept, and Chapter 7 defines the subsystems of the chosen concept and their interrelations. Chapters 8 to 11 present the Power & Propulsion, Aerodynamic, Stability & Control, and Structural analyses respectively, and Chapter 12 lays out what avionics and electronic components are necessary to fulfil the requirements. Chapter 13 presents the mass, cost and power breakdowns of the design, and Chapter 14 analyses and outlines what procedures need to be taken during operations. Chapter 15 outlines the production plan, and Chapter 16 presents the life cycle assessment. Finally Chapter 17 presents the conclusions of this report, and suggests recommendations for further research.

2 Project Description

This chapter elaborates on the objective of the project and the mission of the product in Section 2.1. Furthermore, the functions that the product needs to perform will be evaluated in Section 2.2.

2.1 Mission Description

The Hybrid UAV is designed to have a wide range of missions and applications. The five identified main markets are listed in this section.

1. Search, rescue, and support to disaster relief operations.
2. Precision agriculture by monitoring of cattle and crops.
3. Transportation of parcels at sea and on land.
4. Inspection of extensive industrial assets and infrastructure such as railways, high-tension power lines, pipelines, wind farms, etc.
5. Transportation of organs for transplants.

To help visualise the missions, the mission profile diagram can be found inFigure 2.1. The first type of mission (solid line) corresponds to a mission which requires high range or speed. It starts by going to its cruise altitude, at which it can cruise at the desired speed until it reaches its destination. At the end there is a five minute window for hovering, which will be used to find a suitable landing site. The second mission profile (striped line) applies to missions which focus on endurance and surveillance. It is similar to the first mission profile, except for the fact that it will have a loiter period in between the cruise phases to perform the missions.

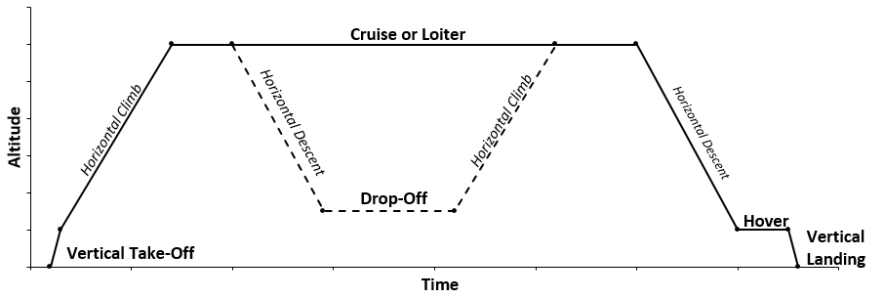

Figure 2.1: Mission Profile for Different Missions

2.2 Functional Analysis

In this section the functions of the UAV are analysed by means of illustrating the functional flow diagram and functional breakdown structure.

2.2.1 Functional Flow Diagram

The functional flow diagram is illustrated in Figure 2.2. The top-level flow of each mission is given on top of the figure. Each rectangle corresponds to a specific function to be performed and can be further elaborated on in a function-branch indicated by REF. Depending on the statement, a GO (G) or NO GO ($\overline{G}$) may follow the function.

The functional flow diagram is applicable to all missions stated in Section 2.1. First, the pre-flight preparations are carried out. Secondly, take-off and transition take place, after which

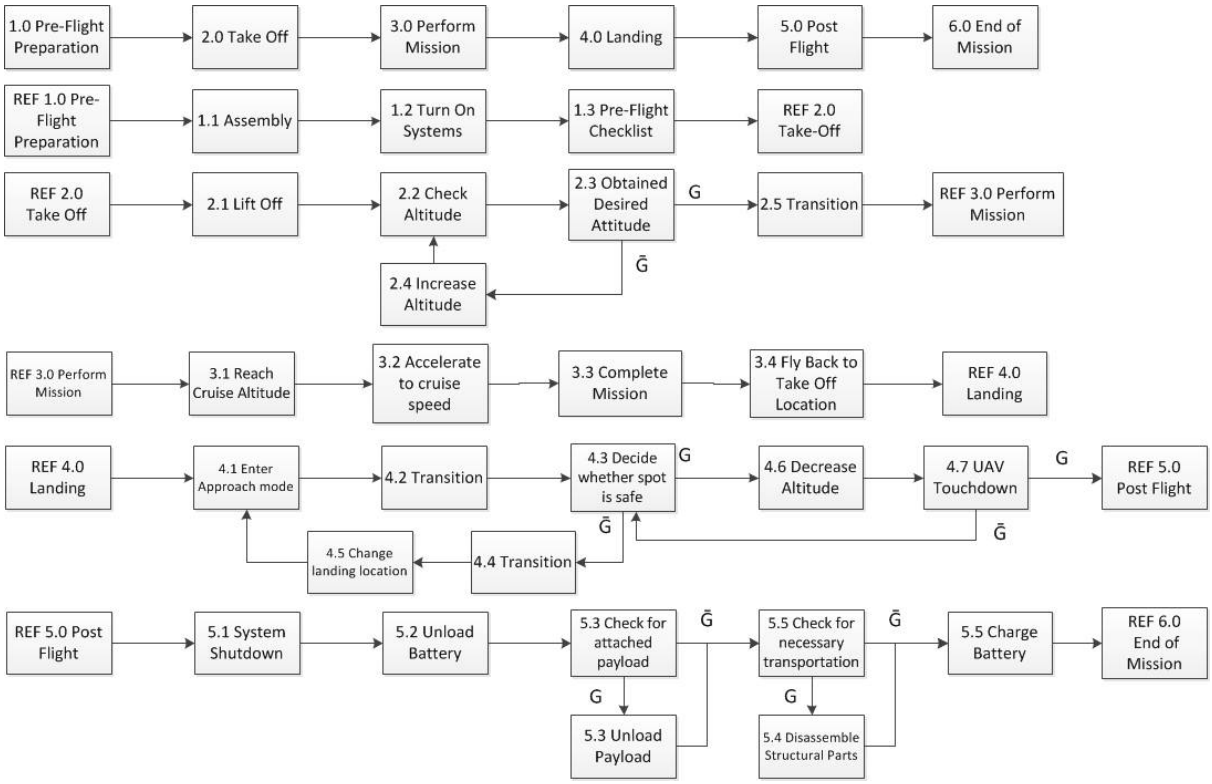

Figure 2.2: Functional Flow Diagram

the mission is performed. Finally, the transition and landing is carried out, followed by the post-flight procedures. Each mission phase consists of flying at cruise altitude and cruise speed towards the mission destination. However, function 3.3 Complete Mission is a mission specific function block. Depending on what mission the UAV has to fly, the UAV will have to perform different functions such as hovering, loitering, dropping of packages, etc.

2.2.2 Functional Breakdown Structure

Figure 2.3 shows the functional breakdown diagram where all top-level functions make the UAV system operative. The structure was adapted from an example air transport mission [3]. The function of performing air transport is separated from performing missions and operates under various conditions. 'Perform air transport' breaks down the pre-flight operations, take-off preparations, flight and post-landing operation mission phases into functions. Since the flight operations are both important and extensive, they have a separate break-down in Figure 2.4.

It can be identified that the main missions are monitoring missions, transport missions between bases, transport mission with aerial drop-off, and combinations of them. Hence, functions must exist that enable those operations, e.g. the ability to follow predefined way points. The conditions under which these missions can be performed can be grouped into: normal operating conditions, under which the UAV can achieve its maximum performance, abnormal conditions, where limited flight operations are still possible, and emergency situations, in which safety considerations overrule the original mission.

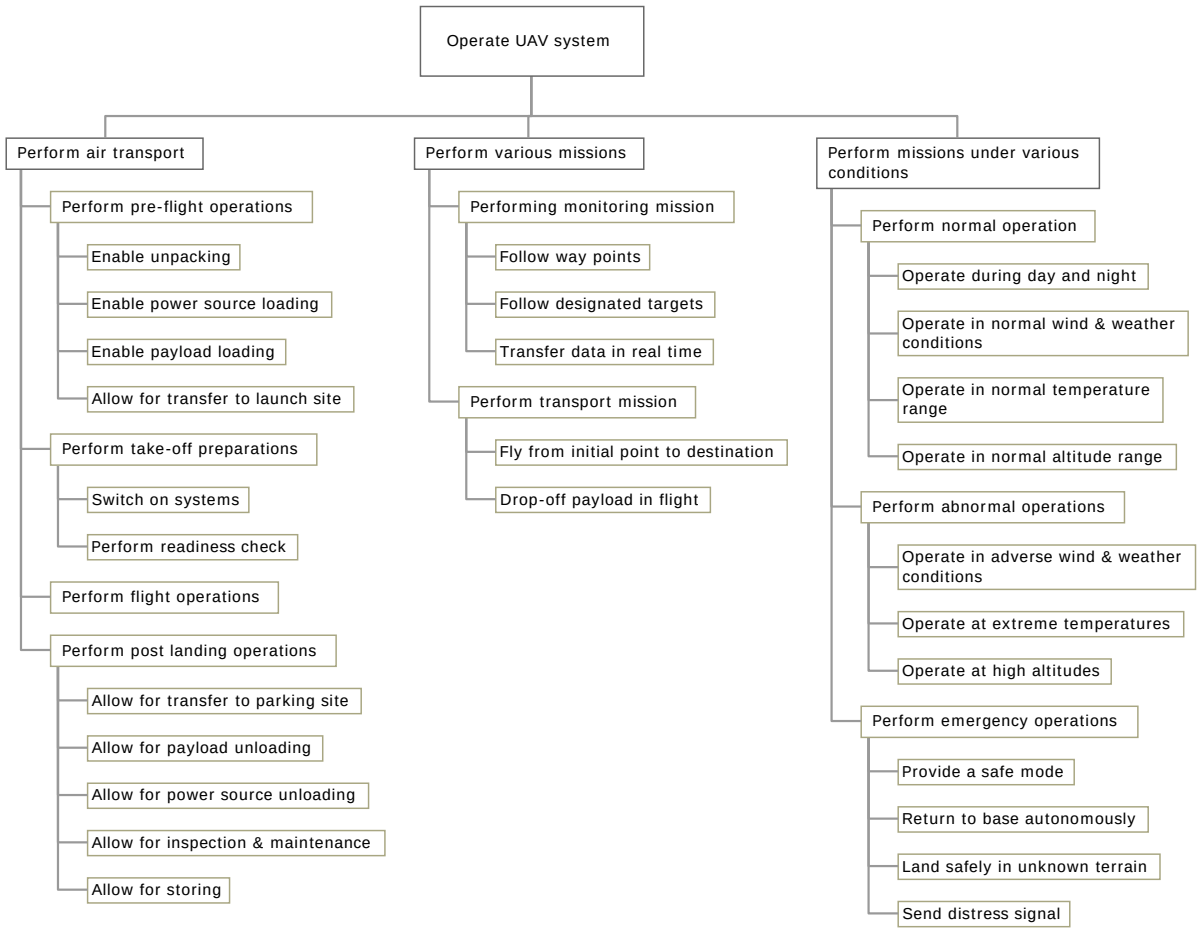

Figure 2.3: Functional Breakdown Structure

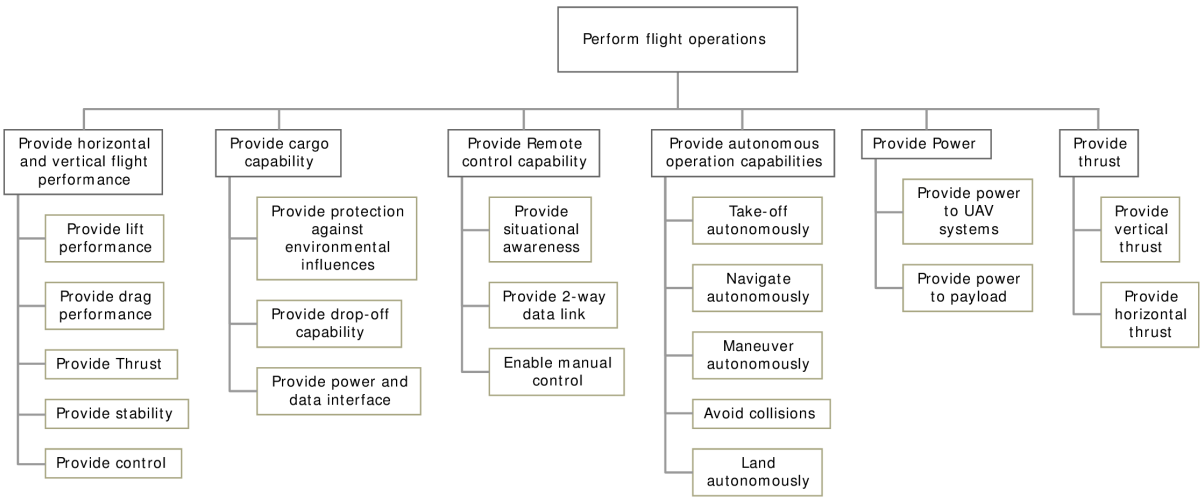

Figure 2.4: Perform Flight Operations Function

3 Project Approach

In this chapter, the design process is described and the approach to verification and validation is explained.

3.1 Design Process

In the baseline report [1], concepts were generated that could deal with the problem at hand. In the midterm report [2], a trade-off was performed to see which concept would be the best to do so. Now that a concept is chosen, detailed design can be done to ensure that the requirements can be met.

3.1.1 Preparation

The first step taken in the detailed design phase is defining the different subsystems. The subsystems are chosen in such a way that the whole aircraft system is accounted for. Departments are then created which will work on the various subsystems, and each subsystem will have one leading department. The departments and subsystems are shown in Table 3.1.

Table 3.1: Departments and Responsibilities

Department	**Leading on**	**Working on**
Aerodynamics	Wing	Wing, Tail, Fuselage and Propulsion Unit
Command & Data Handling	Avionics and Ground Control	Payload, Avionics and Ground Station
Power & Propulsion	Propulsion Unit and Power Unit	Propulsion Unit and Power Unit
Stability & Control	Tail	Wing and Tail
Structures	Fuselage	Payload, Wing, Tail and Fuselage

3.1.2 Tools

The next step taken into the detailed design is coming up with tools to aid the design process. One of the tools that aids the design process is the N^2 chart which shows the interrelations between sub-systems, shown in Section 7.2. With this chart the different departments know what they need from other departments and which constraints are present.

Another tool being used is the work flow diagram. Each department will make a work flow diagram to help visualise the design process, showing the steps and iterations required to arrive at an outcome. This way, when a team member is lost, it is possible to look at this diagram to see how to proceed. The work flow diagrams can be seen in each designing chapter.

The next tool is called the 'Master Set'. This tool contains all the up-to-date values and variables of the design, so that there can be no confusion between departments. To make sure that this tool is implemented correctly, only one team member can bring changes to it. When using python for coding, the Master Set is automatically imported when running the code, meaning the most up to date values are always used. The master set can be seen in Figure E.1.

To be able to have an overview of what is being done, a smart task division tool has been created. This tool is made in Excel and contains all the work that has to be done. Apart from

the work needed to be done, there is also a tab containing all the writing that needs to be in the report, listed to sub-section level detail. Each task has a deadline which changes colour the closer the deadlines approaches. In addition there are columns to indicate who worked on a task, and who is in charge of it (as a contact person). The writing tab shows: the maximum number of pages for each chapter; who wrote which sub-section; who contributed to that sub-section; and which members performed the quality control. On top of all this, a drop down menu was implemented through which each task can be labelled as 'Not Started', 'In Progress or 'Done'. To get an impression of the Task Division tool, it can be seen in Appendix D.

When designing, the different departments want to generate the best result according to their principle. This could cause a problem for the cost and mass of the aircraft, and also the amount of energy it needs. To prevent this, budgets are assigned to each subsystem. Each budget has a certain contingency, these are set in place to account for likely increases in mass, energy and cost as the design phase progresses. The budgets and contingencies are explained in Section 7.4.

3.1.3 Designing

Now that the preparation is done, the designing can start. Each department will start designing according to their work flow diagram. To start-off the design process, values for the variables are estimated. Once new values are known, they will be updated in the Master Set, so the further calculations will be done with these new values. During the design process a lot of iterations are made due to major design changes or due to changes in these same variables. These changes are updated in the Master Set and explicitly communicated to relevant departments if it implies a substantial change.

3.2 Verification & Validation Procedure

In this section, the verification and validation procedures are analysed and explained. First, in Section 3.2.1, the verification method used for each requirement is illustrated. Then, in Section 3.2.2, validation procedures for requirements, tools, models, and the final product are discussed. The actual execution of the verification and validation is not discussed in this section but is documented throughout the report since it is also executed continuously throughout the design phase.

3.2.1 Verification

In order to verify requirements, different methods can be used such as inspecting, analysing, demonstrating or testing. Verifying by inspection means using human senses to verify the requirement. Verification by analysis means verifying with mathematical theorems to determine whether the product satisfies the requirement. Verification by demonstration means verifying by operating the UAV under specific conditions to verify that the results are as expected. Verification by tests can be done by checking the compliance of the product with the requirement under representative circumstances. The difference between test and demonstration is that testing requires a more specialised test setup and equipment. Table 3.2 gives an overview of all of the system requirements and the method that can be used to verify them. In this table abbreviations are used: A = analysis, D = demonstration, I = inspection and T = test. The requirements can be found in Chapter 5. During the Design Synthesis Exercise (DSE) it is not possible to verify requirements by test, demonstration or inspection. In Section 13.2 the compliance matrix is presented which summarises the verification of the requirements.

Table 3.2: Requirements Verification Methods

Requirement	Method	Requirement	Method	Requirement	Method
SYS-C-1	A	SYS-OP-2.7	D	SYS-C-2	A
SYS-OP-2.8.2	D	SYS-S-2	A	SYS-OP-2.8.6	D
SYS-L-2	T	SYS-OP-2.8.7	I	SYS-L-3	T, A, D and I
SYS-OP-2.8.8	D	SYS-R-1	I	SYS-OP-2.9.2	D
SYS-ENV-1.4	T	SYS-OP-2.9.3	D	SYS-ENV-1.5	A
SYS-OP-2.9.4	D	SYS-ENV-1.6	D	SYS-PF-1.1	A
SYS-ENV-2.1	D	SYS-PF-1.2	T	SYS-ENV-2.2	D
SYS-PF-1.3	T	SYS-ENV-2.5	I	SYS-PF-1.4	T
SYS-PH-1.1	I	SYS-PF-2.1	D	SYS-PH-1.2	I
SYS-PF-2.2	D	SYS-PH-2	D	SYS-PF-2.3	D
SYS-PH-4.3	T	SYS-PF-2.4	T	SYS-PH-4.4	T
SYS-PF-3	A	SYS-OP-1.1	D	SYS-PF-4	A
SYS-OP-1.5	I	SYS-VS-1.1	D	SYS-OP-1.7	D
SYS-VS-1.2.1	T	SYS-OP-2.1	A	SYS-VS-1.2.2	T
SYS-OP-2.2	A	SYS-VS-1.2.3	D	SYS-OP-2.3	I
SYS-VS-1.2.4	D	SYS-OP-2.4	D	SYS-VS-2.1	T
SYS-OP-2.5.3	T	SYS-VS-2.2	T	SYS-OP-2.5.4	T
SYS-VS-2.3	T	SYS-OP-2.5.5	T	SYS-VS-3	I
SYS-OP-2.9.5	T				

3.2.2 Validation

In this section, the validation methods for the requirements, the tools and models used, and the final product are presented.

Requirement Validation All system and subsystem requirements are checked and altered in order to be VALID (Verifiable, Achievable, Logical, Integral and Definitive).

Tool Validation Different tools will be used in order to create a model of a system. These include commonly used tools such as CATIA, Excel, and Python but also less common tools can be used such as XFLR5, an analysis tool for airfoils, wings and planes. The calculation methods of the well known programs are validated by experience since they have been continuously validated by experts in various fields within industries and particularly also in the UAV field. The less common tools need to be validated by analysis in order to check if they are the correct tools to use for a certain purpose. The inputs given by the user will be validated using inspection, meaning reviewing all the inputs and checking the formulas for typos.

Model Validation The model validation will check if the models used to analyse systems and products are the correct models and if they reflect the physical phenomenon as accurately as required. Models can be validated in three different ways: by experience, by analysis, and by comparison. Validating a model by experience is checking if the model produces the expected outcome while using various inputs. Validating by analysis means showing that the elements of the model are correct and are correctly integrated. Comparison validation compares the

outcome of the model with independent models of proven validity or actual test data. The model validation procedures differ from model to model. The execution of the model validation will be documented in Chapters 8 to 11.

Product Validation Validation of the product is answering the question if the product accomplishes the intended purpose. In other words, does the product fulfil the Mission Need Statement (MNS). Qualification tests and acceptance tests need to be performed for the system product validation. A stress test and simulations can be used as qualification. Mission scenario tests and operations readiness tests are possible acceptance tests that can be used. Since these tests can only be performed when at least a prototype of the system exits, product validation by analysis needs to take place in this stage of the design. When the product fulfils all the requirements, the product also fulfils the MNS. Hence, the product can be validated by checking if all the requirements are verified. This is documented in Section 13.2.

4 Market and Stakeholder Analysis

In this chapter, both the market and stakeholder analyses are presented. The size of the market and competitors are identified in Section 4.1. Then all stakeholders of the project are listed and their relevance is explained in Section 4.2.

4.1 Market Analysis

In this section, a market analysis relevant to the Hybrid UAV is presented. First, the market is defined, and its current size and expected growth are estimated. Then an analysis of the competition is made. Finally, a customer analysis is made, which is partly based on the stakeholders as discussed in Section 4.2.

4.1.1 Current and Future Market

In the baseline report, the market was already analysed [1]. The Hybrid UAV will be part of the general aviation sector[1]. Its market can be defined as:

> *The subsets of both the general aviation market and military market comprising UAVs and helicopters used specifically for autonomous monitoring and transport missions.*

During the previous analysis, it was also determined that quantifying the market size is extremely difficult. The current estimation is that the entire UAV market is worth United States Dollar (USD) 13.22 billion[2] (12.11 billion EUR), while the market opportunity between now and 2020 is estimated at USD 100 billion[3](92 billion EUR[4]). The relevant part of the market for the Hybrid UAV that is being designed, is estimated at USD 13 billion (12 billion EUR) in this period[5]. Shese values should mostly be considered for their order of magnitude, since the exact market size is nearly impossible to grasp.

4.1.2 Competition Analysis

Since the market is growing, it is expected to provide enough business opportunities. Therefore, an analysis of the competition is made, which is the most important information on the market during the design process. When the design is too similar to a product that is already on the market, chances of success are smaller. In the baseline report, not only UAVs, but also helicopters were included in this analysis. A choice was made to leave helicopters out of the analysis in this report, since even though they are used a lot for the same missions, most customers will specifically look for a UAV. Also UAVs weighing over 25 kg were not considered because of EASA regulations; this ruled out a lot of companies and models, such as Textron and most of Latitudes models. The largest difference between this Hybrid UAVs main market orientation and that of the competition is that other UAVs are much more mission specific.

[1] `http://www.iaopa.org/what-is-general-aviation/`, Accessed on 01-05-2017

[2] `http://www.marketsandmarkets.com/Market-Reports/unmanned-aerial-vehicles-uav-market-662.html?gclid=Cj0KEQjwuZvIBRD-8Z6B2M2Sy68BEiQAtjYS3D4gmcrdpSawOfsX6w4PIEX91fD4cpe7P7stNjVpG9IaAu3c8P8HAQ`, Accessed on 01-05-2017

[3] Exchange rate 1 USD = 0.92 EUR, 26-06-2017

[5] `http://www.goldmansachs.com/our-thinking/technology-driving-innovation/drones/`, Accessed 22-06-2017

[5] See footnote 5.

Table 4.1: List of Competitors

Company, concept	Unique selling points and benefits	Commonalities and outperformed aspects	Price estimate
Latitude, HQ-40[6]	Cooperate with Arcturus and Textron by using their airframes, and also enable the use of other airframes in combination with their quadrotor technology. Gas powered.	Hybrid quadrotor layout. Most competing concept has five hour endurance and 2.5 kg payload capacity.	USD 40,000[7]
Arcturus, Jump-15[8]	Endurance 6+ hours, catapult launch.	Hybrid quadrotor layout. Maximum speed 100 km/h, fuel injection engine.	Unknown
Avy	Prandtl box layout. 400 km range.	Maximum speed 200 km/h, 10 kg payload, fully electric[9].	EUR 30,000 - 60,000[10]
Atmos	Tailsitter concept. MTOW estimated at 5,5 kg[11], fully electric.	Meant for mapping missions, such as precision agriculture. Mapping range 1 square km, endurance 30 minutes.	Estimated at EUR 30,000
Carbonix, Volanti[12]	Multiple modular options. Endurance 1.5 h when operated fully electric.	Hybrid twin- or quadrotor layout. Optimal loiter speed 65 km/h. Payload bay ca. 0.4x0.2x0.1 m, capacity 6 kg.	Estimated at USD 114,000[13]
Sky-watch, Cumulus and Heidrun[14]	Deep stall landing, hand launched.	Up to 600 g payload capacity, 25 km range or 40 square km coverage in monitoring, top speed 100 km/h.	Unknown

4.1.3 Customer Analysis

There exist different types of potential customers. These are defined by the mission types the Hybrid UAV can perform, and have some overlap with the stakeholders. Some customer groups are: governmental organisations, non-governmental non-profit organisations (charities), farmers, logistics companies, internet retailers, offshore companies, infrastructure companies, and hospitals.

Both opportunities and difficulties arise because of this large range of potential customers. A lot of UAVs can be sold, yet promoting the product in so many different sectors is time consuming. Also, the versatile nature of the Winged Quadcopter design might not be as attractive as a UAV solely designed for the customers intended purpose.

Aspects regarding the potential sales of the Hybrid UAV combined with the estimated market size from Section 4.1.1, the amount of UAVs team 14 will sell can be estimated. The estimated

[6] `https://latitudeengineering.com/products/hq/`, Accessed 08-06-2017

[7] `http://www.popularmechanics.com/flight/drones/a9351/this-unmanned-plane-can-land-on-a-helo-pad-15812116/`, Accessed 08-06-2017

[8] `https://www.uav-africa.com/.../11_arcturus-jump-spec-sheet.pdf`, Accessed 08-06-2017

[9] `www.avy.eu`, Accessed 08-06-2017

[10] Private contact with Avy

[11] Private contact with Atmos

[12] `http://carbonix.com.au/wp-content/uploads/2017/02/17-02-22-Carbonix-VTOL-Hybrid-UAV-Information-Brochure.pdf`, Accessed 08-06-2017

[13] `http://newatlas.com/carbonix-volanti-vtol-fixed-wing-industrial-uav/48253/`, Accessed 08-06-2017

[14] `http://sky-watch.com/products/`, Accessed 08-06-2017

sales price is 60,000 euros (EUR). Looking at the worldwide market and at the competitors, sales are estimated. When team 14 is able to take 0.25% of the civil UAV market, that would mean that the team could sell for EUR 32 million on drones[15]. That means around 500 Hybrid UAVs can be sold.

4.2 Stakeholder Identification and Analysis

Stakeholders of a project are actors, namely persons or organisations who have a vested interest in the success of the project [4]. They are individuals or groups who are affected by or who can exert influence on the project's outcome. The stakeholders can range from organisations who govern policy of the project, to citizens who may benefit or be disadvantaged depending on the outcome of the project. The success of a project in project management terms is partially defined by stakeholder satisfaction and therefore, in order to successfully execute the project, it is crucial to conduct a stakeholder analysis.

In order to conduct a stakeholder analysis, the relevant stakeholders must first be identified. Once the stakeholders are identified the analysis can be conducted which would include investigating the ability of each stakeholder to affect the project as well as their interest in the project. Each stakeholder will be presented followed by both an individual analysis and a potential management strategy. Finally a graphical representation of the analysis will be presented.

4.2.1 Identification and Analysis

In this section the direct stakeholders will be identified and analysed based on a few key aspects. Each stakeholders' knowledge of the project and interest in the project will be examined as well, to identify whether they are in favour of or opposing the project. Each stakeholders' power (ability) to affect the project will be assessed as well as whether potential alliances amoung stakeholders are imminent. Each stakeholder will be rated from 1 to 4 on both power and interest, 1 being given to stakeholders who have little power or interest, and 4 to stakeholders that have significant power over or interest in the project. The ratings will be presented as (***interest, power***).

A. Avy Avy has laid out the primary requirements of the design of the Hybrid UAV and therefore, by definition, has significant power over the outcome of the project as well as substantial knowledge about the project. Avy might adopt the findings of the project, however that is at their own discretion and therefore their interest in the project is moderate. Rating (***2, 3***)

B. EASA EASA is responsible for regulating European Aviation and therefore, in order to get certification to operate the Hybrid UAV developed throughout this project, EASA airworthiness regulations must be met. The project cannot be a success without meeting these requirements and therefore EASA has substantial power over the project. Rating (***1, 4***)

C. General Public Ultimately the goal of the project is to develop a product that serves the general public and therefore the public in theory has a high interest in the project. However, it is most likely that the vast majority of the public will not have much knowledge about the project and it's goals. Since the Hybrid UAV is to be operated in the public domain, there needs to be transparency as pertains to the development and operation of the UAV. There will be a subset of the general public who will oppose the project as they might see the product as

[15]Exchange rate USD 1 = EUR 0.92, 23-06-2017

being potentially harmful to their quality of life (privacy and noise pollution). The wishes of the public must be considered and therefore the public's ability to affect the project is moderate. Rating ***(2, 2)***

D. National Fire Department National fire departments are potential customers as fire departments are generally in charge of search and rescue efforts. Fire departments will therefore be in support of the successful execution of the project and will be interested in the capabilities of the Hybrid UAV. As potential operators of the UAV, input from the fire departments must be considered and therefore the fire departments exercise moderate power over the project. Rating ***(3, 2)***

E. Health Care Institutions As potential customers of a product aiming to decrease the transport time of emergency medical supplies and samples, health care institutions will be beneficiaries of the successful execution of the project. They will therefore be interested in the progress made throughout the development phase. Medical institutions will have substantial power over the design as the UAV must meet the stringent requirements on the conditions required for delicate transportation missions. Rating ***(3, 2)***

F. Infrastructure & Asset Owners The Hybrid UAV will have the capabilities required for highly accurate surveillance. This makes it an attractive product for owners and operators of extensive infrastructure and expensive assets as monitoring costs can be drastically decreased. As the outcome of the project is simply a product that can be bought and configured for specific missions, infrastructure and asset owners do not have significant power or leverage over the execution of the project. Rating ***(3, 2)***

G. Logistics Companies As potential customers, logistics companies will be interested in the capabilities of the Hybrid UAV. They will be particularly interested in the relationship between range and payload. Ultimately, the logistics companies do not have substantial leverage over the project. However, as potential customers, whether or not their wishes are met dictates to some degree the success of the project. Rating ***(3, 2)***

H. Suppliers of Parts & Services During the production phase of the project, various 'off the shelf' components as well as a number of services will be required to successfully produce the Hybrid UAV. The costs dictated by the suppliers have a substantial effect on the overall production costs of the UAV and therefore the suppliers have significant power over the project. Suppliers are not particularly interested in the project but rather in the business opportunity of supplying parts or services. Rating ***(1, 3)***

I. Air Traffic Control Air traffic control is responsible for regulating air traffic to ensure safety for all. Air traffic control needs to keep an overview of all air traffic in certain airspace regions and has the authority to stipulate what class of aircraft is allowed to be operated in what regions of airspace. For this reason, they, along with the EASA regulatory body, pose constraints on the outcome of the project and the types of missions that can be carried out. Air traffic control agencies have no particular interest in the project and are likely to be neither for or against the project. Rating ***(1, 3)***

J. Sponsors Sponsors give something of value to the project (money, expertise, a service, access to facilities, etc.) and in return receive good publicity. Because of providing something of value to the project (usually vital to the success of the project), sponsors have significant power over the project and are particularly interested in the successful execution of the project. Rating ***(4, 3)***

4.2.2 Summary of Stakeholder Analysis

Having analysed the direct stakeholders and rated each on the basis of interest and power, each stakeholder can be mapped to a specific management strategy as shown in Figure 4.1. These management strategies are:

Manage Closely which would entail constantly keeping the stakeholder up to date with progress. This can be done with, for example, status meetings. Stakeholders in this category are in the top right of the figure.

Keep Satisfied through close conversation with the stakeholder about goals and wishes along with keeping the stakeholder up to date with progress. Stakeholders in this category are in the top left of the figure.

Keep informed about the general progress. This might be done in-person or through the media. Stakeholders in this category are in the bottom right of the figure.

Monitor by keeping the stakeholder in contact. Stakeholders in this category are in the bottom left of the figure.

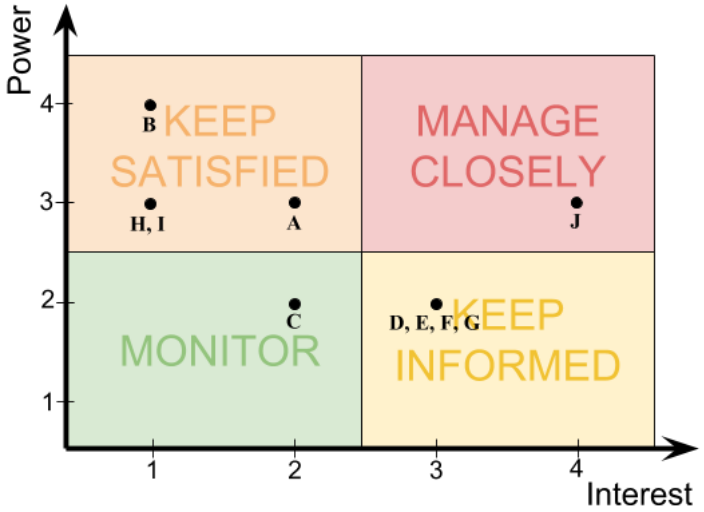

Figure 4.1: Mapping of Stakeholders Based on Interest and Power

5 System Requirements

System requirements describe the system in terms of constraints and functions, and guide the design such that the final product meets the expectations of the stakeholders. Therefore they allow to gain insight into the basis for the design choices that have been made so far.

This chapter presents the system requirements for the Hybrid UAV. The requirement coding is explained in Section 5.1 and the requirements themselves are listed in Section 5.2. At the end of this section, requirements which currently make it impossible to complete the project within the set constraints are mentioned, and their revision is briefly justified.

5.1 Legend

Table 5.1 presents the legend explaining the meaning of the requirement coding.

Table 5.1: Requirements Coding Legend

Requirement Code	**Related to**
SYS	**Sys**tem
C	**C**ost
S	**S**chedule
L	**L**egislation
R	Available **R**esources
ENV	**Env**ironmental Conditions and Footprint
PH	**Ph**ysical Characteristics
OP	**O**perational **P**erformance
PF	**P**erformance of **F**light
VS	**V**ehicle **S**ystems
*	Non-critical Requirements (stakeholder wishes)
†	Key Requirements[1]
‡	Driving Requirements[2]
x	Killer Requirements [3]

5.2 Requirements

The revised requirements can be found in the following list.

SYS-C-1: †‡ The production and distributed development cost per unit shall be limited to an amount of 30k EUR.

SYS-C-2: The cost of the UAV support service shall not exceed 5k EUR per year.

SYS-S-2: The design (up to and including preliminary phase) of the UAV shall be done in 11 weeks.

[1] A requirement which is of primary importance for the customer.
[2] A requirement that dramatically affects the outcome of the design process.
[3] Not meeting such a requirement leads to a product without value to the stakeholders.

SYS-L-2: †	The UAV shall notify the operator when an above ground level altitude of 110 m is reached.
SYS-L-3: x	The UAV shall conform with EASA regulations (A3-Category).[4]
SYS-R-1:	The design shall be performed with 10 team members.
SYS-ENV-1.4: ∗	The UAV shall be able to operate at wind conditions up to 6 on the Beaufort scale.
SYS-ENV-1.5:	The UAV shall have resistance against corrosion of safe-life components for its entire planned lifetime.
SYS-ENV-1.6: ∗	The UAV shall be able to operate nominally in temperatures ranging from -30 to +40 degrees Celsius.
SYS-ENV-2.1: †	The UAV shall not produce any carbon emissions during operation.
SYS-ENV-2.2:	The UAV noise emission shall not exceed a limit of 68 dB.
SYS-PH-1.1: ‡	The combined UAV and support equipment shall occupy a maximum volume of 2.3 x 1.7 x 1.4 meters.
SYS-PH-1.2: †	The UAV shall have a payload bay volume of 100 x 15 x 15 cm minimum.
SYS-PH-2: x	The UAV shall have a MTOW of maximum 25 kg.
SYS-PH-4.3:	The UAV shall have no single point of failure.
SYS-PH-4.4:	The UAV shall be bale to sustain accelerations from maximum -1g up to minimum +3g.
SYS-OP-1.1:	The UAV shall be able to airdrop its payload during operation.
SYS-OP-1.5: ∗	The payload bay shall provide a connection to the power storage.
SYS-OP-1.7: ∗	The UAV payload bay shall allow for payload mounting with basic tooling.
SYS-OP-2.1:	The UAV shall have an operational life of at least 1500 flying hours.
SYS-OP-2.2:	The UAV shall perform missions with a reliability of at least 75%.
SYS-OP-2.3:	The UAV shall be constructed with off-the-shelf electrical components.
SYS-OP-2.4: ∗	UAV fail-safe components shall not require specialised skills to be replaced.
SYS-OP-2.5.3:	The UAV shall avoid collisions with other aircraft autonomously.
SYS-OP-2.5.4:	The UAV shall be able to avoid collisions with birds autonomously.
SYS-OP-2.5.5:	The UAV shall avoid collisions with ground objects autonomously.
SYS-OP-2.7:	The UAV shall be able to operate in night conditions.
SYS-OP-2.8.2: ∗	The UAV shall have a maximum turnaround time of 20 minutes.
SYS-OP-2.8.6: ∗	The transport of the UAV shall require a maximum of two persons.
SYS-OP-2.8.7: ∗	The in-flight operation of the UAV shall be performed by one person.
SYS-OP-2.8.8: ∗	The UAV energy source shall be replaceable within 5 minutes.
SYS-OP-2.9.2:	The safe mode of the UAV shall have a return-to-base function.

[4] EASA Regulations received through contact with AVY

SYS-OP-2.9.3:	The safe mode of the UAV shall contain an autonomous emergency landing function.
SYS-OP-2.9.4:	The safe mode of the UAV shall be able to send a distress signal to the UAV operator, in case of an emergency.
SYS-PF-1.1: ‡	The UAV shall be able to carry a payload of at least 10 kg.
SYS-PF-1.2: ‡	The UAV shall be able to fly at a horizontal velocity of at least 200 km/h at cruise altitude carrying 10 kg of payload.
SYS-PF-1.3: †	The UAV shall have a minimum range of 200 km carrying 10 kg of payload.
SYS-PF-1.4:	The UAV shall have a minimum endurance of 1 hour carrying 10 kg of payload.
SYS-PF-2.1: †‡	The UAV shall be capable of vertical take-off.
SYS-PF-2.2: †‡	The UAV shall be capable of vertical landing.
SYS-PF-2.3:	The UAV shall be able to hover for a minimum of 5 minutes carrying 10 kg of payload.
SYS-PF-2.4:	The UAV shall have a climb speed of at least 4 m/s.
SYS-PF-3:	The UAV shall be controllable in all flight conditions when fully operational.
SYS-PF-4:	The UAV shall be longitudinally, directionally and laterally stable during operation.
SYS-VS-1.1:	The UAV shall be remotely controllable within visual line of sight.
SYS-VS-1.2.1:	The UAV shall be able to navigate autonomously.
SYS-VS-1.2.2:	The UAV shall be able to manoeuvre autonomously.
SYS-VS-1.2.3:	The UAV shall be able to land autonomously.
SYS-VS-1.2.4:	The UAV shall be able to take-off autonomously.
SYS-VS-2.1:	The UAV shall communicate with a ground station with a minimum frequency of 50Hz.
SYS-VS-2.2:	The UAV shall communicate with other air vehicles within a 1000 m radius.
SYS-VS-2.3:	The UAV shall communicate the current flight conditions to the pilot.
SYS-VS-3:	The UAV shall have electrical propulsion.

As seen above, requirements SYS-L-3 and SYS-PH-2 were regarded as killer requirements due to the fact that a range of 200 km or an endurance of one hour is not achievable with a MTOW of 25 kg and 10 kg of payload. Not meeting requirement SYS-L-3 would make it illegal to operate the UAV in Europe unless it were to be classified as a civil aircraft leading to much greater legislation costs exceeding the budget. The solution yielding a useful product was found in the form of exchanging payload capacity with additional energy storage. The direct consequence is the need for the change of requirements SYS-PF-1.3 and SYS-PF-1.4 which state that the UAV shall be able to have the maximum range and endurance while carrying a payload mass of 10 kg. The redefined requirements are as follows:

SYS-PF-1.3R: The UAV shall have a minimum range of 200 km.

SYS-PF-1.4R: The UAV shall have a minimum endurance of 1 hour.

6 Concepts & Trade-Off

In this section, an overview is given on the concepts generated during the baseline, how they were filtered and how the final trade-off was performed. Some more information is given on the Winged Quadcopter concept, the concept that was carried to the final design phase.

6.1 Concepts Generation

In a previous phase of the project, concepts were generated through a brainstorm session and a design option tree [5]. From this, five concepts were chosen to be analysed further in order to obtain one concept on which the final design is based. This was done based on feasibility calculations and selecting the designs that seemed most promising.

The five concepts are: a tailsitter, a tiltable wing in tandem configuration, a Prandtl boxed wing with tiltable propellers, a 'tiltrotor' configuration where the propellers (located at the wing tips) can rotate, and a winged quadcopter layout. Detailed information about these concepts can be found in the baseline report [1]. All of these concepts have their own strengths and weaknesses. A trade-off was first performed, as elaborated on in Section 6.2 and in the midterm report [2]. The best-performing concept was carried to the final design phase.

The final concept layout that was chosen was the Winged Quadcopter. It consists of a fuselage with one wing and a tail. On both sides, tiltable propeller engines are installed on the front and aft sides of the wing. This allows the UAV to fly both like a quadcopter and like an airplane. In the initial design, the entire payload module could be taken out of the payload bay. However, it was decided to slightly adapt the mounting mechanism in the final design, such that individual segments of the payload can be taken out separately. This is explained in Section 12.3.

6.2 Trade-Off

The trade-off performed to determine which concept should be further developed in the the current final phase of the project will be presented here. This section is a summary of the trade-off process performed in the midterm report [2]. The trade criteria and their corresponding weights will be discussed in Section 6.2.1, followed by the actual trade-off in Section 6.2.2. Finally, the sensitivity analysis will be presented in Section 6.2.3.

6.2.1 Trade Criteria & Weights

The trade criteria have an important impact on the end results of the trade-off. Choosing a criterion which shows no difference in grade for the concepts will adversely impact the trade-off because it will average the results and decrease diversity. This diversity is what should be aimed for to see a distinct difference between the final grades of the concepts, so that the choice for the final concept will be clearer. The explanation of how each criterion affects each concept, and the score achieved by each concept can be found in the midterm report [2]. Each concept can score between 0 (bad) and 100 (good).

The first criterion is the performance of the concepts. This criterion has been chosen because there are a lot of requirements on the performance of the aircraft. For this criterion the following elements are examined: the mass, the geometric properties, the endurance, the range, and the power required of each concept. The next criterion is the manoeuvrability and stability where a sub-trade-off was performed using the manoeuvrability, stability, and control of each concept as criteria. Next, the concepts were analysed it terms of ground handling, taking into account how the concepts can be handled during pre- and post-flight procedures. The fourth criterion is the development risk. This criterion was not split into sub-criteria. It inspected the feasibility,

complexity and the available knowledge of the concepts, to assess the risk associated with the development phase. The next criterion is the production cost. This criterion is split into manufacturing costs, material costs, mechanisms costs, power and propulsion costs, and finally cost due to weight influence. This criterion has been chosen due to the set limit of 30k EUR for the production cost, limiting the design possibilities for the aircraft. The sustainability criterion is also taken into account and was split into a manufacturing and noise emission analysis. Finally, the reliability criterion took into account the reliability of the propulsion subsystem, the control surfaces, and the wing subsystem.

Assigning weights to the criteria influences the final grades of the trade-off. If a less significant criterion is weighed more than an important criterion, the results will be misleading and the final results might change drastically. Furthermore, it is possible to get biased weights when only one person is responsible for weighing the criteria. Therefore, each member of the team was tasked with filling out a form comparing each criterion to all the other ones. The averages of the weights for each criterion were taken. These averages were normalised to ten and converted into percentages to use for the trade-off.

6.2.2 Final Trade-Off

This section will present the results of the final trade-off, which can be seen in Table 6.1. The outcomes of the trade-off will be briefly discussed to get a grasp as to why the concepts scored as they did. Detailed explanation of the separate criteria scores are the result of extensive research on each criterion. The reasoning behind these scores can be found in the midterm report [2]. For clarity, the table contains colours to give an overview of the severity of the scores. Five colours have been used in a 30-15-10-15-30 spacing (Red, Orange, Yellow, Light Green, Dark Green). This spacing has been used to show more detail around the average than around the extremes. In the event that the table cannot be viewed in colour, each score has a superscript showing which category it scores: 1 = Red, 2 = Orange, 3 = Yellow, 4 = Light Green, 5 = Dark Green. The best performing concept according to the trade-off is the Winged Quadcopter as it scores best in all criteria.

Table 6.1: Final Trade-Off

Concept \ Criterion	Performance	M&S	Reliability	Production Cost	Development Risk	Sustainability	Ground Handling	Outcome
Tailsitter	50^{3}	46^{3}	50^{3}	50^{3}	75^{5}	84^{5}	59^{4}	**55^{3}**
Tandem	17^{1}	41^{2}	43^{2}	35^{2}	35^{2}	25^{1}	38^{2}	**33^{2}**
Prandtl Box	67^{4}	41^{2}	68^{4}	50^{3}	70^{4}	58^{4}	54^{3}	**58^{4}**
Tiltrotor	17^{1}	73^{5}	66^{4}	25^{1}	45^{2}	17^{1}	51^{3}	**42^{2}**
Winged Quad.	83^{5}	85^{5}	84^{5}	55^{3}	95^{5}	84^{5}	82^{5}	**81^{5}**
Weight	24	22	16	14	11	8	5	

6.2.3 Sensitivity Analysis

The goal of the sensitivity analysis is to determine to what extent the final concept selection depends on a change in the weighting of the trade criteria. It alerts whether the chosen concept greatly outperforms all other concepts in one area whilst being poor in the remaining areas. Therefore it is desirable that during the sensitivity analysis the ranking of the concepts do not change. More so, the concept performing best initially, should remain ranked highest at the end of the analysis.

The sensitivity analysis is carried out by successively increasing the weighting of one of the trade criteria, and recalculating the relative score between the concepts. In order to ensure that the analysis is somewhat reliable, the change in weighting should not be too small. An increase of 20% in the weighting of one criterion yields such results.

Figure 6.1 presents a comparison between the scores of the concept corresponding to the changed trade criteria weightings, starting with the original setup. The horizontal axis indicates the type of modified weighting used to achieve the corresponding scores of the concepts. These are the original (normal) weighting and weightings with one criteria increased by 20%. The score of each concept is shown on the vertical axis.

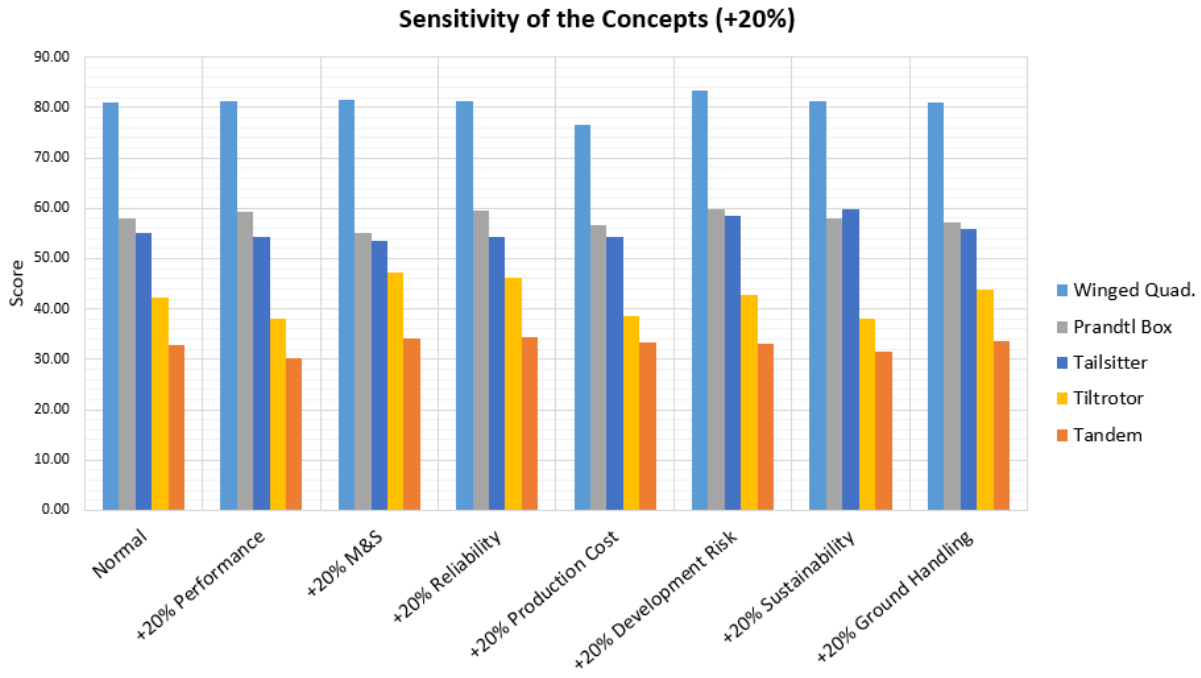

Figure 6.1: Sensitivity Analysis of the Final Trade-Off

The figure shows that even though the weights of the criteria are changed, The Wing Quadcopter scores highest every time. The gap between the first best and second best does not decrease drastically during the sensitivity analysis, showing that the weighting will not influence the end results. The overall rankings of the concepts also remain unchanged everywhere except when sustainability is weighted 20% more, this is because the Tailsitter scores 26 higher than the Prandtl Box for that criterion.

Since the Winged Quadcopter greatly outperforms all other concepts throughout the entire sensitivity analysis, it is safe to say that this concept has the greatest potential to satisfy all requirements. Therefore it is sensible to further develop this concept into the preliminary design phase.

6.3 Concept Risk Analysis

Having selected the Winged Quadcopter configuration, it is possible to asses the potential dangers of not meeting the requirements with this concept. These risks are then mitigated, to ensure the concept can be developed as intended.

Not all requirements are investigated here. Some were deemed not relevant enough for the risk analysis, while others were found to be met naturally. Further explanation of these choices can be found in the midterm report [2]. Only the crucial requirements posing a risk larger than 4, and the ones that have changed since the preliminary design phase, are elaborated on here. This can be seen in Table 6.2, where the likelihood of occurrence (L) and impact (I) are marked between 1 (impossible, negligible respectively) and 4 (very likely, catastrophic respectively). The product of these forms the risk (R). All requirement codes can be found in Section 5.2. After investigating the risks, they are mapped in Table 6.3; here the SYS- proposition was left out for clarity. Mitigation measures have been taken for all the requirements with a risk score of 4 and higher. These can also be found in Table 6.2, where L, I and R have the same meaning, but now applied to the mitigated risk.

Table 6.2: Overview of Applicable Technical Risks and Mitigation Measures

Requirement	**Impact and likeliness explanation**	**L**	**I**	**R**
SYS-PH-1.1	The wingspan is 2.92 m, which means it can not fit in a van as a whole. However, it is possible to dismantle the wings, which solves the problem.	1	3	3
SYS-PF-1.1	The 10 kg requirement can be met, however, when maximum range or endurance is desired, part of this payload should consist of batteries.	2	2	4
SYS-PF-1.2	When the UAV does not reach a maximum velocity of 200 km/h it will perform less in missions where endurance is the driving factor.	3	2	6
SYS-PF-1.3R	Since the payload can carry extra batteries, it will be possible to meet this requirement.	1	3	3
SYS-PF-2.3	Hovering is one of the most power-intensive flight phases, and therefore this severely reduces the endurance.	2	3	6
Requirement	**Mitigation measure**	**L**	**I**	**R**
SYS-PF-1.2	When the maximum velocity that is *designed* for is 200 km/h, the maximum attainable velocity will still be very high. Therefore, the impact is decreased.	3	1	3
SYS-PF-2.3	The payload mounting mechanism will be designed such that the UAV is able to release it within one minute. Therefore less hovering time is required.	2	1	2

Table 6.3: Risk Map of the Winged Quadcopter Before Mitigation

	(Almost) impossible	Improbable	Probable	Very likely
Catastrophic				
Critical	PH-1.1, PF-1.3R	PF-2.3		
Marginal		PF-1.1	PF-1.2	
Negligible				

7 System Description

In this chapter, the system will be described in greater detail by breaking it down into subsystems. In Section 7.1 these subsystems are defined and the elements they are comprised of, are identified. Section 7.2 deals with the interrelations between the individual subsystems on design level; this is illustrated by means of an N^2 chart. Section 7.3 states the subsystem requirements and constraints, which create the design space in which the designing has to be performed. Section 7.4 describes the mass, cost and power budgets; the total budget is broken down and divided among the different subsystems. Since there is still an aspect of uncertainty at this stage of the design process, contingencies are incorporated in the budgets.

7.1 Subsystem Definition

Subsystems are groups of elements within a system which have a physical or functional commonality. Systems are divided into these groups in order to have a better overview of both the functionality and the design process, making the system more approachable. The latter is especially valuable when working on larger projects such as the UAV system at hand. Therefore, it is sensible to split this system into subsystems. The subsystems and the respective responsible engineering departments are explained below, whilst the elements contained within each subsystem are listed in Table 7.1.

Structure: fuselage, wing and tail Primarily, the main structural subsystems are addressed; the fuselage, the wing and the tail section. The fuselage is regarded as the main subsystem. The attachments with the wing and the tail are regarded as 'fuselage' responsibility.

The first allocated department is the aerodynamics, due to the influence these subsystems have on the aerodynamic characteristics of the UAV. Next, the structures department is involved because the fuselage, wing and tail form the main structural framework and thus they must provide the structural integrity to the UAV. Furthermore, the stability and control department gets involved mainly in the design of the tail and wing.

Propulsion unit Next to the main structural aspect, the propulsion is regarded as an individual subsystem; both physically and functionally. Physically it is developed and assembled separately, due to its external mounting. Furthermore, there are several top level requirement related to the VTOL capability and the high speed performance that are specific to the propulsion unit. Thus, functionally speaking, the propulsion subsystem is regarded a separate subsystem.

The propulsion subsystem includes the pylon, which forms the interface with the wing. This is regarded as a structural aspect. That is why the structural department is consulted in the development of the propulsion subsystem. Furthermore, there are several factors related to aerodynamics as well; not only the shape of the pylon, but also the feathered or folded propeller has strong affinity with the aerodynamics department. The propeller design itself is treated by the power and propulsion department. Finally, the control and stability department will be involved, since stability and control is significantly related to the propulsion system, especially in vertical take-off and hovering.

Power The power management and distribution on board of the UAV is included in the power subsystem. The main reason is that the only power source for all the other subsystems is electrical, making the power subsystem an essential and significant element of the system. The power and propulsion department is the only department that will be involved in the design of the power subsystem.

Avionics and ground station Aviation related electronics that enable autonomous and manual remote control lead up to the avionics and ground station subsystems. These two systems are composed of enough elements to be individual subsystems.

The responsible department will be the Command and Data Handling, since this department specialises in the data collection and processing within the UAS.

Payload bay The payload bay subsystem needs to have a broad operational flexibility; there are several mission related requirement that result in a more complicated payload bay design. The resulting increased effort required for the design is so substantial, that it justifies the choice of making the payload bay a separate subsystem.

The structures department is one of the involved parties, both for the implementation in the fuselage and for the payload hatches which enable drop-off mission. Besides structures, command and data handling will be involved to design the interface between the payload and the communication system. Also the interface with the power subsystem has to be considered. In some mission settings, the payload bay will be used to extent the battery capacity. That is why there is a connection with the power and propulsion department.

Table 7.1: Elements Incorporated within Subsystems

Subsystems	**Elements**	
Fuselage	Internal layout	Attachment fuselage - wing
	Structure	Attachment fuselage - tail
	Payload bay integration	Battery mounting
Wing	Control surface	Structure
	Actuator	Landing gear
	High lift device	Attachment wing - propulsion unit
	Wingtip devices	
Tail	Structure	Actuator
	Control surface	
Propulsion unit	Motor	Storing/feathering mode
	Propellers	Motor controller
	Tilting mechanism	Pylon structure
Power unit	Battery unit	Electrical elements
	Cable harness	
Avionics	Flight Control Module	Communication system
	Sensors	Autopilot
	Navigation system	Safety system
Payload	Payload mounting	Data transmission
	Payload hatch	Power connector
Ground station	CPU	Controller (input device)
	Display (visual interface)	Casing
	Communication system	Power supply
	Maintenance unit	Antenna tracking system

7.2 Subsystem Interrelations

Although the definition of the subsystems gives a general overview of the design process, it is not sufficient to be useful during the design process itself. To solve this problem, it is necessary to define the relations between the subsystems in the form of an N^2 chart. This makes it possible to determine which subsystems are most complex and allows to plan a strategy in order to prevent any setbacks. In addition, it shows which subsystems are highly dependent on each other. Both of these features of the N^2 chart hint which subsystems should be designed first and which subsystems will be subject to larger changes at later design stages. Finally, the N^2 chart informs all the departments working on each of the subsystems about what information they need to supply to the other subsystems, resulting in a smoother design process.

The relations between the different subsystems in the design process of the Unmanned Aerial System (UAS) are shown in the N^2 chart found on the next page. This chart should be interpreted clockwise; the outputs of the blocks are shown horizontally, the inputs are shown vertically. In the diagonal, the subsystems are shown with the corresponding responsible departments underneath.

As the fuselage is the main framework of the UAV, it has a substantial number of inputs. First, there are the general inputs: the subsystem masses, locations, forces and moments introduced by other subsystems. These are needed for the structural aspect of the interfaces between the fuselage and the other subsystems. For stability purposes also the masses, locations of components and c.g. positions are needed. Furthermore, the aerodynamic centres' positions and lift magnitudes of the wing and tail are needed.

The wing can be, for the most part, designed independently from the rest of the UAV. Although it greatly depends on the masses of the other subsystems, the design is only influenced by the overall mass, not single contributions. The wing design is also influenced by the fuselage, yet to a much lesser extent since this subsystem only defines the design of the connection points on the wing. Therefore those areas will require design inputs such as the wing configuration (high, mid, or low wing). The only major influence on the design of the wing is the propulsion subsystem. Apart from the engine mount (pylon) geometry which influences the connection points, the forces and moments introduced by the propulsion units, as well as the motor configuration (pusher or puller) greatly impact the structural and aerodynamic design of the wing.

The inputs to the tail subsystem mostly consist of the aerodynamic interference-related parameters of the wing and propeller with the tail (wash) and c.g. location. Since the tail has to provide stability and controllability, some control and stability related parameters are input to the tail design as well.

The propulsion subsystem is critical to the VTOL stability and controllability, therefore its inputs relate to the disposition of the engine mounts on the wing, and the c.g. of the aircraft.

The power subsystem needs to provide sufficient power to overcome drag and (in the case of VTOL) the weight. That is why there is a relation between the drag generated by different subsystems and the power system. For the weight input, the overall mass is used (similarly to the mass input for the wing). Furthermore, the power consumption of the avionics and payload is influencing the power system and therefore it is also part of the inputs.

The payload bay requires outputs from the fuselage such that it is possible to integrate it inside the fuselage structure. In addition, several missions require the payload to send data to the ground station. Therefore this subsystem needs outputs from the avionics subsystem, ensuring a compatible communication, and outputs from the power subsystem in order to be able to power the payload equipment.

Finally, the ground station is only directly related to the avionics subsystem. The input from the avionics are the signal related parameters, such as the signal strength. Vice versa, avionics is also just linked directly to the ground station, meaning that the inputs to the avionics will also be signal related parameters.

Fuselage A, S, CNS	A,S, CNS: Wing Location on fuselage	A: Fuselage tail shape CNS: c.g. position fuselage	CNS: Fuselage c.g. PNP: Zero lift drag coefficient		-	S: Available volume Available mass	-
A: Wing root Chord S: Wing inner structure geometry Wing geometry (fairing) Forces and moments CNS: c.g. position Wing mass	**Wing** A, S, CNS	A: Wing location Wing configuration Wing stall angle CNS: Wing aerodynamic center Wing CL-α	CNS: Wing c.g. PNP: Wing configuration Wing location Zero lift drag coefficient Surface area Aspect ratio Oswald factor		-	-	-
A: Tail configuration/geometry Vert. stabiliser root chord S: Tail inner struc. geometry Tail weight Forces and moments CNS: c.g. of Tail Aerodynamic center Tail mass and arm	-	**Tail** A, S, CNS	CNS: Tail c.g. PNP: Zero lift drag coefficient		-	-	-
PNP: Max thrust single engine Engine locations	A: Pylon geometry Pylon location Motor configuration S: Pylon geometry Pylon location Forces and moments CNS: c.g. propulsion sub-system	-	**Propulsion** PNP, S, CNS	PNP: Required power	-	-	-
PNP: Number of batteries Battery masses Battery dimensions CNS: Required c.g. batteries	-	-	PNP: Power harness CNS: Power c.g	**Power** PNP		PNP: Power harness	-
CDH: Sensor masses Sensor dimensions Sensor location constraints Electrical cabling CNS: Avionics c.g	CDH: Pitot tube placement Electrical cabling	-	CNS: Avionics c.g	PNP: Power consumption Avionics locations CDH: Power consumption	**Avionics** CDH	CDH: Data transmission type	CDH: Data protocol Data type Data rate Antenna type Uplink/Downlink frequency
S: Payload bay geometry Door mechanism CNS: c.g + corresponding mass	-	-	CNS: Payload c.g.	-	CDH: Data output strength	**Payload** S, CDH, PNP	-
-	-	-	-	-	CDH: Coding/Encryption Maximum data rate Uplink/Downlink frequency Ground station software	-	**Ground Station** CDH

7.3 Subsystem Requirements

The subsystem requirements are presented in this section and are ranked per subsystem. The legend can be found in Table 7.2.

Table 7.2: Requirements Coding Legend

Requirement Code	Related to
SUB	**Sub**system
AV	**Av**ionics
PR	**Pr**opulsion
PW	**Pow**er
W	**W**ing
T	**T**ail
F	**F**uselage
P	**P**ayload
GS	**G**round **S**tation

Avionics Requirements

SUB-AV-1.2: The avionics subsystem shall be insulated to withstand temperatures of -30 to 40 degrees.

SUB-AV-2.1: The avionics subsystem shall have a database of restricted geographical areas where it is not allowed to fly.

SUB-AV-2.2: The avionics subsystem shall be able to update the restricted areas database.

SUB-AV-2.3: The avionics subsystem shall be able to determine its position with an accuracy of at least 5 m.

SUB-AV-2.5: The avionics subsystem shall be able to determine its attitude at an accuracy of at least 0.5 degrees per axis.

SUB-AV-2.7: The avionics subsystem shall be able to get updates on weather forecasts.

SUB-AV-2.8: The avionics subsystem shall be able to return the UAV to the base autonomously in case the data link to the ground station is lost for more than 10 sec.

SUB-AV-3.1: The avionics subsystem shall be able to trigger obstacle avoidance manoeuvres.

SUB-AV-3.2: The avionics subsystem shall be able to detect objects, larger than 1 m^2, within 3 km in front of it.

SUB-AV-4.1: The UAV shall be able to fly autonomously.

SUB-AV-4.2: The avionics subsystem shall be able to autonomously detect a suitable landing spot.

SUB-AV-4.3: The UAV shall be able to take-off autonomously.

SUB-AV-4.4: The UAV shall be able to land autonomously.

SUB-AV-5.2: The UAV shall be able to automatically descend to 110 m when reaching a height of 130 m.

SUB-AV-6.1: The avionics subsystem shall provide an electrical connection to the payload module.

SUB-AV-6.2: The avionics subsystem shall provide a data connection to the payload module.

SUB-AV-7.1: The avionics subsystem shall make use of a fly-by-wire system.

SUB-AV-8.2: The avionics subsystem shall be able to receive inputs from the ground station within a distance of 200 km from the ground station.

SUB-AV-8.3: The avionics subsystem shall be able to transmit data to the ground station within a distance of 200 km from the ground station.

SUB-AV-8.4: The data sent by the UAV shall be integrous and authenticated.

SUB-AV-9.1: The avionics subsystem shall provide throttle control for motors.

SUB-AV-9.2: The avionics subsystem shall control the orientation of motors.

Propulsion Requirements

SUB-PR-2.2: The propulsion subsystem shall provide thrust in vertical and horizontal flight.

SUB-PR-2.4: The propulsion subsystem shall be capable of providing a thrust of 392 N.

SUB-PR-2.5: The propulsion subsystem shall be capable of sustaining a flight velocity of 200 km/h.

SUB-PR-3.4: The propulsion subsystem shall be able to provide an angular acceleration of 0.8 rad/s^2 in roll.

SUB-PR-3.5: The propulsion subsystem shall be able to provide an angular pitching acceleration of 0.8 rad/s^2.

SUB-PR-3.6: The propulsion subsystem shall be able to provide an angular acceleration of 0.1 rad/s^2 in yaw.

SUB-PR-5.1: The propulsion subsystem shall have a maximum noise emission of 68 dB.

Power Requirements

SUB-PW-1.2: The power subsystem shall have a nominal capacity of minimum 3 kWh.

SUB-PW-1.3: The power subsystem shall provide a voltage of 37 V.

SUB-PW-1.4: The battery shall be detachable.

Wing Requirements

SUB-W-2.1: The wing shall provide a minimum lift of 245.25 N in horizontal flight.

SUB-W-2.2: The wing shall have a maximum stall velocity of 20 m/s.

SUB-W-2.3: The wing tip shall not stall first.

SUB-W-2.4: The wing shall have a maximum span of 4.8 meters.

SUB-W-2.5: The wing shall have a maximum cantilever ratio of 25.

SUB-W-3.1: The wing shall provide sufficient space for its internal components.

SUB-W-3.2: The wing shall provide mounting points for the engine pylons.

SUB-W-3.4: The wing shall protect its internal components from dust particles.

SUB-W-3.5: The wing shall protect its internal components from precipitation.

SUB-W-3.9: The wing shall have a maximum wing tip deflection of 15% of the wing span.

SUB-W-3.10: The wing shall have a maximum wing tip twist angle of 2°.

SUB-W-3.11: The wing shall be designed for a load safety factor of 1.5.

SUB-W-3.14: It shall be possible to detach the wing from the fuselage by one person within 2 minutes.

SUB-W-3.16: The wing shall not experience aeroelastic flutter at velocities below 220 km/h.

SUB-W-5.6: The engine pylons shall not experience aeroelastic flutter at velocities below 220 km/h.

SUB-W-7.2: The wing airfoil shall start stalling at the leading edge.

SUB-W-7.3: The wing subsystem shall provide a minimal angular roll acceleration of 45 deg/s^2.

Tail Requirements

SUB-T-1.1: The tail shall not experience deep stall conditions.

SUB-T-1.2: The tail shall stall after the wing.

SUB-T-2.1: The tail shall provide a longitudinal balancing moment for all flight velocities.

SUB-T-2.2: The tail shall be able to provide an angular pitch acceleration of 45 deg/s^2 in horizontal flight.

SUB-T-2.3: The tail shall be able to provide an angular yaw acceleration of 6 deg/s^2 in horizontal flight.

SUB-T-3.1: The tail shall provide sufficient internal space for relevant components.

SUB-T-3.2: The tail shall protect internal components from wind.

SUB-T-3.3: The tail shall protect internal components from dust.

SUB-T-3.4: The tail shall protect internal components from precipitation.

SUB-T-3.5: The tail shall protect internal components from UV radiation.

SUB-T-4.1: The tail elevator shall have a maximum deflection angle of 28°.

SUB-T-4.2: The tail rudder shall have a maximum deflection angle of 25°.

SUB-T-5.1: The tail shall not contain materials posing a health or environmental threat.

Fuselage Requirements

SUB-F-1.1: The fuselage shall contain at least 1 kg of permanent batteries.

SUB-F-2.1: The fuselage shall protect internal components from wind.

SUB-F-2.2: The fuselage shall protect internal components from dust.

SUB-F-2.3: The fuselage shall protect internal components from precipitation.

SUB-F-2.4: The fuselage shall protect internal component from UV radiation.

SUB-F-3.1: The fuselage shall not fail when a belly landing of 4 m/s is performed.

SUB-F-4.1: The fuselage shall not contain materials that pose health or environmental threats.

Payload Requirements

SUB-P-2.1: The payload subsystem shall have a two-way power link with the fuselage.

SUB-P-2.2: The payload subsystem power link shall be rated for a minimum of 50 W.

SUB-P-3.3: The payload subsystem shall provide mounting points for the payload (including additional batteries).

SUB-P-3.4: The payload subsystem shall allow for payload release during flight.

Ground Station Requirements

SUB-GS-2.1: The ground station shall be able to process all data received by the UAV.

SUB-GS-3.2: The ground station battery shall enable at least two hours of continuous operation.

SUB-GS-4.1: The ground station shall transmit inputs to the UAV within a distance of 200 km.

SUB-GS-4.2: The ground station shall be able to receive data from the UAV within a distance of 200 km.

SUB-GS-4.3: The ground station shall send data towards the UAV securely.

SUB-GS-4.7: The ground station shall be able to communicate with the drone in stormy weather conditions.

SUB-GS-5.1: The ground station casing shall fit within 100x50x30 cm.

SUB-GS-5.2: The ground station shall weigh at most 7.5 kg.

SUB-GS-6.3: The ground station shall allow for direct control of the UAV.

SUB-GS-6.4: The ground station shall be able to make the UAV drop the payload.

SUB-GS-7.1: The ground station shall display a warning when exceeding a height of 140 m from the ground.

SUB-GS-7.2: The ground station shall display a warning when approaching a restricted area.

7.4 Budgets & Contingencies

To ensure that the departments do not exceed any limits during the designing, some budgets have been made. On top of the budgets a contingency is added. There are two budgets: the mass budget and the cost budget. The ground control is not considered in the budgets as it is seen as a separate system. The final budgets and contingencies for mass and cost can be found in Table 7.3.

Table 7.3: Mass and Cost Budget for the Aircraft

Subsystem	Mass Budget	Contingency	Cost Budget	Contingency
Power	8.0 kg	5%	800 EUR	5%
Propulsion	4.0 kg	5%	2200 EUR	10%
Avionics	1.0 kg	5%	2200 EUR	10%
Wing	3.5 kg	10%	800 EUR	10%
Tail	1.5 kg	10%	400 EUR	10%
Fuselage	2.5 kg	10%	800 EUR	10%
Payload	4.5 kg	5%	300 EUR	5%

Mass Budget The mass budget has been estimated by comparing it to a similar UAV, the Avy One[1]. This aircraft has a Manufacturing Empty Weight (MEW) of 13 kg, meaning that if this design has a maximum mass of 25 kg, 12 kg are allotted to the battery and payload. The other 13 kg are destined for the structure of the aircraft[2]. The mass budget can be seen in Table 7.3. To have an allowable margin of freedom, contingencies are put in place for each subsystem. The percentage of the contingency varies with the certainty of the mass budget. The contingency should decrease over time as the project progresses, and the mass prediction becomes more precision.

Cost Budget Analysing the cost budget has been done in a similar fashion as the mass budget. Contact has been established between Atmos, a company which produces the Marlyn[3], a Hybrid UAV. This company provided information about how much percent of the cost their subsystems take up of the unit production cost. Before budgeting the cost of each subsystem, the choice has been made to separate the cost of materials from the cost of manufacturing. The assumption has been made that 75% of the production costs are attributed to manufacturing. This leaves 7.5k EUR for the materials and purchase of the subsystems.

The Marlyn spent 10% of the cost on their payload subsystem, 20% on power & propulsion, 20% on the avionics and 40% on the wing, tail & fuselage combined. The remaining 10 % are used as contingency value[4]. With these values, it is possible to construct the cost budget. The Atmos UAV has its cameras added to the payload cost, which this design does not have. This means that a part of their payload cost can be neglected. Atmos has said that the avionics will take up a larger percentage of the total cost for this design since they have designed and built parts of the avionics by themselves. The wing and fuselage turn out to cost the same amount, while the tail costs half of the wing [6]. Using the preliminary energy calculation from the midterm report [2], the cost of the power subsystem is estimated to be 800 EUR. The rest of the cost is attributed to the propulsion subsystem, which turns out to be close to 20% as estimated by Atmos. The final cost budget can be seen in Table 7.3.

[1] `avy.eu`, Accessed on 21-06-2017
[2] Private Contact Avy, 22-05-2017
[3] `http://www.atmosuav.com/`, Accessed on 22-06-2017
[4] Private Contact Atmos, 08-06-2017

8 Power & Propulsion

This chapter describes the design process of both the propulsion unit and the power subsystem. In Section 8.1, the design approach is discussed, followed, in Section 8.2, by the used assumptions. In Section 8.3, the complete analysis is documented and the result of the design process is discussed. Finally, in Section 8.4 the validation & verification process is described.

8.1 Design Approach

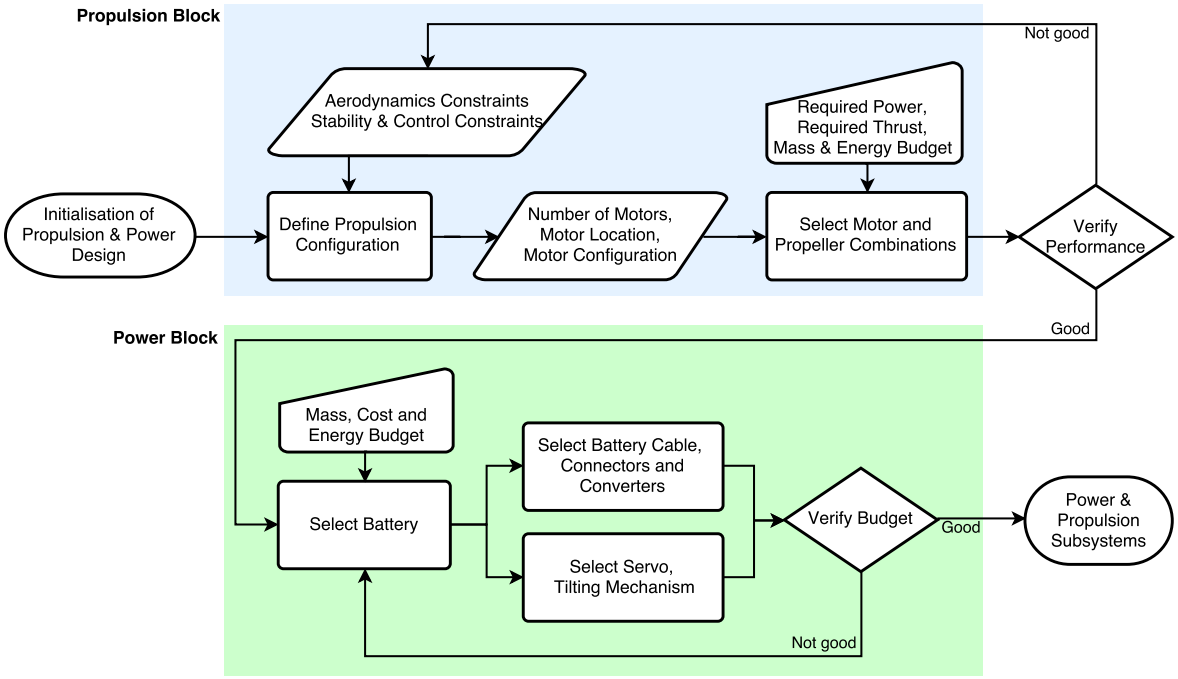

Figure 8.1: Work Flow Diagram for Power & Propulsion Design

Figure 8.1 shows the work flow diagram for the power & propulsion design process. It includes the systematic approach and selection of the motor with propellers and power source with power distribution system based on a series of calculations. The propulsion block indicates the design process of a propulsion unit. With aerodynamics and stability & control constraints, a series of propulsion configurations can be defined. The number of motors, motor location and motor configuration can be obtained as an output, which is used as an input for selecting a motor and propeller combination. Along with the input parameters, performance parameters such as required power, required thrust and mass & energy budget are considered. A verification loop is performed afterwards to check if a chosen motor and propeller combination as well as a configuration is feasible based on other departments' judgements. For example, a certain combination and a configuration are passed to the stability & control department to determine effects of the configuration. If it creates conflicts with a certain department and budgets, the department can provide the power & propulsion group with suggestions such that a new propulsion configuration can be generated. If it is deemed feasible, the combination and configuration can be processed and relevant information is used for a battery selection process. The power block indicates the design process of a power unit. Motor specifications such as power, voltage and current are used as an input for a battery selection process. The energy budget of other systems is taken into account, as the battery has to provide enough power for them. After a

battery is chosen, battery-related components such as battery cables, connectors and converters are chosen based on battery specifications. Servos and tilting mechanism are selected simultaneously, as it is independent from the battery selection process. Budgets are verified to see if the chosen power unit meets budgets and requirements. After the verification loop, a complete power & propulsion subsystem is obtained.

8.1.1 Propulsion Unit Design Approach

The first step in the propulsion unit design block is defining a propulsion configuration which consists of the number of motors and their mounting location. A motor quantity analysis from three to five motors is carried out and different motor mounting systems are assessed. Limiting the analysis to just three to five motors is explained as follows: a quantity of three motors was the bare minimum in order to still have a stable vehicle. Having two motors would require a configuration change to a tilt rotor or tilt wing concept. A quantity of five motors was investigated in order to determine whether it is more efficient than four motors. Since five was not possible due to budgetary constraints, a configuration of six or more motors was left out.

As the number of motors and corresponding location are chosen, off-the-shelf motors are selected. Requirement SYS-VS-3 states that the UAV shall have electrical propulsion. Although the propulsion type is constrained to be electric, a motor type still has to be determined. Two choices for a motor type are brushed and brushless. Advantages and disadvantages of each motor type are used to perform a qualitative analysis for choosing a certain motor type.

As the number of motors, motor type and location are determined, propellers can be selected. Finding a right motor and propeller combination requires a trial and error process and iterations, since a powerful motor with an arbitrary propeller does not necessarily meet desired performance requirements for VTOL and horizontal flight. Motor and propeller specifications are taken from a Hacker data set [7].

Step 1: The high-velocity requirement SYS-PF-1.2 is a driving requirement. The most important design aspect to attain the high velocity of 200 km/h is the propeller design. Generally, a high-pitched propeller is required for high velocity.

Step 2: After constraining the aft-propeller pitch, a propeller diameter and aft motors can be chosen. Since both the propeller diameter in combination with the after motors need to be determined, one way approach cannot be applied. There are more design parameters than the number of design constraints. An iterative approach and a Static Thrust Calculator (STC) is used to find a right combination of a propeller diameter and aft motors. The team had consulted ATMOS and received advice that motors from Hacker-motors could be considered as Hacker-motors is a prominent motor manufacturer specialised in brushless motors. After a series of iterations, the right aft motor-propeller combination is found.

For this step, a required thrust value is an input. The motors should provide sufficient thrust to overcome drag at the maximum velocity, which results in the highest drag. During the horizontal flight phase, only aft motors are operational, while the propellers on the front motors are folded in a feathering mode to minimise drag. To calculate the required thrust and power for maximum velocity cruise flight, a PDC tool is used.

Step 3: After constraining the complete aft motor-propeller combination, the VTOL performance is analysed. Since the aft motor is optimised for horizontal flight, its performance is relatively poor in VTOL. Knowing VTOL capabilities of the aft motor allows the required front motor VTOL performance to be computed. This front motor-propeller combination is to be optimised for VTOL; it means that a different motor category is considered. The required forward performance parameters such as required thrust are found by using a Python VTOL

Thrust Calculator. By means of trial and error along with an iterative approach, a suitable front motor-propeller combination is selected.

8.1.2 Power Subsystem Design Approach

The power subsystem requires motor specifications and power budget of other subsystems. Unlike the propulsion subsystem design approach, the power subsystem design approach does not require intensive iterative processes. The battery is primarily sized based on extreme flight scenarios and essential flight phases, which are shown in the following list.

- Extreme flight scenarios
  - Max. speed horizontal flight
  - Max. range horizontal flight
  - Max. endurance horizontal flight
- Essential flight phases
  1. VTOL
  2. Hovering

The other subsystems such as avionics and payload draw power from the battery, and the battery sizing increases further based on their energy budget.

As flight phases and other subsystems are considered for the battery sizing, the method for calculating a required battery capacity needs to defined. The Python Drag Calculator (PDC) determines a required battery capacity of extreme flight conditions by calculating the required power per scenario then converting it to the battery capacity in [mAh]. The most extreme flight scenario is identified as well as two essential flight phases and power usage of other subsystems for the final battery sizing.

8.2 Assumptions

This section contains the made assumptions in the design process of both the propulsion and the power subsystem and the effect on them.

General simplifications:

- Power used by servos are minimal, thus negligible.
- The relation between battery capacity and range is linear, due to the fact that power consumed during horizontal flight is approximately constant.

Hardware related:

- Chosen servos are waterproof, by means of an internal waterproof construction or an external protective casing.
- Propellers do not have to be designed completely, as only off-the-shelf components components will be considered.
- Motors are chosen from off-the-shelf motors, from a data sheet of the manufacturer Hacker-motors.
- Back propellers can be used as pusher propellers, regardless of availability of pusher propellers for right dimensions.

Efficiency related:

- Front motor efficiency is 90%.
- Aft motor efficiency is 95%
- Calculations are done for optimally-performing propellers.

Motor efficiency was not provided by the manufacturer. By means of a efficiency calculator, the order of magnitude of the motor was estimated and included as an assumption. Because no exotic propeller configurations (such as propeller wash phenomena due to aligned propellers) are applied, and the propeller used for this UAV is an of-the-shelf component, no further research was done for propeller efficiency.

Flight condition related:

- Operational temperature is 15 degrees Celsius.
- Air density at operational altitude is equal to sea level density, which is 1.225 kg/m^3

8.3 Analysis

This section contains the analysis of a motor configuration and a motor type. Then tools used are elaborated; the required inputs and outputs, theoretical background and equations are stated.

8.3.1 Motor and Propellers

Motor configuration Different number of motors with corresponding locations are analysed. The different locations are leading-edge mounted, wing-mounted quadcopter setting and body-mounted. The number of motors varies from three to five. The analysed configurations can be seen in Figure 8.2.

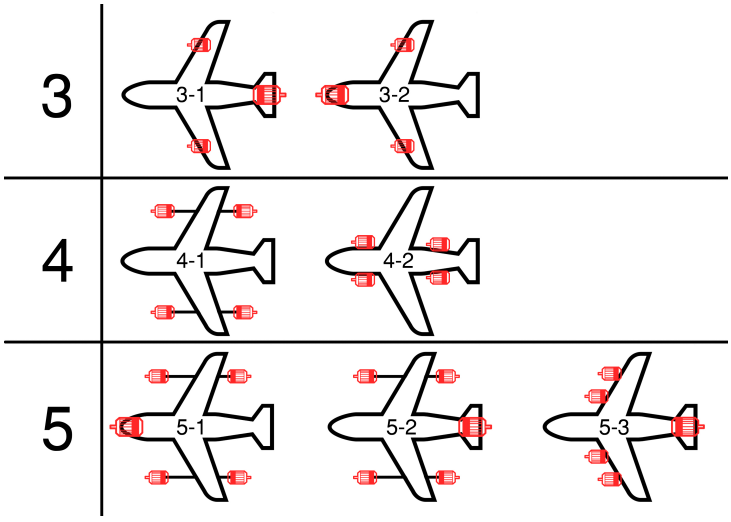

Figure 8.2: Overview of Different Motor Configurations

- **Three motors:** Consultation with the stability & control department resulted in a conclusion that three-motor configurations (3-1 and 3-2) shall not be considered, since they do not generate sufficient controllability in VTOL operations.

- **Four motors:** Based on calculations, four-motor configurations turned out to be sufficient to meet both the required thrust and power output in VTOL and high-velocity cruise. Consultation with the stability & control department resulted in a conclusion that a quadcopter setting (4-1) is advantageous over a body-mounted configuration (4-2), since a greater moment arm increases effectiveness of motors for VTOL stability.
- **Five motors:** Five-motor configurations (5-1, 5-2 and 5-3) were regarded as a solution to problems with propeller designing, however, the fifth motor solely dedicated for horizontal flight would allow the total cost and mass budget to easily exceed its limits.

Motor types There are two kinds of motors: brushed and brushless motors. Both types have advantages and disadvantages: brushed motors have relative lower efficiency but are cheaper to produce than brushless motors. Table 8.1 shows a qualitative trade-off between the two type of motors. The superior option is indicated and the result is explained in the note column.

The major criteria are performance efficiency and cost. The capability to operate with high velocity is also important, since it is linked to the top-level performance requirement of max horizontal flight velocity of 200 km/h. Because of requirement SYS-PH-2.2 and SYS-OP-2.2 related to noise emissions and reliability respectively, these aspects are also taken into account. Furthermore, due to the broad range of missions and operational conditions, the environmental resistance is also evaluated as a criterion.

Table 8.1: Brushed vs. Brushless Motor Analysis

	Brushed	Brushless	Note
Efficiency		✓	Brushed ranges from 75% - 80% in contrast to brushless, which ranges from 85% - 90%[1].
Cost	✓		Brushed motors have lower cost due to simplicity and established production techniques [8].
Velocity		✓	Brushless motors typically generate higher angular velocity and torque, meaning it can operate with the higher-pitch propeller. The combination of a high pitch and RPM enable higher velocity for the brushless motor [9].
Reliability		✓	Brushless motors have less parts that can potentially break or wear-out[2].
robustness	✓		Due to the simplicity of brushed motors, they can handle more hostile environmental conditions towards electronics and motor components [9].
Noise Emission		✓	Brushless motors emit less noise due to complete enclosure of internal components[3].

A brushed motor has two main advantages: the lower cost and better environmental resistance. However, the rest of the criteria show that the brushed motor performs worse than a brushless motor, especially in the performance-related criteria. The cost increase can be compensated by the budget and the environmental resistance can be drastically improved by the motor pylon. Thus, a brushless motor type is chosen for the Hybrid UAV design. Upon recommendation of ATMOS, the catalogue of Hacker-motors[4] is chosen for getting necessary components.

[4] `https://www.hacker-motor-shop.com/`, Accessed 19-06-2017

8.3.2 Utilised Tool Collection

Static Thrust Calculator The main tool used to find the right motor-propeller combination optimised for horizontal cruise flight is STC.[5] The steps in the design approach in which this tool was utilised can be found in Section 8.1. The STC tool uses the propeller parameters (propeller pitch, diameter and type), RPM generated and the operational altitude as inputs. The provided thrust, required power and estimated operational speed are given as outputs.

By using STC, required power and RPM output for a motor with a certain propeller diameter can be checked. Since there are more design parameters than constraints, an iterative process has to be initiated. Combinations of different propellers and motors with correct specifications have to be found. Using the Hacker-motors data set[7], an optimal motor-propeller combination is found.

Python Drag Calculator To determine how much thrust the horizontal-flight optimised motor needs to produce, the drag in horizontal flight is computed. For that the PDC and Equation 8.1 are utilised. The equation is derived by replacing C_L with the weight (W) divided by the dynamic pressure (q) and wing surface (S)[6]. As the drag calculation is complete, it is processed into the P_{req} and required battery specifications. The P_{req} for maximum velocity operations is derived by multiplying the drag at maximum airspeed by that airspeed. The P_{req} can be found in Equation 8.2. The values of the wing surface, aspect ratio, Oswald factor and C_{D_0} are inputs provided by the aerodynamics department. The weight is taken from the mass budget and the corresponding requirement SYS-PH-2, which states that the maximum MTOW shall be 25 kg.

$$T_{req} = D = C_D qS = (C_{D_0} + \frac{C_L^2}{\pi ARe})qS = C_{D_0} qS + \frac{\frac{W^2}{qS}}{\pi ARe} \tag{8.1}$$

$$P_{req} = DV = (C_{D_0} + \frac{C_L^2}{\pi ARe})qSV = \frac{1}{2}\rho V^3 S C_{D_0} + \frac{\frac{W^2}{\frac{1}{2}\rho VS}}{\pi ARe} \tag{8.2}$$

Python VTOL Thrust Calculator This tool computes the required thrust output in the VTOL mode as a function of the maximum power output of the motor and the propeller area. For the development of the tool, the conservation of momentum in helicopter climb/hover theory is used.[7] The equation for required thrust for hovering and climb is shown in Equation 8.3.

$$T_{req,max} \leqslant T_{max,out} = (2\rho A_{prop} P_{out,max}^2)^{\frac{1}{3}} \tag{8.3}$$

The required thrust value is provided by the stability & control department by means of a moment equilibrium analysis. The maximum required thrust values are computed by analysing the moment with the extreme c.g. positions. For instance, when the c.g is most aft, the aft motors have to provide significantly higher thrust levels than when the c.g. is most forward. This is because the effective moment arm decreases with the c.g. moving aft.

Furthermore, a margin has to be taken into account for the case of a motor having to stabilise the UAV from an incoming gust or for performing various manoeuvres. A factor of 1.5 of the thrust required to hover is sufficient to encompass the power splits required during the mission profile including for corrections required to counter disturbances.

[5] `http://www.godolloairport.hu/calc/strc_eng/index.htm`, Accessed 21-06-2017

[6] `http://nptel.ac.in/courses/101104007/Module2/Lec6.pdf`, Accessed 09-06-2017

[7] `http://s6.aeromech.usyd.edu.au/aerodynamics/index.php/sample-page/aircraft-performance/hoverclimbdescent-analysis/`, Accessed 19-06-2017

8.3.3 Propeller performance analysis

Within the motor-propeller design, several parameters have to be considered. To give an indication of the complexity of the cohesion between the parameters within the motor-propeller design process, a visual is shown in Figure 8.3. The black outlined columns in the figure are the two degrees of freedom. In the design process the propeller and motor with their corresponding parameters are selected. The difficulty however, is that the required output is in the form of the blue and red rows. It is the combination of parameters from both these two components that must meets the requirements. For instance, both the pitch (a propeller parameter) and the rotational speed (a motor parameter), determine whether of not the high-velocity requirement is met. So a right combination of motor-propeller is looked for. However, it is not just the high-velocity requirements. Also the thrust output, which is depending on both the propeller diameter and the motor power output, is a requirement where the motor-propeller selection should be optimised for. The two requirements both pose constrains on the selection process, but are also conflicting one another; optimising for requirement one, might be a very inefficient or even infeasible combination for requirement two. The difficulty is to find a motor-propeller selection that meets both the requirements in the optimal way.

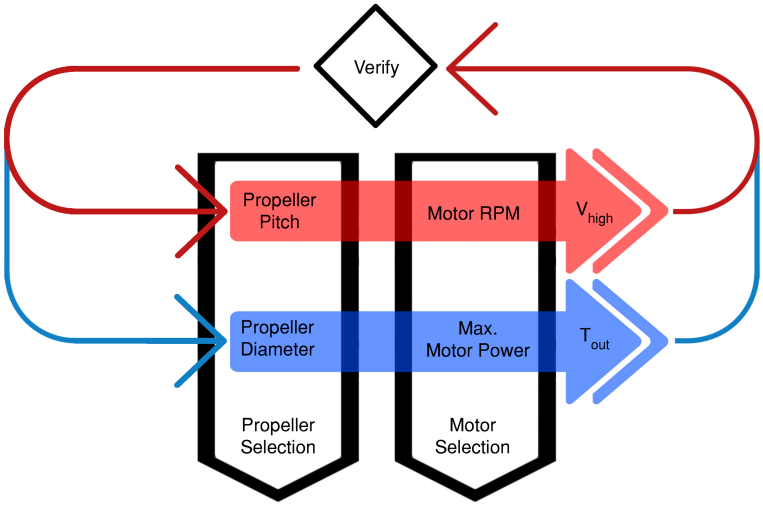

Figure 8.3: Parameter Relationship within Motor-propeller Design

The optimal motor-propeller selection is done by means of an iterative process. For different propeller and motor choices, the requirements are verified and fed back into the system. In this way, the design converges to the propeller and motor selection that is optimal for both performance requirements.

The performance of a propeller is very sensitive to operational conditions; propellers are designed for specific conditions such as flight speed and RPM inputs. As seen in Section 8.1, the first step in the design approach is related to the propeller design. The propeller design, especially the pitch, is highly significant to the operational airspeed at which the UAV can operate.

A propeller is essentially a wing in rotating motion and acts as a fixed wing, as a propeller also experiences stalling phenomena in certain flight conditions. In case a propeller pitch is high, the desired airspeed is also high; a high-pitched propeller has an increased risk of stalling at low airspeed. Figure 8.4[8] shows that a propeller with higher pitch will have an equal angle of attack as a lower pitched propeller if the flight velocity is higher.

Within the specifications list of a propeller, the pitch is often indicated in inches and not as an angle. The inch value is the distance that the propeller would travel during one revolution.

[8] `http://www.pilotwings.org/propellers.html`, Accessed 21-06-2017

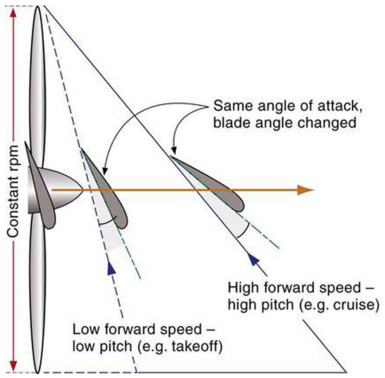

Figure 8.4: Theoretical Relation between Propeller Pitch and Flight Velocity

It means that the pitch together with the angular velocity with which it rotates determines the cruise velocity, as indicated in Equation 8.4.

$$V_{cruise} = \text{Pitch} \cdot \frac{\omega}{60} \tag{8.4}$$

This shows that differently pitched propellers (given a constant RPM) have their own 'preferred operational regime'. It means that the different operational phases should be addressed and analysed for the design. In this UAV design, the two critical flight phases are VTOL and high-velocity horizontal flight.

1. In case of the VTOL phase, the flow velocity is relatively low and the required thrust is high. The propeller that is optimised for VTOL will have a low pitch and a large diameter.
2. In case of high-velocity horizontal flight, lower thrust is required, but the flight velocities are significantly higher. This will result in a significantly higher required propeller pitch, with a low desired propeller diameter.

Since propellers only perform optimally in their specific operational regime, there is a challenge to perform hybrid operations with the same propellers. Propellers optimised for VTOL will perform poorly in horizontal flight and vice versa. Several solutions are considered to optimise the propulsion system for both VTOL and horizontal flight. By means of brainstorming and consulting experts in the field of propeller design, the following solutions are found to be worthy for further analysis.

Solution 1 Use four propellers purely for the VTOL operation and install a fifth motor as either a pusher or a puller configuration to sustain the horizontal cruise flight.

This solution is proven to be infeasible regarding both the mass and cost budget which are related to requirements SYS-PH-2 and SYS-C-1 respectively; a fifth motor for horizontal flight will increase the total cost and mass to an unacceptable extent. Also, not using four of the five motors during horizontal flight is regarded as highly inefficient; the VTOL phase is just a small fraction of the mission scenarios, and the four propellers will simply be inducing extra drag during the rest of the missions.

Solution 2 Equip all four motors with double propellers; one optimised for VTOL and the other for horizontal flight. During VTOL operations, the horizontal propellers are folded, and the VTOL propellers are folded during horizontal flight.

The double propeller solution is not feasible either, since the concept is still in an experimental phase. Double propellers introduce great complexity to the system; the rotating of an extra pair of propellers may cause difficulties in balancing the rotors. Furthermore, this foldable propeller system also increases the drag. For these reasons, this solution is regarded as infeasible.

Solution 3 Implement four similar propellers that are not optimised for specific operations; this means implement a kind of propeller that has both in VTOL and horizontal flight a moderate performance. To investigate the feasibility of this solution, further analysis is required. First, the 200 km/h cruise flight capability has to be ensured, which means, according to Equation 8.4 choosing a motor-propeller configuration with sufficient pitch and RPM output. Next to that, the propeller should have a sufficient diameter to generate enough thrust for VTOL operations. Equation 8.3 shows how the propeller diameter and thrust output relate.

For the horizontal high-velocity flight performance analysis the STC tool used. For the VTOL performance, the VTOL Thrust Calculator was utilised. By trial and error, it was concluded that there exist no motor that could provide enough power to operate a sufficiently pitched propeller with large diameter at high RPM[9]. If such a motor would exist, it would certainly exceed the cost and mass budget. Furthermore, if both the front and aft propellers operate at the same time in horizontal flight, another undesirable phenomena will occur; since the propellers are longitudinally aligned, a propeller wash is created by the front propellers affecting the aft propellers by decreasing their efficiency and thrust output [10].

Solution 4 Using only one pair of propellers for horizontal flight and providing the other pair of propellers with folding/feathering capability. The advantage of this solution is that there is no wash of the front propeller that influences the aft propeller, since the front propeller is folded in horizontal flight. The downside of this solution is that during VTOL, the front propellers have to compensate for the poor performing aft propellers; the aft are after all optimised for horizontal flight. This means that the front motor-propeller combination has to be optimised for VTOL and needs to provide a significant thrust output. This solution needs further analysis to see if motor-propeller combinations can be found that fit in the cost and mass budget and still meet the performance requirements; this is done in the next paragraph.

8.3.4 Propeller and Corresponding Motor Selection

First of all the required pitch was determined; the highest propeller pitch on the market was found to be approximately 14 inch. Due to limited time and resources, the choice was made not to go into the effort of designing the propellers, but instead to go with of-the-shelf propellers; a propeller of 14 inch pitch with 11 inch diameter was chosen (11x14). By rewriting Equation 8.4 and transforming the units to the metric system, a required rotational speed of 9380 RPM was obtained. The motor that is most optimal to fulfil the performance requirements is the A50-12L, which has a maximum rotational speed of 9429 RPM[10]. The next step was to verify that the motor specifications met the required values; this was done first for vertical operations and secondly for horizontal flight.

$$\omega = \frac{V_{cruise}}{\text{Pitch}} \cdot 60 = \frac{55.6}{14 \cdot 0.0254} \cdot 60 = 9380\text{RPM}$$

Vertical performance analysis aft motor unit For the vertical performance, the maximum power output of the selected A50-12L motor was used for the thrust calculation. As a side note, the motor can only provide the maximum power for a limited time; the manufacturer states in the specifications that after a certain time it will overheat. However, even if a reduced maximum power is taken to be 5%[11] less than the actual value, the thrust output is still sufficient, since it only decreases to a value of 80.4 N. Table 8.2 shows that the A50-12L motor can

[9] Motors from the Hackers-motor data set

[10] `https://www.hacker-motor-shop.com/Brushless-Motors/Glider-drives/Glider-10kg/A50-12-L-V4.htm?shop=hacker_e&SessionId=&a=article&ProdNr=15726840&p=7202`, Accessed 22-06-2017

[11] A five percent power reduction will prevent overheating, however, as stated in recommendations, thermal control is an aspect worthy of further considerations.

easily provide the 71.9 N of required thrust. There are two reasons for the difference in required and provided thrust; first, since the options in motor selection were limited by the consulted Hacker data catalogue, the most optimal choice can still contain some over-design'. Secondly, as redundancy an extra thrust of approximately 10 N was incorporated in the motor selection.

Table 8.2: Vertical Performance Analysis of A50-12L V4 Motor

	Value	**Used Tool**
T_{req} [N]	71.9	Moment equilibrium
$T_{max,out}$ [N]	84.6	Python VTOL Thrust Calculator
$T_{reduced,out}$ [N]	80.4	Python VTOL Thrust Calculator

Horizontal performance analysis aft motor unit In horizontal maximum velocity cruise flight the required thrust, which equals the drag, was calculated using the Python Drag Calculator. This turned out to be a total of 12.42 N per motor. The thrust provided by the motor-propeller combination was computed by the STC; that turned out to be approximately 4.5 N more per motor, clearly sufficient to compensate for the drag. Also the power required for the most critical operational phase (maximum velocity flight), that was computed by the Python Drag Calculator, turned out to be lower than the maximum power output of the selected motor. The result shown in Table 8.3, show as well that the A50-12L V4 is an good choice.

The high power output level seems an over design with respect to the required power (1381 Watts vs. 2009 Watts), however, this is not the case. Due to the fact that this motor-propeller combination is optimised for horizontal flight, it operates very inefficient in vertical operations. That is why the high power level is required to ensure VTOL capabilities. Table 8.2, the table indicating the A50-12L motor performance in vertical flight, shows that the maximum thrust (which is reached during maximum power output) is within the desired order of magnitude. The maximum power is thus not an over design, but something that compensates for the low efficiency of the propeller in vertical flight operations.

Table 8.3: Horizontal Performance Analysis of the A50-12L V4 Motor

	Value	**Used Tool**
$T_{req,max}$ [N]	12.42	Python Drag Calculator
$T_{out,max}$ [N]	16.97	Static Thrust Calculator
P_{req} (Max. speed) [W]	1381	Python Drag Calculator
P_{req} (Max. range) [W]	314	Python Drag Calculator
P_{req} (Max. endurance) [W]	260	Python Drag Calculator
$P_{out,max}$[W]	2009	Given specification

Vertical performance analysis front motor unit: Finally, the front motor-propeller combination has to be chosen, this motor is optimised for VTOL. This means it only performs vertical operations; no horizontal flight, since then the front propellers are in folded or feathering mode.

After some iterations, the chosen selection is the Q60-7M F3A motor. Just as with the aft motor, the aim was to have approximately 10 N more thrust output in vertical flight operations as redundancies to account for when example the efficiency turns out to be lower as expected[12]. Although Section 8.3.1 shows only the analysis of one motor-propeller combination, several

[12]Inaccurate efficiencies are a serious concern, that is also why a test with an experimental set-up is a future recommendation as stated in Chapter 17

combinations were analysed after all the entire approach was iterative. The A50-12L V4 motor with a 11x14 propeller proved to be optimal. That is why only the analysis of this engine unit is treated.

Table 8.4: Vertical Performance Analysis of Q60-7M Motor

	Value	**Used Tool**
T_{req} [N]	124.0	Moment equilibrium
$T_{max,out}$ [N]	135.6	Python VTOL Thrust Calculator
$T_{reduced,out}$ [N]	81.5	Python VTOL Thrust Calculator

Conclusion All the chosen components for the propulsion subsystems can be seen in Table 8.5. Besides all the product names, it also shows the unit mass and cost, based on this there can be concluded that the selection meets the budget constraints. The table shows a total mass for the propulsion subsystem of 2387 grams and a cost of 1953.70 EUR. These values meet the corresponding mass and cost budgets, which are 4000 grams and 2200 EUR, respectively. Further elaboration on the budgets can be found in Section 7.4.

Table 8.5: Off-the-shelf Component Selection propulsion unit Subsystems

Component	**Product Name**	**Q.**	**Unit Mass [g]**	**Unit Cost[€]**
Front Motor	Hacker Q60-7M (10S)	2	520	410
Front Propeller	AC Carbon 16x10	2	25	11.8
Front Speed Controller	MasterSPIN 99 Pro	2	105	229
Front spinner	Spinner RFM 40x6	2	n.a	30.9
Aft Motor	Hacker A50-12L (8S)	2	445	184
Aft Propeller	APC 11x14	2	40	3.50
Aft Speed Controller	X-70-SB	2	54	99.0
Aft spinner	Ae-spinner A/K 45	2	n.a	8.65
Total			2387	1950

8.3.5 Battery and Power Subsystem Components

The required power can be found using Equation 8.2. Velocity for each extreme flight scenario is defined based on the performance analysis in the midterm report [2]. Important parameters such as wing surface area, aspect ratio, Oswald factor and zero-lift drag coefficient are redetermined for the velocity calculation. The required power is divided by voltage to obtain current. With the determined current, Equation 8.5 is used to calculate the required battery capacity for each extreme flight scenario, which can be seen in Table 8.6. The maximum range flight scenario requires the highest battery capacity of 16100 mAh. The duration of the maximum speed flight is defined to be 15 minutes, as longer maximum speed flight puts high loads on motors and battery packs.

$$C_{req} = I \cdot \frac{t_{flight}}{60} \cdot 1000 \tag{8.5}$$

The essential flight phases are defined by requirements SYS-PF-2.3 and SYS-PF-2.4. Thus, the duration for hovering is 5 minutes while the duration for VTOL is 1 minute. In order to

Table 8.6: Battery Capactiy for Extreme Flight Scenarios

Flight Scenario	**V [m/s]**	t_{flight} **[min]**	**D [N]**	P_{req} **[W]**	$C_{req,efs}$ **[mAh]**
Max. speed	55.6	15	24.4	1360	9180
Max. range	29	115	10.7	311	**16100**
Max. endurance	24	60	10.8	258	6980

compute the required power for VTOL and hovering, Equation 8.6 can be used. It computes the required power for front and aft motors during VTOL and hovering, which can be seen in Table 8.7. The required battery capacity is 8090 mAh, by summing $C_{req,efp}$ for VTOL and hovering.

$$P_{req} = \sqrt{\frac{T_{req}^3}{2 \cdot \rho \cdot A_{prop}}} \tag{8.6}$$

Table 8.7: Battery Capacity for Essential Flight Phases

	t_{flight} **[min]**	$P_{req,front}$ **[W]**	$P_{req,aft}$ **[W]**	**Sum [W]**	$C_{req,efp}$ **[mAh]**
VTOL	1	1660	955	$2 \cdot (1660 + 955)$	**2360**
Hovering	5	600	672	$2 \cdot (600 + 672)$	**5730**

Power usage of other subsystems must be considered to determine the final battery size. Based on an estimation by the command & data handling department, the power usage of avionics is 9.23 W. Then, the final required battery capacity is determined to be 16100 + 8090 + 9.2 = 24200 mAh. Since the front motors are 10S, a battery pack with 10S is used. Aft motors are 8S, but a DC-DC converter will be installed in order to downscale the voltage. 'ZIPPY Compact 5800 mAh 10S 25C Lipo Pack' is selected, as it provides sufficient current and capacity for the propulsion subsystem. To determine the number of battery packs, the total battery capacity has to be divided by the capacity of a chosen battery pack: 24200 mAh/5800 mAh = 4.17. Thus, five battery packs will be used.

Table 8.8: Total Mass and Cost of Power Subsystem Components

Power components	**Total mass [kg]**	**Total cost [€]**
Battery packs	6.340	673
Battery cables	0.480	13.3
Battery connectors	0.078	8.43
Total	**6.898**	**695**

As the battery is chosen, battery cable and connectors must be selected resulting in a 'Turnigy High Quality 8AWG Silicone Wire 1m' and 'Nylon XT90 Connectors Male/Female'. The cable is estimated to be 4 meters based on the layout of the UAV.

The cost and mass budget has to be reviewed to see if chosen power subsystem components are within the budgets. According to Table 7.3, the mass budget and cost budget for the power

subsystem are 7.6 kg and 950 EUR respectively, including 5% contingency. Table 8.8 shows that the actual mass and cost of the power subsystem excluding rotating mechanism are 6.898 kg and 695 EUR respectively. Thus, the chosen components are within the budgets.

Payload range diagram For certain ranges, part of the payload capacity has to be sacrificed to be exchanged with additional battery. To show the payload capacity for different ranges, a payload range diagram is shown in Figure 8.5.

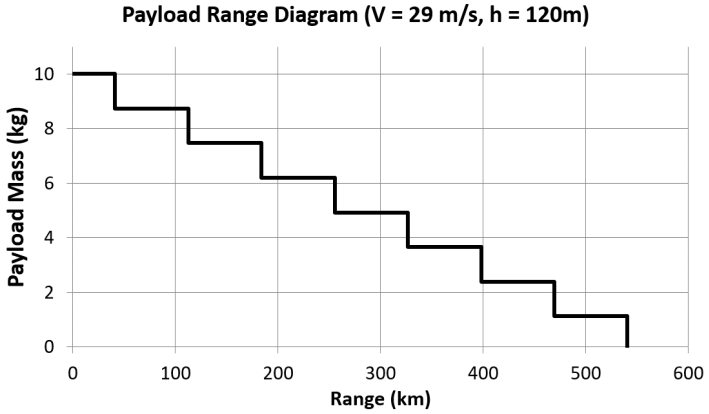

Figure 8.5: Payload Range Diagram

The equation for the range is found by dividing the battery, which is obtained by multiplying the battery mass by the specific capacity, by the battery capacity required for 200km range. This gives a C_{bat}/C_{200km} - ratio. Furthermore, due to the assumption that the power output during operation is approximately constant, the capacity is assumed linearly related with range. This enables the range to be calculated by multiplying the capacity ratio by 200km, as shown in Equation 8.7. First of all, the curve shows first a horizontal line segment, after which it at a certain range starts descending in a linear way with a slope of 56 km/kg. With a maximum payload capacity of 10kg, the UAV has a range up to a 41.2km. For top level range requirement SYS-PF-1.3R, the corresponding payload capacity for a maximum range of 200km will be 7.2kg. The absolute maximum range, which can be covered if all payload capacity is used for additional battery, is 603.9km.

$$R = \frac{C_{bat}}{C_{200km}} \cdot 200 = \frac{M_{bat} \cdot \frac{C}{M}}{C_{200km}} \cdot 200 \tag{8.7}$$

8.3.6 Rotating Mechanism Components

A simple rotating mechanism with fiberglass reinforced nylon parts and a servo is chosen, as very few off-the-shelf rotating mechanism components exist. After a market research, a tilt mechanism for a tricopter is considered, although it may require minor modifications to be retrofitted to the Hybrid UAV. A specific servo is recommended along with the mechanism, as they are designed to be used as a set. The quantity, mass and cost of rotating mechanism components can be seen in Table 8.9 as well as the total off-the-shelf components for the power subsystem. The total mass is within the budget including the contingencies, but the cost exceeds the budget by 100 EUR.

Table 8.9: Off-The-Shelf Component Choice Power Subsystem Including Rotating Mechanism

Component	**Product Name**	**Q.**	**Unit Mass [g]**	**Unit Cost[€]**
DC-DC Converter	LM2596 DC 3.2-40V to 1.25-37V	2	n.a	2.70
Rotating Mechanism	Tricopter Tilt Mechanism	4	10.6	8.50
Servo	BMS-210DMH	4	17.5	24.2
Servo wire	DITEX Servowire Extension	4	n.a	7.30
Battery	Zippy Compact 5800mAh 10S Lipo	5	1268	135
Power cabling	Turnigy HQ 8 AWG Silicon wire	4	120/m	3.50/m
Connector	Nylon XT90 Connectors	5	78.0	8.40
Total			7010	860

8.4 Verification & Validation

In order to ensure accuracy of the power & propulsion analysis, the methods used to perform the analysis have to be verified, and the corresponding results as well as tools used have to be validated.

Validation Python is primarily used to generate models for the analysis. It is assumed that Python is validated by experts of various industries.

The STC contain models for the analysis. Since the STC itself does not provide any codes, the validation of STC is done with a method of 'analysis'. In order to check if the model of the STC is correct, a set of real life data is used as an input for the method of analysis. Five arbitrary motor and propeller combinations are used to validate the model, which can be seen in Table 8.10. Input parameters for the validation are propeller diameter and pitch, RPM and propeller type. The output parameter is power. The STC power values have difference of less than 5 % with respect to the reference power value from the Hacker-motor data sheet [7]. Thus, values generated by STC are assumed to be valid and the model is validated.

Table 8.10: STC Validation

	Reference power value [W]	**STC power value [W]**	**Difference [%]**
A50-16S	1117	1127	0.887
A40-10L	945	909	3.96
C50-13XL	2592	2611	0.728
A200-8	8820	8741	0.904
Q80-11S	3038	2908	4.47

Verification Inputs used for the PDC have to be checked. The input parameters of PDC that are dependent on other departments are the following: weight, air density, zero-lift drag coefficient, wing surface area, aspect ratio and Oswald factor. In the beginning of the iteration process, the parameters were approximated from the previous phase of the project. Initial

calculations were carried out and components were chosen based on the calculations. Since the parameters directly come from the aerodynamics department, inter-communications between the power & propulsion department and aerodynamics department were established and finalised values are used for the final power & propulsion subsystem design. Thus, the parameters used in PDC are up to date and correct.

9 Aerodynamic Analysis

The aerodynamic analysis for horizontal flight only will be performed in this chapter, seeming that for vertical flight the airspeed will be low. The aircraft will need to fulfil a set of requirements which concern the aerodynamic properties of the aircraft. The most important aerodynamic property is the lift, since the aircraft will need to generate enough lift to be able to fly. The problem is that with lift comes drag. The challenge will be to design an aircraft which satisfies the requirements, while producing as little drag as possible.

The first section in this chapter is the approach, which is important to ensure that the process of designing goes well. The next section contains the assumptions made to ease the design process. The following section contains the actual analysis made for all the aerodynamic parts of the aircraft. Finally, once the analysis is done, the used methods are verified and validated.

9.1 Design Approach

There are several subsystems of the plane that need an aerodynamic analysis, each of these subsystems will be designed to have the least amount of drag as possible. The problem that arises is that the design with the least drag probably will not coincide with the requirements or the constraints put up by other departments. This results in an iterative process which will ensure that the design with the least drag, and that complies with requirements and constraints, comes out best. To get an overview of the design process, Figure 9.1 shows the process followed in the form of a work flow diagram.

The work flow diagram shows four differently coloured regions. These are the separate processes that have been carried out, though not only four processes have taken place. The first region is the preparatory work needed to be done before the designing can start. The literature study will help with understanding how to perform the design, and the assumptions will be made to give an overview of how the design can be done. Once that is finished, it is possible to go to any of the other regions based on what needs to be designed.

The second region contains the work flow diagram for the sizing and shaping of both the wing and the tail. The processes for both these subsystems are very similar, hence they have the same work flow diagram. The first step of the process is to define the optimal planform, which would be the one with the least amount of induced drag. Once that is done, it needs to be checked if the planform is feasible with the constraints set by the structures department. If feasible, then the planform is done. If it is not feasible, then an alternate solution has to be determined. With the help of a Python code the optimal alternative can be found, and again checked to be feasible. Now, if it is not feasible, the iteration starts to find the correct planform.

The third region is the work flow diagram for the airfoil selection for both the wing and the tail. Before this process can start, code has to be written to collect all airfoil data and select the optimal airfoil. Verification and validation will check if the code used is correct. Once all the data is collected and the optimisation is made, the airfoil will be checked for feasibility, constrained by the structures department and the stability & control department. If the airfoil turns out to be infeasible, a new airfoil optimisation will be run with new constraints to find the new best airfoil.

The fourth region is used for the design of the fuselage and the pylon. To start off the process, several parametric equations are selected which are used to make preliminary calculations. Once the calculations are done, it is possible to find the major influences of the fuselage shape on the drag. Knowing these influences, the optimal fuselage characteristics can be found, with which it is possible to design the fuselage. Once again, when the fuselage is designed, it needs to be checked for feasibility. This time the constraints come from the structures department, the aerodynamics department and the mass budget. If the design is feasible, a Computational

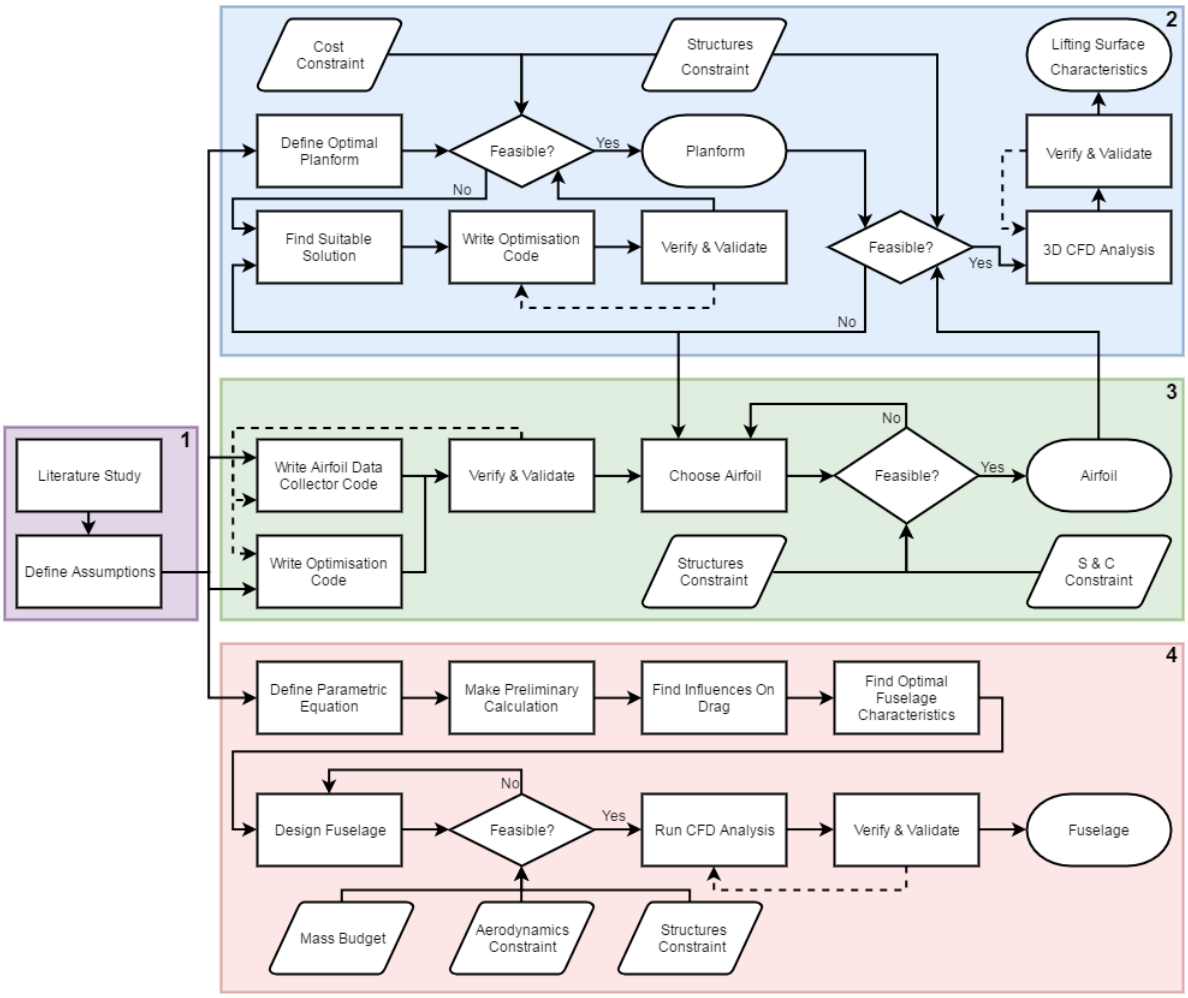

Figure 9.1: Work Flow Diagram for the Aerodynamic Design Process

Fluid Dynamics (CFD) analysis can be done to find more precise aerodynamic characteristics. The results of the CFD analysis are reflected against the parametric equations to check whether the CFD analysis has been implemented correctly.

9.2 Assumptions

- The flight condition is assumed to be at an altitude of 120 meters. This has been chosen because the majority of missions will not be flown at higher altitudes, so it will be optimised for an altitude of 120 meters. When flying at a higher altitude, the aircraft will need to fly at a higher angle of attack to achieve enough lift, increasing the drag and decrease the overall performance.
- The increment in velocity due to the pusher propellers is assumed to be negligible, not affecting the wing aerodynamics. In reality the propellers will increase the speed over the wing and decrease the amount of detached airflow, which increases the lift over the wing.
- The lifting surfaces are assumed to be completely smooth. In reality there are imperfections and other aspects, e.g. attachments, which decrease lift and increase drag.
- The drag of the propellers and motors is neglected. In reality they produce drag, but due to a lack of resources it was not possible to analyse this.
- The upwash and downwash of the wing on the pylons is neglected. In reality this effect

would create a destabilising positive pitching moment. Nevertheless, ignoring this is acceptable as the pylons are narrow and the resulting pitching moment will be orders of magnitude smaller than the one created by the wing and tail.

- It is assumed that for the CFD analysis the boundary layer is completely laminar. In reality, the boundary layer will transition to a turbulent flow, yet it is assumed that the transition point is near the aft of the relevant geometries, such as the fuselage or wing. The direct effect is a lower skin friction drag than in the case when the transition is not neglected. [11, p. 75], [12, p. 170].
- It is assumed that for the CFD analysis the turbulence model is laminar. Since most geometries of the UAV are smooth, slender, and have a small angle of attack, it is assumed that the transition from a laminar to a turbulent flow does not occur.

9.3 Analysis

This section will contain the analysis of the various subsystems. The goal of the analysis is to find the optimal solution to the problems at hand by meeting the requirements given with the set of constraints set by other departments. The first subsystem to be analysed is the wing in Section 9.3.1. Next, the tail will be analysed in Section 9.3.2, and the fuselage is analysed in Section 9.3.3. The last subsystem analysed is the power & propulsion subsystem, though only the pylon will be analysed. This analysis can be seen in Section 9.3.4.

9.3.1 Wing

There are five aspects that need to be analysed for the wing. The first aspect to be analysed is the shape & size of the wing, which gives the wing planform. Afterwards, the airfoil can be chosen which will give the wing the best aerodynamic properties. When that is done, it is possible to see whether high lift devices are necessary. Finally, with the basic wing shape designed, it is possible to analyse the wing in a 3D environment, to see if the aerodynamic characteristics are still satisfied. Finally, the winglets are the last aspect of the wing to be checked.

Shape & Size

Literature Study For low speed aircraft, there is one major influence of the wing on the drag, namely the induced drag[1]. Seeming this UAV flies at low speeds (20-55 $\frac{m}{s}$), the induced drag will be the biggest source of drag of the wing. To minimise the drag, the lift distribution of the wing needs to be elliptical, which can be achieved by having an elliptical planform. This would be the optimum planform of the wing, as can be seen in Figure 9.1. However, an elliptical wing is harder to manufacture due to its complex shape [13]. Due to this, an alternative has to be found, which still resembles an elliptical lift the best. This can be done by using several taper ratios or having a different airfoil at different spanwise locations. Due to the seeming complex manufacturing of different spanwise airfoils, the choice has been made to have several different tapers to resemble an elliptical lift distribution.

Another aspect of the planform which has been looked at is the sweep of the wing. Usually the front is swept to reduce Mach bubbles being created on the wing, which reduces lift drastically and generates a lot of drag. But this effect occurs only at high speeds (M >0.8) so it is not necessary for this UAV to have it. Having a swept wing will only have an adverse effect by reducing the chord wise speed over the wing, hence reducing lift. If the lift decreases, a bigger surface area will be needed which would only increase the drag. The dihedral of the wing has been left for the stability & control department.

[1] `https://www.grc.nasa.gov/www/k-12/airplane/induced.html`, Accessed on 14-06-2017

Having a wing stall can have an adverse effect on the safety of the aircraft, it gets even worse if the tip stalls before the root. This is because this will create a moment on the aircraft, which will roll the aircraft uncontrollably. This rolling can cause the aircraft to plummet to the ground, especially when close to the ground during landing. To prevent the tip stalling before the root, the tips will have washout. This causes the wing tips to have a lower incidence angle with respect to the rest of the wing, making it have a lower angle of attack. Due to the lower angle of attack, the tips will stall later and hence prevent tip stalling.

Method The sizing of the wing has been done by looking at the wing loading. The surface area needed to generate enough lift depends on various factors, see Equation 9.1.

$$S = \frac{2 \cdot W}{C_L \cdot V^2 \cdot \rho} \tag{9.1}$$

Using air density at sea level and the stall speed of 20 $\frac{m}{s}$, it is possible to find the wing loading for different C_L values. The C_L at a feasible wing loading is 1.3. With this number the surface area of the planform is calculated to be 0.8 m^2.

Since the optimum solution (an elliptical planform) is not feasible, it is necessary to find the best alternative solution. With the choice to have several different taper ratios, it has been chosen to use two different taper ratios on the wing. This choice has been made because the wing has to be detachable for ground handling, so the location of the taper change will be where the wing is detachable. Having more than two tapers would implicate the manufacturing while improving the planform slightly.

To find the best planform, a python code has been made. The code has been made in such a way that it would iterate through all variables directly or indirectly to find all possible combinations of planforms. The variables can be seen in Table 9.1. Each planform generated has been compared to an elliptical planform, using the mean squared error of the differences of normalised chord lengths. This way the planform which resembles an ellipse the most could be chosen. To verify the planform for its elliptical lift, the program XFLR5 has been used, which can generate the lift of a 3D wing and show its distribution. The resulting lift distribution can be seen in Figure 9.10 in Section 9.4.

Results With the design process done, the planform of the wing is finalised. The result can be seen in Figure 9.2. The dimensions of the planform are summarised in Table 9.1.

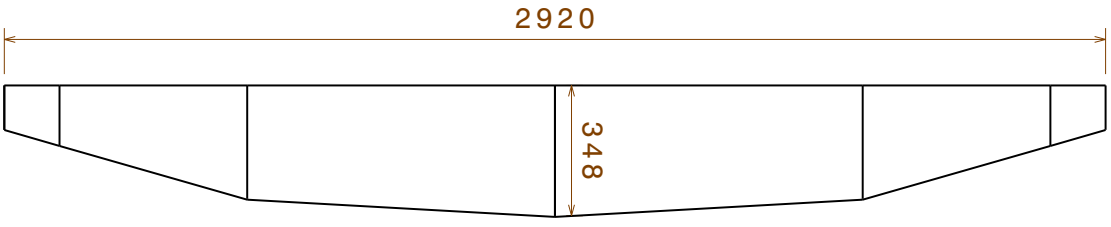

Figure 9.2: Planform of the Wing, Dimensions in mm

Table 9.1: Dimensions of the Wing

Variable	Value	Variable	Value
c_{t_w}	118mm	c_{r_w}	348mm
b_w	2920mm	AR_w	10.
λ_{tip}	0.39	λ_{root}	0.8
l_{twist}	146mm	$l_{taperchange}$	642mm
$\Delta\alpha_{tip}$	5 deg		

Airfoil

Literature Study Airfoils are used to achieve high lift while generating little drag (in relative terms). They are classified into families, and depending on which family the airfoil belongs to, different parameters are used to describe the geometry. This in turn determines the lift and drag coefficients. Airfoils within one family will show similar shape characteristics, which also distinguish them from the other families. Since the aerodynamic performance is directly influenced by the shape, every airfoil family will therefore have distinct aerodynamic characteristics. Thus the application of the airfoil serves as the starting point for airfoil selection, beginning with the selection of the airfoil family.

The most common airfoil families are the NACA 4-, 5-, and 6-digit series. The geometries of these airfoils are defined by the maximum camber value and position, the maximum thickness, and the family-specific parametric equations. Since the Hybrid UAV must be able to transition from horizontal to vertical flight, it is essential that the airfoil has a gradual stall behaviour ensuring a safe transition. Therefore, the airfoil chosen for the Hybrid UAV must demonstrate gentle stall behaviour, which is true only with the NACA 4-digit series [14]. For this series, the first digit indicates the maximum camber, the second specifies the position of the maximum camber, and the last two digits indicate the maximum thickness of the airfoil. All these values are shown as a percentage of the chord.

Apart from the general aerodynamic behaviour, the airfoil's lift and drag (or C_l and C_d) relationship must also be considered since it dictates the efficiency. In the case of the Hybrid UAV, two ratios are of greatest importance, namely $\frac{C_l}{C_d}$ influences the maximum range, and $\frac{C_l^{1.5}}{C_d}$ influences the maximum endurance [15]. Since the Hybrid UAV will mostly fly in cruise condition, the aim is to maximise both of these ratios for the lift coefficient required at cruise velocity, effectively yielding the optimal airfoil.

Method The selection of the airfoil was done in two steps. Firstly, a list of all possible NACA 4-digit series airfoils was generated, with parameters ranging from 0008 to 5530. These were then inspected for their maximum lift coefficient and all airfoils which had a $C_{l,max}$ lower than 1.3 (dictated by the stall velocity) were discarded.

The second step consisted of calculating the $\frac{C_l}{C_d}$ and $\frac{C_l^{1.5}}{C_d}$ at a C_l value of 0.56 ($C_{l,cruise}$) for the remaining airfoils. Next, the airfoil with the highest $\frac{C_l}{C_d}$ ratio, and the airfoil with the highest $\frac{C_l^{1.5}}{C_d}$ ratio was found, yielding two airfoils optimised either for maximum range, or maximum endurance.

Results The result of the airfoil selection yielded only one airfoil, namely the NACA 4417. This means that this airfoil has the highest $\frac{C_l}{C_d}$ and $\frac{C_l^{1.5}}{C_d}$ at $C_{l,cruise}$, and therefore is optimal for both maximum range and endurance. Its geometry can be seen in Figure 9.3.

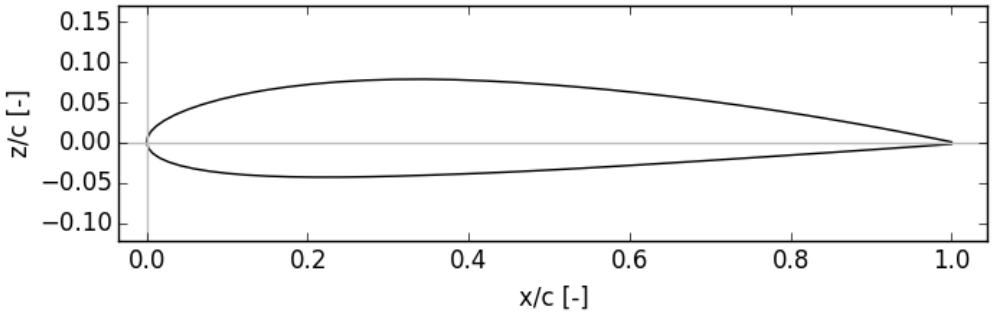

Figure 9.3: NACA 4417 Airfoil Geometry

The aerodynamic characteristics of this airfoil are summarised in Table 9.2. It should be noted that according to this analysis, the wing incidence angle is 1° ensuring the highest efficiency in cruise flight.

Table 9.2: NACA 4417 Lift and Drag Characteristics

	Value	α **[deg]**
$C_{l,max}$	1.53	14
$(C_l/C_d)_{Cl,cruise}$	57.6	1
$(C_l^{1.5}/C_d)_{Cl,cruise}$	41.4	1

High Lift Devices

Literature Study High lift devices are necessary in aircraft to be able to fly at lower stall speeds, because the high lift devices increase the C_L of the wing. This proves to be useful for large aircraft, so that the landing speed can be reduced significantly, ensuring a safer landing. However, the Hybrid UAV does not need to land horizontally, meaning that this is not a problem. High lift devices can still be implemented to be able to ensure a lower stall speed, but adding high lift devices brings forward more disadvantages than advantages. They will increase the overall cost of the aircraft due to extra material cost and manufacturing costs and it brings complexity in the wing which is unnecessary. More loads will be introduced, hence more structural integrity will be needed. These factors alone are the reason why the choice has been made not to use high lift devices.

3D Wing

Literature Study Determining the total lift and drag of the wing is essential when assessing the feasibility of the design. To do so, a three-dimensional analysis has to be performed which would mainly take into account the effect of the wingtip vortexes caused by the finite span and the corresponding pressure gradients. Two tools capable of such an analysis were found.

The first tool is XFLR5. It is an airfoil analysis tool also suitable for basic 3D wing analyses. For this software it was found that the horseshoe Vortex Lattice Method (VLM) is most fitting for the analysis since it allows non-flat wings to be analysed (the current wing has wing tip washout resulting in an out-of-plane geometry) [16, p. 26]. In addition, XFLR5 has the option to include the effects of viscosity in the horseshoe VLM.

The second tool is the SimScale Workbench, a CFD software. Starting with the meshing, it was found that the hex-dominant parametric meshing algorithm (included with the software) was most efficient and lead to faster convergence times [17, p. 9]. Next, due to the low Mach

numbers (not greater than 0.15), the fluid dynamics were selected to be incompressible. Furthermore, the turbulence model was selected to be laminar as explained previously in the assumption section. Finally smooth solvers were used as it was found that they are more efficient[18].

It is expected that, with the use of the 3D analysis tools, the total lift will be smaller than the one found in the 2D analysis, the stall behaviour will be more gradual [19, p. 72], and the total drag will be higher than the one found in the 2D analysis.

Method The 3D analysis was first carried out in XFLR5. The wing geometry was created within the tool and the surface was divided into panels. The panel distribution along the span is uniform (constant panel width), but along the chord a cosine distribution is used (panel size decreases towards the leading and trailing edge). Next, the viscous horseshoe vortex lattice method was chosen as the analysis definition. The analysis was ran with an initial velocity of 30 m/s and an angle of attack of 1°. The results were exported and analysed to find the total lift, drag, pitching moment, and lift distribution. Due to the iterative nature of the wing design, this process was repeated whenever necessary, and the results were updated. During the design iterations only XFLR5 was used for the 3D analysis since it could produce updated results within minutes, ensuring a smoother design process.

Once the wing design was fixed, the SimScale Workbench was used to determine the lift and drag with higher accuracy. First the wing geometry was imported into the program, and the corresponding surface and bounding-box meshes were created. The bounding box was made sufficiently large such that the boundary effects could be neglected. In addition, a second smaller mesh box was defined around the wing which consisted of a finer mesh. Next the inlet, outlet, and wall boundary conditions were set for the bounding box and wing surface. Finally, the simulation was started with an initial inlet velocity of 30 m/s. The analysis yielded the lift as well as the pressure and viscous drag.

Results The first results of the XFLR5 analysis are seen in Table 9.3. As predicted, the total lift is lower than the one required to achieve flight at cruise conditions. Therefore an iteration was performed by increasing the $C_{l,cruise}$ and checking whether the previous airfoil remained the most efficient one. Since this was indeed the case, the wing incidence angle was changed to 2.5°, according to the 2D airfoil angle of attack corresponding to the new cruise lift coefficient. The results of the updated incidence angle are also seen in Table 9.3. The lift-drag polar for the wing can be seen in Figure 9.4.

Table 9.3: Main Wing XFLR5 Results

	First Results	**Iterated Results**	
$C_{L,cr}$	0.444	0.622	[-]
L_{cr}	195.8	274.3	[N]
$C_{D,cr}$	0.015	0.02	[-]
D_{cr}	6.615	8.82	[N]
$C_{M,ac}$	-0.137	-0.137	[-]

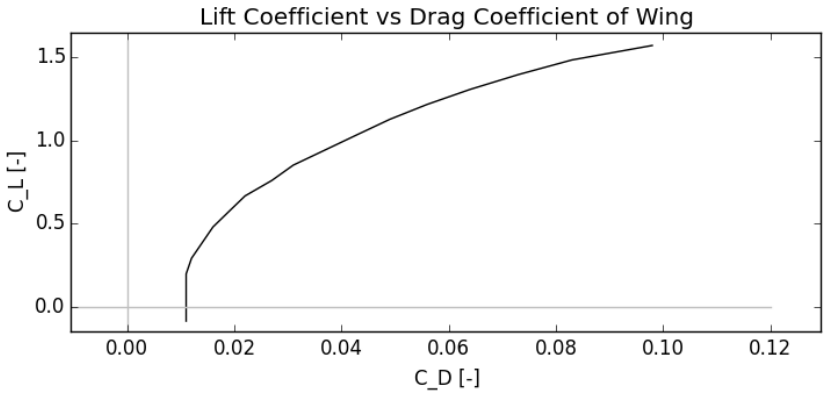

Figure 9.4: Lift-drag Polar of the Wing

The results of the SimScale Workbench CFD analysis with the updated wing incidence angle yielded a total lift of 173 N and a total drag of 6 N at cruise velocities. The validity of this result is discussed in Section 9.4.2.

Wingtip Devices

Literature Study Wingtip devices such as winglets decrease the drag of a wing by reducing the magnitude of the tip vortices. This means the efficiency of the plane increases when using wingtips, although the factor it increases by is too low for further consideration[2]. Having the improved efficiency from the winglets does not overcome the disadvantages it brings with it. Having winglets increases the overall cost due to extra material for the surface and the internal structures (higher wing loading). Seeming the efficiency gained is not worth it, it has been decided not to use winglets.

9.3.2 Tail

Three aspects have to be analysed for the tail. The three aspects are similar to the wing, the shape, the airfoil and the 3D tail. The size of the tail will not be designed by the aerodynamics department because the surface area of the tail is of more value for the stability & control department. The aspect to be analysed is the shape, which is done to design the planform of the tail (with the given surface area of the stability & control department). The second aspect is the airfoil of the tail, which needs to comply with constraints set by the stability & control department. The final aspect is the 3D tail, which is an aspect to be analysed because the 3D characteristics will differ compared to the 2D characteristics.

Shape

Literature Study There are two parts of the tail which need to be shaped and sized, namely the horizontal and the vertical tail. The empennage will be a T-tail type, chosen by the stability and control department. This means that the vertical tail will be closed in by the horizontal tail and the fuselage. Due to this, the vertical tail has been shaped in such a way that it would just fit between these two other parts of the aircraft. The horizontal tail however, has been shaped to minimise the drag. Just as for the wing, the minimal drag occurs when there is an elliptical lift distribution. This time, it is possible to achieve this with an elliptical planform due to three reasons. The first reason being that the loads on the horizontal tailplane are low, meaning the inner structure can be small and less complex. Furthermore, the size of the tailplane is much smaller than that of the wing, easing the manufacturing. The last reason is that the tailplane

[2]Prive Meeting with Mark Voskuijl, 15-06-2017

is not as complex as the wing. Due to these reasons the horizontal tailplane has been chosen to have an elliptical planform.

Method The key to getting an elliptical lift distribution is to have the chord lengths follow the size of an ellipse. This means it is possible that the centre line of the ellipse can be moved up or down. Keeping in mind that the elevators are most efficient if perpendicular to the flow, the horizontal centre line of the planform has been moved down to the three-quarters chord point. This way the elliptical lift distribution is kept while having a more effective controllability with the elevators.

Having an elliptical lift distribution is not indicative of the root chord and span of the tailplane, so to size these dimensions reference aircraft have been used. The usual aspect ratio of a horizontal tailplane is between four and five[3], for the vertical tail a taper ratio between 0.3-0.6 is common [20]. With these values, and the surface areas acquired from the stability & control department, the final dimensions could be calculated for both the vertical and horizontal tailplane.

Results With the shaping done, it is possible to find the dimensions of the tail surfaces. The dimensions of the tailplanes can be seen in Table 9.4, the planforms of the horizontal tailplane and the vertical tailplane can be seen in Figure 9.5 and Figure 9.6, respectively.

Table 9.4: Tail Dimensions

Horizontal Tail		**Vertical Tail**	
Parameter	Value	Parameter	Value
c_{r_h}	196mm	c_{r_v}	181mm
b_h	694mm	b_v	220mm
AR_h	4.5	AR_v	3.35
λ_h	-	λ_v	0.45

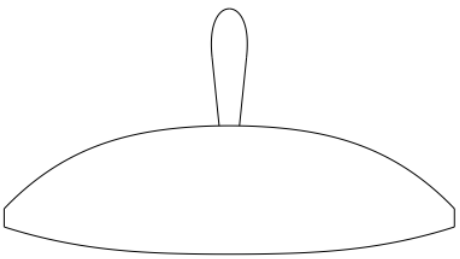

Figure 9.5: Top View of the Horizontal Tailplane, On Top Of The Vertical Tailplane

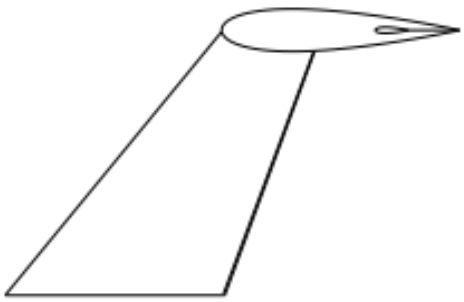

Figure 9.6: Side View of the Vertical Tailplane

Airfoil

Literature Study The horizontal tail must stall later than the main wing to ensure stability, therefore the corresponding airfoil must have a larger critical angle of attack (the angle of

[3] `http://nptel.ac.in/courses/101106035/035_Chapter%206_L26_(04-10-2013).pdf`, Accessed on 20-6-2017

attack at which the airfoil stalls) than the one of the main wing. Although the function of the horizontal plane is different from the main wing, the 4-digit NACA series is chosen here again as the starting point. This, again, is due to the predictable stall characteristics. In addition, this family is also common amongst tail airfoils [21, p. 23]. Nevertheless, the main difference between the wing and the tail is that the tail usually uses a symmetrical airfoil since it must provide positive and negative lift.

The required C_{l_h} at cruise conditions (dictated by the stability & control department) must also be kept in mind when selecting the airfoil, such that the tail will produce as little drag as possible during cruise, while keeping the UAV stable. Apart from the airfoil itself, the tail cruise lift coefficient can be changed by the horizontal plane incidence angle, yet the aim is to minimise this angle too.

The vertical tail must produce the least amount of drag, therefore an appropriate airfoil must be chosen. The 4-digit NACA series is chosen for the vertical tail as well since, again, it is commonly used on tails. The only constraint on the vertical tail airfoil is the minimum thickness (dictated by the structures department), which in turn also depends on the vertical plane planform.

Method The optimal horizontal tail airfoil was found by inspecting symmetrical NACA airfoils ranging from 0008 to 0029 for both the C_{l_h} required at cruise conditions and the stall angle. It was decided that the stall angle should be about 4° greater than the stall angle of the main wing. Out of all possibilities, the airfoil with the lowest thickness was chosen.

The optimal vertical tail airfoil was found by calculating the thickness of the vertical tailplane and comparing it to the structures department's requirement. The airfoil with the lowest sufficient thickness was chosen.

Results The horizontal tailplane airfoil with the lowest thickness that satisfied the lift and stall requirements was the NACA 0018. The aerodynamic characteristics are summarised in Table 9.5.

Table 9.5: NACA 0018 Aerodynamic Characteristics

$C_{l,cruise}$	0.18	[-]
$C_{l,max}$	1.24	[-]
$C_{d,cruise}$	0.009	[-]
α_{crit}	17.1	[deg]

The vertical tailplane airfoil with the lowest thickness that satisfied the Structures department's requirement was the NACA 0012. The zero lift drag coefficient ($C_{d_{0,v}}$) is 0.007.

3D Tail

Literature Study The knowledge gained from the 3D Wing literature study is directly applicable to the 3D tail analysis. Again, it is expected that the 3D total lift will be smaller than the estimated 2D lift, and the 3D drag will be larger than the estimated 2D drag.

Method The horizontal and vertical tailplane 3D analyses were first carried out in XFLR5 in the same manner as the main wing. The only difference is the angle of attack, which was now set to 0° for both the horizontal and vertical plane. Hence, the horizontal plane has a incidence angle of 0° as dictated by the stability & control department.

Once the tail design was fixed, the SimScale Workbench was used again to determine the lift and drag with higher accuracy. This analysis was also carried out in the same manner as the main wing.

Results The results of the XFLR5 tail analysis are seen in Table 9.6. As predicted, the 3D lift coefficient of the horizontal tailplane is lower than the one required at cruise conditions. Therefore an iteration was performed by increasing the incidence angle of the horizontal plane to 2.6°. The iterated results are also shown in Table 9.6.

Table 9.6: XFLR5 Tail Results

	Horizontal	**Iterated Horizontal**	**Vertical**	
$C_{L,h}$	0.118	0.181	0	[-]
$L_{h,cr}$	6.96	10.68	0	[N]
$C_{D,h}$	0.0015	0.0016	0.0003	[-]
$D_{h,cr}$	0.65	0.71	0.128	[N]

The results of the SimScale Workbench indicate a lift of 12.57 N and a drag of 1.11 N for the combined vertical and horizontal planes. The validity of these results is discussed in Section 9.4.2.

9.3.3 Fuselage

Literature Study From the point of view of the aerodynamics, the fuselage shape must be designed such that it produces the least amount of drag as possible during cruise flight. Based on the Roskam parametric equations for the fuselage drag, the two independent variables directly influencing the drag are the maximal frontal area and the length of the fuselage [22, p. 44].

Parametric equations serve as a starting point for the optimisation of the fuselage shape and provide an estimate on the drag, yet to gain more accurate results 3D analysis must be performed. Unfortunately XFLR5 does not support body analysis, therefore only the SimScale Workbench CFD tool is used for this purpose. Here, the knowledge gained from the 3D Wing literature study is directly applicable to the 3D fuselage analysis as well.

Method First, the subsonic parametric equations for the drag of the fuselage were coded in python. These equations took into account the wing-fuselage interference, the skin friction contribution, the lift induced drag, and the influence of the general shape of the fuselage on the drag. Next, since the maximum frontal area and the length of the fuselage are independent variables, the drag of the fuselage was calculated for a range of both of these two inputs and plotted. This plot indicated how these two inputs influenced the drag, and made it possible to optimise the fuselage shape for minimal drag.

Once the fuselage shape was fixed, the CFD analysis was performed in order to gain more accurate drag values. This analysis was also carried out in the same manner as the main wing.

Results The influence of the maximum frontal area and the fuselage length on the drag is shown in the plot in Figure 9.7. It can be seen that for fuselage lengths smaller than 3 meters, a smaller frontal area results in a smaller drag coefficient. Furthermore, for each frontal area there is an optimal fuselage length resulting in a minimal drag coefficient.

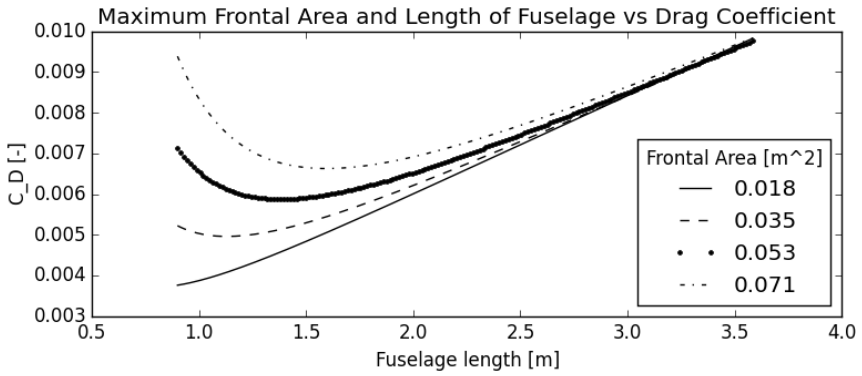

Figure 9.7: Influence of Maximum Frontal Area and Fuselage Length on Drag Coefficient

Since the cross sectional area of the fuselage is mostly dictated by the payload bay and the structures department, the maximum frontal area is fixed at $0.053m^2$. At this frontal area, the optimal fuselage length is 1.4 meters. The minimal length was limited to 1.7 meters by the stability & control department, nevertheless the final fuselage length was set to 1.8 meters. The reason for this was to have a less abrupt fuselage ending by elongating the empennage by 10 centimetres, in anticipation of a lower pressure drag. Although this contradicts the optimisation, it should be noted that the parametric equations assume that the fuselage's empennage cross sectional area gradually decreases towards the aft of the UAV, and this is not the case for the Hybrid UAV with a fuselage length of 1.7 meters. To approximate this situation, the empennage is elongated, resulting in a C_D of 0.0062 and a drag of 2.7 N at cruise velocities.

The results of the SimScale Workbench indicate a drag of 2.2 N during cruise. The validity of this result is discussed in Section 9.4.2.

9.3.4 Pylon

Literature Study The design of the pylon is performed in a similar fashion to the design of the fuselage, with the goal to minimise the drag. Therefore the knowledge gained from the fuselage literature study is directly applicable to the pylon design. Furthermore, the same parametric equations can be used as for the fuselage [22, p. 73]. The pylon-fuselage interference is considered significant enough to be included in the analysis, therefore the relevant parametric equations should also be used [22, p. 77].

Method The parametric equations for the pylon were coded in the same manner as the one for the fuselage, with the addition of the pylon-fuselage interference equation. In this case, the two independent variables were the pylon length and the pylon diameter, and the output was the drag coefficient of the pylon. The results were plotted which made it possible to optimise the design for minimal drag.

Once the pylon shape was fixed, the CFD analysis was performed in order to gain more accurate drag values. This analysis was also carried out in the same manner as the main wing.

Results The influence of the pylon diameter and length on the drag is shown in the plot in Figure 9.8. It can be seen that the smaller the diameter, the smaller the drag coefficient. Furthermore, for each diameter there is an optimal pylon length resulting in a minimal drag coefficient.

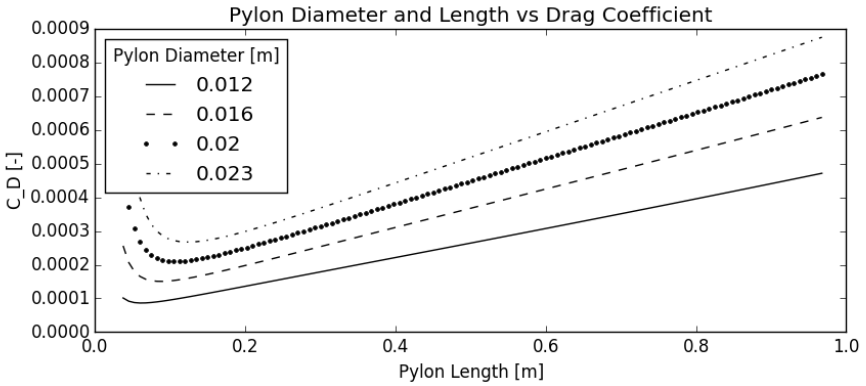

Figure 9.8: Influence of Pylon Diameter and Length on Drag Coefficient

The minimal diameter is dictated by the structures department, therefore it is fixed at 2 cm. The corresponding optimal pylon length is 10.5 cm, yet the minimal possible length set by the stability & control department is 90 cm. The result of the parametric analysis is a C_D of 0.00072 and a drag of 0.317 N at cruise velocities.

The results of the SimScale Workbench indicate a drag of 0.248 N during cruise. The validity of this result is discussed in Section 9.4.2.

9.4 Verification & Validation

In order to ensure that the 3D analyses were carried out correctly, the methods have to be verified, and the results validated. The verification of the XFLR5 tool is considered first. The validation of the wing, tail, fuselage, and pylon results is treated afterwards.

9.4.1 XFLR5 Verification

XFLR5 uses an inviscid linear-vorticity panel method to calculate the aerodynamic characteristics of airfoils [23, p. 1]. Therefore, in order to test whether this model produces accurate results within XFLR5, two verification methods are used. For convenience, the NACA 4417 airfoil will be used as an example.

Analytical The first method consists of finding the $C_l - \alpha$ curve using the classical cambered thin airfoil theory [11, p. 348], where the lift coefficient is described by Equation 9.2:

$$C_l = \pi\Big(2\alpha + \frac{2}{\pi}\int_0^\pi \frac{dz}{dx}\cos\theta d\theta - \frac{2}{\pi}\int_0^\pi \frac{dz}{dx}d\theta\Big) \tag{9.2}$$

Here, z describes the mean camber line geometry as a function of the chord position $\frac{x}{c}$. For the 4-digit NACA family, the derivative of the mean camber line geometry with respect to the chord position is given by Equation 9.3 and 9.4[4]:

$$\frac{dz}{dx} = \frac{2m}{p^2}\big(\frac{p}{10} - \frac{x}{c}\big) \quad for \quad 0 \leq x \leq pc/10 \tag{9.3}$$

$$\frac{dz}{dx} = \frac{m}{50(1-p/10)^2}\big(\frac{p}{10} - \frac{x}{c}\big) \quad for \quad pc/10 \leq x \leq c \tag{9.4}$$

Here, the variables m and p are the first two digits of the NACA airfoil description (i.e. NACA mpXX). In order to be able to insert the above equations into Equation 9.2, the variable change shown in Equation 9.5 must take place:

[4] `http://airfoiltools.com/airfoil/naca4digit`, Accessed on 20-06-2017

$$\frac{x}{c} = \frac{1}{2}(1 - \cos\theta) \tag{9.5}$$

Solving the equation for the NACA 4417 airfoil yields Equation 9.6:

$$C_l = 2\pi\alpha + 0.356 \tag{9.6}$$

Numerical The second method consists of finding the $C_l - \alpha$ curve using the vortex panel numerical method [11, p. 361], where the lift coefficient is found by dividing the airfoil into panels and solving for the vortex strength (Γ) at each panel using Equation 9.7.

$$V_\infty\left(\alpha - \frac{dz}{dx}\right) + w_{induced} = 0 \tag{9.7}$$

Here, the induced velocity ($w_{induced}$) is given by Equation 9.8 for an n-number of panels. Here x_{cp} denotes the position of the control point, and x_Γ denotes the position of the vortex, both as a fraction of the chord length.

$$w_{induced} = \sum_{i=1}^{n} \frac{-\Gamma_i}{2\pi(x_{cp,i} - x_{\Gamma,i})} \tag{9.8}$$

For the purpose of this verification, the airfoil was divided into two equal panels, the vortices were placed at the quarter chord points of each panel, and the control points were placed at the three-quarters chord points of each panel. Solving for the NACA 4417 airfoil, the two panel vortex strengths are given by Equation 9.9:

$$\Gamma_1 = \frac{3\pi c V_\infty}{8}\left(2\alpha + \frac{67}{720}\right) \quad \Gamma_2 = \frac{3\pi c V_\infty}{8}\left(\frac{2\alpha}{3} + \frac{79}{720}\right) \tag{9.9}$$

Plugging the values for the vortex strengths into Equation 9.10 yields the $C_l - \alpha$ relationship.

$$C_l = \frac{2(\Gamma_1 + \Gamma_2)}{cV_\infty} \tag{9.10}$$

From the comparison between the analytical, numerical, and the XFLR5 $C_l - \alpha$ curves seen in Figure 9.9, it can be said that XFLR5 produces accurate results in the linear region of the curve. Therefore the model used by XFLR5 can be considered to be verified.

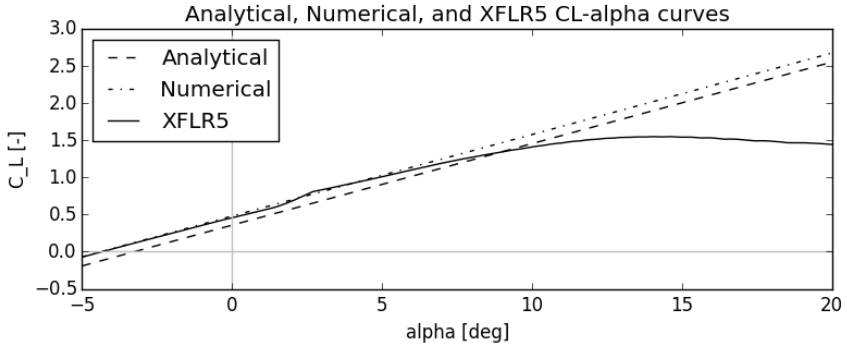

Figure 9.9: Comparison of the Analytical, Numerical, and XFLR5 $C_l - \alpha$ Curves

9.4.2 Results Validation

Wing The validation of the wing results begins with the visual inspection of the spanwise lift distribution in order to ensure that it is elliptical (as intended). A comparison between the two is plotted and seen in Figure 9.10. It can be seen that the lift distribution closely approximates an elliptical one, therefore this result is considered to be valid.

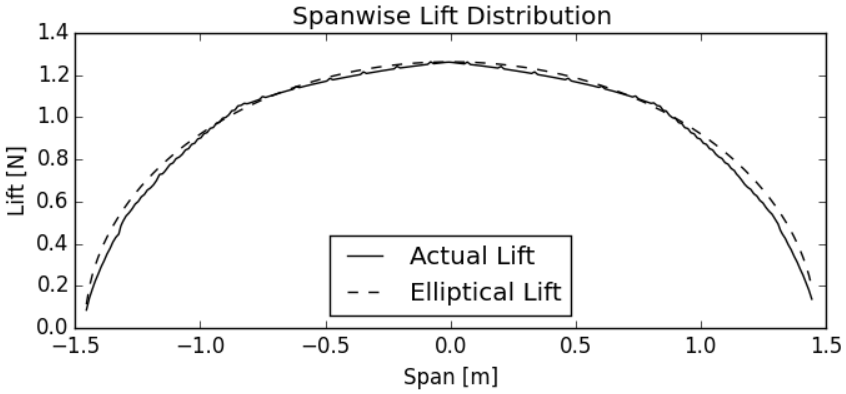

Figure 9.10: Comparison of Actual and Elliptical Lift Distribution

The next step is to validate the lift and drag obtained from the SimScale Workbench tool. This is done by comparing the SimScale results to the XFLR5 ones. As seen in the 3D Wing Results in Section 9.3.1, the discrepancy is too large and thus this result is not considered valid. One possible reason for the discrepancy is an improper boundary condition implementation, yet due to resource constraints this claim was not proven. However, since the XFLR5 tool was verified, its results are considered to be valid. Therefore the final lift and drag coefficients of the wing are 0.444 and 0.015 respectively.

Tail The validation of the tail results consists of only a comparison between the SimScale Workbench and XFLR5 results. These forces (as seen in the 3D Tail Results in Section 9.3.2) are similar and in the same order of magnitude as the XFLR results, therefore it is concluded that the setup of the CFD was correct, and the tail lift and drag coefficient is updated to 0.213 and 0.0026 respectively.

Fuselage and Pylons The validation of the fuselage and pylon results consists of a comparison between the SimScale Workbench and parametric results.

As seen in the Results in Section 9.3.3, the fuselage drag force obtained from the SimScale Workbench tool is similar and in the same order of magnitude as the parametric result, therefore it is also concluded that the setup of the CFD (including the initial and boundary conditions) was correct and the results are considered valid. Hence, the fuselage drag coefficient is updated to 0.005.

The results in Section 9.3.4 show that the pylon drag force obtained from the SimScale Workbench tool is also similar and in the same order of magnitude as the parametric result, therefore it is assumed that the setup of the CFD was correct and the results are considered valid. Hence, the pylon drag coefficient is updated to 0.00056.

10 Stability & Control

The stability and control design and analysis will be explained and presented in this chapter. First of all, Section 10.1 will clarify the approach followed in order to design and analyse the UAV for stability and control. Secondly, the assumptions used for the analysis are stated in Section 10.2. Next, Section 10.3 explains the methods used to design and analyse the UAV and presents the results of the design and analysis. Finally, the verification and validation of the analysis models, the tools used, and the results are presented in Section 10.4.

10.1 Design Approach

Figure 10.1 shows the work flow diagram for the stability and control design process. Here, the blue rectangle indicates the design phase for longitudinal stability, the green rectangle indicates the design phase for lateral and directional stability, and the yellow rectangle indicates the design phase comprising the manoeuvres in transition, horizontal, and vertical flight. Different design options can be considered in order to control the UAV and to ensure stability. In the concept selection phase, the decision has been made to have a tail for stability and control surfaces for control in horizontal flight, whereas propellers are used for control and stability in vertical flight. First of all, the tail was sized for longitudinal and lateral control and stability considering the critical case of one engine failure. A tail configuration was selected based on effectiveness and controllability. The required surface area of the vertical and horizontal tail were calculated and the optimal incidence angle of the horizontal tail was found. Simultaneously, the c.g. range needed to be estimated and controlled using the position of the wing as a balancing tool. Secondly, the control surfaces and actuators were sized in order to provide the required angular acceleration in horizontal flight. Thereafter, the propeller power split in order to perform manoeuvres in vertical flight was calculated. Finally, the transition phase was considered and a series of actions was defined in order to have a smooth transition.

The design process of the tail is an iterative process where the global c.g. position and the position of the leading edge of the wing change throughout the design. In order to know the global c.g. the tail needs to be sized. Vice versa, in order to size the tail, the c.g. needs to be known. By using the mass budget and an initial placement of the subsystems, an initial c.g. estimation was made. This estimation was used as a starting point for the tail sizing and wing positioning. Eventually, an updated c.g. was found using CATIA, so the design could be iterated. Likewise, in order to calculate the position of the leading edge, an initial position needs to be assumed. This leading edge position is needed to calculate the control and stability curves. When the control and stability curves are combined with the c.g.range curves, a new optimal leading edge position can be found. This new leading edge position has to be iterated into the control and stability curves.

Also the design process of the control principle is an iterative process. Similar to the c.g., the moment of inertia (MOI) changes throughout the design phase. Again, an initial estimation of the MOI was made in order to estimate the required control moments. Next, in order to size the control surfaces, the arm needs to be known which depends on the size of the control surface. Therefore, another iteration process was needed.

10.2 Assumptions

- It is assumed that the c.g. of the UAV coincides with the a.c. of the wing. With the actual c.g. range located between 0.55 m and 0.74 m from the nose, and the a.c. of the wing located at 0.60 m from the nose, the maximum distance between them is 0.14 m. Therefore, this assumption can be used in the design process without heavily affecting the

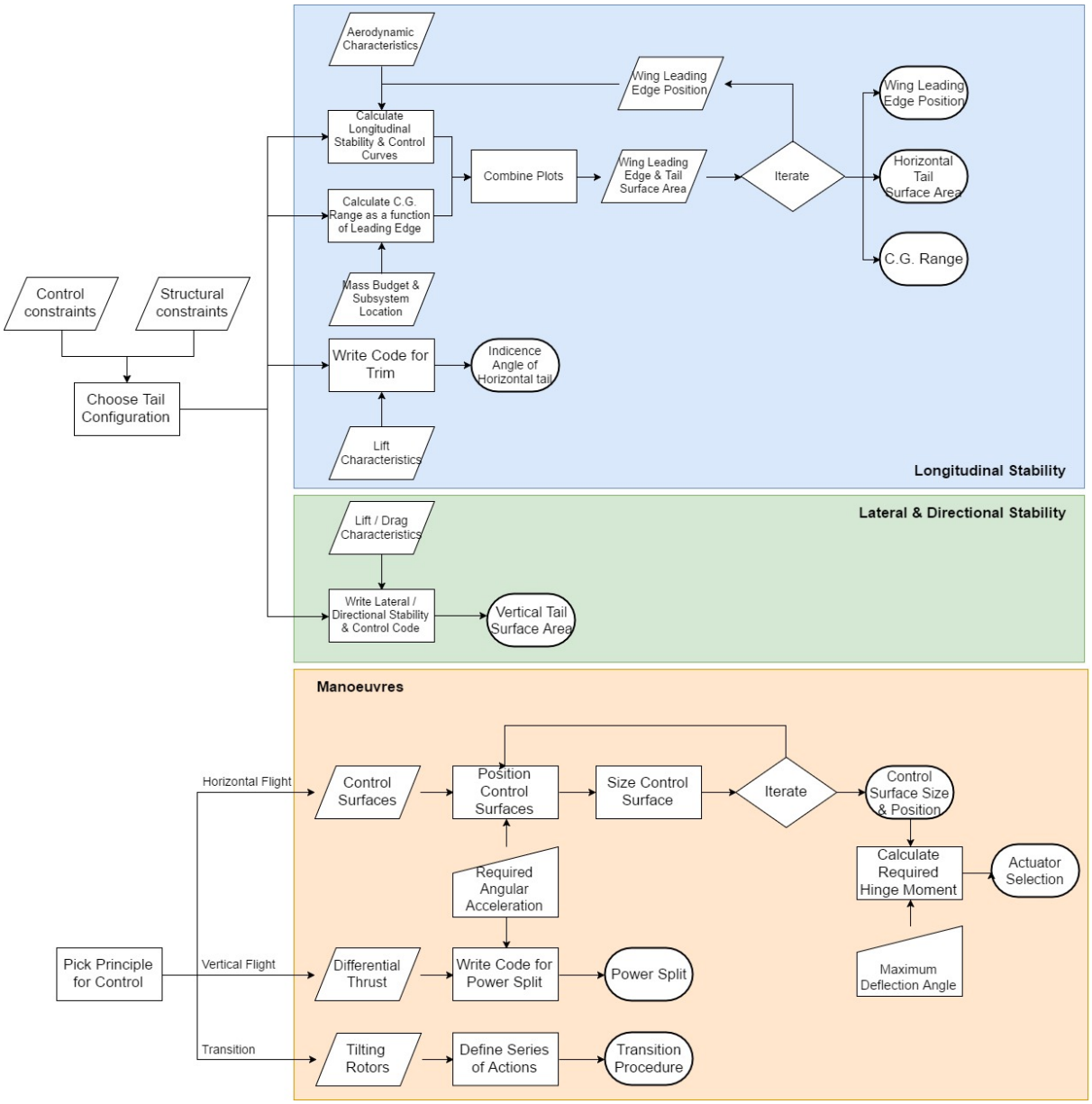

Figure 10.1: Work Flow Diagram for the Stability & Control Design Process

final results.

- It is assumed that the lift coefficient of the horizontal tail during stall, with elevator fully deflected, is equal to -0.8. This value is derived from statistical data for aircraft with adjustable tails [24].
- It is assumed that the resultant force of a control surface goes through half the chord of the control surface. Conventionally, the resulting force of a wing is taken through a quarter chord. However, the flow over the control surface is heavily affected by the airfoil in front of it. By assuming the resultant force goes through half the chord, the arm of the force to the hinge is slightly larger than the actual arm. Therefore, the actuators will be slightly over-designed.
- It can be assumed that the downwash at the horizontal tail-plane is negligible. Based on statistical relations based on the horizontal and vertical distance between the wing and tail, the downwash at the tail will have a magnitude of 10^{-3} [25]. Hence, this assumption can be considered valid.

- It can be assumed that the tail/wing speed ratio, $\frac{V_h}{V}$, is equal to one. This is a valid assumption since a T-tail is used with sufficient distance between the tail and the vortex shed of the wing. Hence, the perturbations in the flow at the tail caused by the fuselage are negligible.
- It is assumed that the UAV has a plane of symmetry across in the x,z-plane. Hence, the c.g. can be assumed to lie on the plane of symmetry. This assumption can be considered valid since the layout of the plane is symmetrical. Some small deviations may exist because of a non-symmetrical placing of internal components or non-symmetrical payload bay mass distribution.
- It is assumed that the fuselage doesn't generate lift. From the CFD analysis done by the aerodynamic department, the fuselage lift coefficient has an order of magnitude of 10^{-3}. Therefore, this assumption can be used without affecting the results.
- The centre of gravity of the payload bay is assumed to lie between the 10 cm and 50 cm mark measured from the front of the payload bay. This takes into account two loading cases: 1. the need to carry batteries and at the same time having sufficient continuous space for useful payload; 2. the need to carry heavy payloads (i.e. 10 kg) which occupy the entire payload bay. The mass of heavy payloads which occupy the entire payload bay is assumed to be distributed homogeneously throughout the payload volume.
- Whilst sizing the vertical tailplane it is assumed that the aerodynamic force induced as a result of side-slip acts perpendicular to the moment arm from the centre of gravity. In reality, the perpendicular component of this aerodynamic force is slightly smaller (scaled with the cosine of the side-slip angle) resulting in a slightly smaller required surface. This assumption therefore makes the calculated surface slightly conservative.
- Conservation of momentum and energy laws are assumed to provide sufficient accuracy when calculating the power required during the vertical flight phase. In reality, the motor and propeller efficiency must also be considered. The use of conservative inputs (namely a higher power required to hover) offsets whatever uncertanties the conservation of momentum and energy laws might introduce.
- The torque delivered by the motors is assumed to be proportional to the current delivered. It is also assumed that the angular velocity of the motors is proportional to the voltage applied. In reality this is loosely accurate, however, it not entirely correct to assume both torque and angular velocity vary linearly. This does not affect the required power splits, however, the motor-propeller combination must be tested experimentally to see how the output power varies with varying current and voltage.

10.3 Analysis

This section shows the methods used to analyse and design the UAV for stability and control, and presents the final results. The values used in the equations in this chapter can be found in Table B.1.

10.3.1 Tail Configuration

First of all, a tail configuration was picked based on the effectiveness, structural weight, and controllability of the tail-planes. Since downwash caused by the vortex of the wing reduces the effectiveness of the tail, a horizontal tailplane located outside of the downwash is preferred. Furthermore, it would be favourable to have tailplanes where pitch and yaw, and longitudinal and lateral control are separated from each other. The structural weight of the tail was also taken into account when choosing a tail configuration. For example, a V-tail has a reduced

amount of components. A T-tail was chosen as the final tail configuration mainly because downwash can be completely neglected and the control surfaces can be completely separated. At the same time, the structural weight can stay within the budget.

$$C_{L_h} = C_{L_{cruise}} \frac{S}{S_h} \frac{(x_{c.g.} - x_{a.c._w})}{(x_{a.c._h} - x_{c.g.})} \tag{10.1}$$

Next, the incidence angle of the horizontal tailplane was calculated in order to be trimmed without the need of deflecting the elevator. The required tail lift coefficient was calculated for cruise conditions using Equation 10.1 which is derived from the trim equation. The optimal incidence angle can be found by finding the corresponding angle of attack in the C_L-α curve of the tail.

10.3.2 Longitudinal Stability & Control

The UAV is required to be longitudinally statically stable. This means that it is able to react to a change in the angle of attack by generating an opposite pitching moment to restore the former state of equilibrium. In order to achieve stability, the c.g. should be positioned in front of the neutral point. The position of the neutral point is dependent on the ratio of tail/wing surface areas. When taking into account a Safety Margin (SM) of 0.05[1], the maximum position of the c.g. (in order to be stable) can be calculated as a function of the tail/wing surface ratio, as can be seen in Equation 10.2. In this equation, a macron (the bar on top of a symbol) indicates it is divided by the mean aerodynamic chord of the wing. The downwash is assumed to be zero and tail/wing speed ratio can be assumed to be equal to one since a T-tail configuration is used. The distance between the wing a.c. and tail a.c., l_h, can be estimated by assuming an initial position of the leading edge of the wing and iterating it. The other parameters are aerodynamic characteristics.

$$\bar{x}_{c.g._{max}} = \bar{x}_{a.c.} + \frac{C_{L_{\alpha_h}}}{C_{L_{\alpha_{A-h}}}} \Big(1 - \frac{d\epsilon}{d\alpha}\Big) \frac{S_h l_h}{S\bar{c}} \Big(\frac{V_h}{V}\Big)^2 - SM \tag{10.2}$$

Additionally, the UAV is required to be controllable. An aircraft is said to be controllable when it is able to be trimmed for a certain aircraft configuration. In other words, a combination of wing and tail lift coefficient should result in a zero total aircraft moment coefficient. In order to achieve controllability, the c.g. has to be positioned behind a certain limit point. This point can be found as a function of the tail/wing surface area by using the trim equation. Here the moment generated by the wing around the c.g. has to be equal to the moment generated by the tail around the c.g.. When rewriting this equation, the minimum position of the c.g. (in order to be controllable) can be calculated as a function of the tail/wing surface area, as can be seen in Equation 10.3. Again, the tail/wing speed ratio can be assumed to be equal to one. The distance between the wing and tail can be estimated and iterated. The aerodynamic characteristics are put in the remaining parameters.

$$\bar{x}_{c.g._{min}} = \bar{x}_{a.c.} - \frac{C_{M,a.c.}}{C_{L_{A-h}}} + \frac{C_{L_h}}{C_{L_{A-h}}} \frac{S_h l_h}{S\bar{c}} \Big(\frac{V_h}{V}\Big)^2 \tag{10.3}$$

These two equations can be plotted with the c.g. measured from the leading edge divided by the mean aerodynamic chord on the x-axis, and the tail/wing surface area on the y-axis. This plot is called the scissor plot, presented as the blue curves in Figure 10.2. In between the two curves lies the region where, if the c.g. is positioned there, the aircraft is stable and controllable. The position of the wing is used as a balancing tool in order to get the actual c.g. range shifted to the optimal position in order to have the lowest tail/wing ratio. Visually, this means that a

[1] AE3211-I Lecture 5 - Requirement Analysis and Design principles for A/C stability & control (Part 1)

plot of the c.g. range as a function of the leading edge has to be combined and shifted vertically to the scissor plot until the range of the c.g. plot matches with the width of the scissor plot.

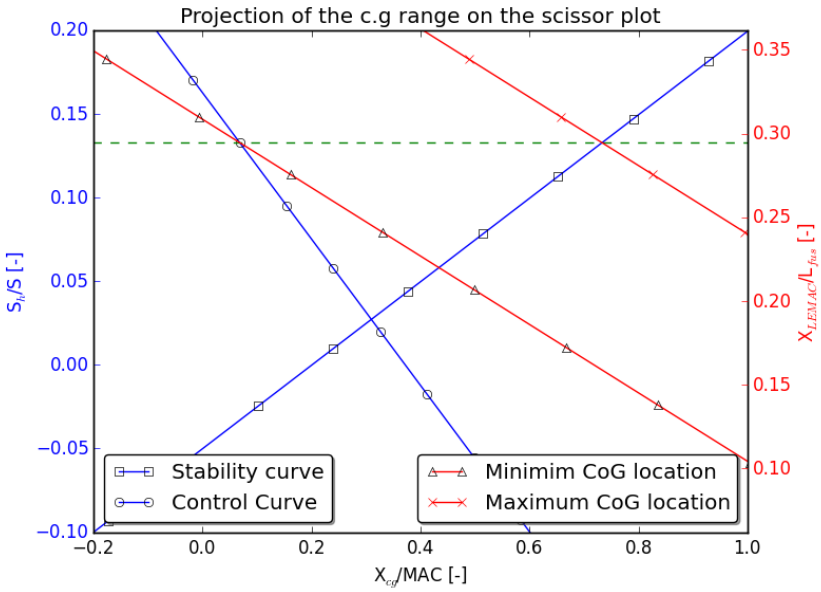

Figure 10.2: Projection of the C.G. Range on the Scissor Plot

Now the c.g. plot needs to be calculated. Here, the c.g. range is plotted with the c.g. measured from the leading edge divided by the mean aerodynamic chord on the x-axis, and the wing leading edge divided by the length of the fuselage on the y-axis. Hence, the x-axes of both the scissor and c.g. plots are the same. In order to calculate the c.g. range, Equation 10.4 is used. Here, m_i is the mass of a subsystem, x_i is the c.g. of the subsystem, and n is the number of subsystems. The subsystem masses and locations can be found in Table 13.11. Since the c.g. of the payload bay has a minimum and a maximum value, a range of c.g. values is found. Furthermore, the c.g. value depends on the x-location of the wing, which depends on the position of the leading edge of the wing. Hence, the c.g. range can be expressed as a function of the wing leading edge over the length of the fuselage. The curves for the maximum and minimum c.g. ranges are presented as the red curves in Figure 10.2.

$$x_{c.g.} = \frac{\sum_{i=1}^{n} x_i \cdot m_i}{\sum_{i=1}^{n} m_i} \tag{10.4}$$

By shifting the c.g. plot over the scissor plot, one can see in Figure 10.2 that an optimal value for the tail/wing ratio, and leading edge over fuselage length ratio can be found. This is indicated by the green striped line extended between both y-axes. The final results are presented in Table 10.1. The final values used to calculate the total c.g. position can be found in Table 13.11.

Table 10.1: Results of the Scissor and c.g. Plot

Parameter	**Value**	**Unit**
$x_{cg_{min}}$	0.55	m
$x_{cg_{max}}$	0.74	m
x_{LE}	0.53	m
S_h	0.106	m^2

10.3.3 Lateral/Directional Stability & Control

In this section, the lateral and directional stability and control of the UAV is analysed. In order to achieve this, the vertical tail area of the system has to be designed. Using wing mounted engines, the critical design case for vertical tail sizing is obtained in the one-engine-inoperative condition. In this case, the remaining engine creates a yaw-moment which needs to be counteracted using the vertical tailplane. Although a rudder deflection might also be used for this, the moment should only be based on the vertical tailplane, as directional yaw control of the aircraft in both directions is still needed and achieved using rudder deflections.

First, a necessary yaw angle at which equilibrium is achieved needs to be defined. It was assumed, that in one-engine-inoperative condition, equilibrium will be obtained at a yaw angle of 5 deg. It was decided that higher yaw angles in one engine out condition are not preferred as this would alter the flight path of the UAV too much. It should be noted, that higher yaw angles will be possible in one engine out condition, however this will require a rudder deflection. Then, the UAV velocity will be reduced to maximum range speed, $V_{range} = 27m/s$, in order to be able to fly to the best landing location. In case the engine fails at a lower velocity, the drag of the failed engine will be lower and in turn less thrust is required. This will reduce the yaw moment and thus flying at lower velocities will also be possible. In case the engines fail at a higher velocity, settling to the required thrust for maximum range will decrease the velocity and drag automatically. Using aerodynamic properties, the thrust required for the remaining engine due to the drag of the inoperative engine is now obtained with Equation 10.5.

$$T = C_D \cdot \frac{1}{2} \cdot \rho \cdot V_{range}^2 \cdot S \tag{10.5}$$

Then, considering the fact that the engines are all mounted at the same distance y_{engine} from the centre of gravity, the yaw moment created by the one-engine-out condition is obtained using $M = T \cdot y_{engine}$. This yaw moment has to be counteracted by the vertical tailplane. As the moment arm, airfoil, velocity, and the sweep angle of the vertical tailplane are known, the required surface area can be calculated using Equation 10.6. For lateral stability, the vertical tail must have a surface area of 0.026 m^2. The actual surface area of the tail is 0.03 m^2.

$$S_v = \frac{2 \cdot M_{yaw}}{l_v \cdot C_{L_v} \cdot \rho \cdot (V_{range} \cdot cos(\Lambda_v))^2} \tag{10.6}$$

10.3.4 Control Surfaces

In this section the size and position of the control surfaces are determined. These are ailerons for roll control, an elevator for pitch control, and a rudder for yaw control. Then, the hinge moment is calculated in order to select suitable servos.

The design of the control surfaces is dependent on the angular accelerations required. From requirements SUB-W-7.3, SUB-T-2.2, and SUB-T-2.3, the following angular accelerations are defined [26].

$$\ddot{\phi} = \ddot{\theta} = 45\frac{deg}{s^2} \quad \ddot{\psi} = 6\frac{deg}{s^2}$$

Using the moments of inertia, the torque required is obtained using Equation 10.7. These torques have to be created by the control surfaces and hence depend strongly on the physical location of the control surfaces. The elevator is located at the trailing edge of the horizontal tailplane. The ailerons are positioned as far away from the fuselage as possible in order to maximise the moment arm. In order to avoid twisting the control surfaces themselves, they can not be positioned at the wing tips. Therefore, they will be positioned just before the start of the wing twist. The rudder is located at the trailing edge of the vertical tailplane. The locations of the control surfaces lead to the moment arms.

$$T = I \cdot \alpha \tag{10.7}$$

With the moment arms and the torque required, one can calculate the required force for the surface. The force generated by deflecting the surfaces to an angle of δ is given by Equation 10.8.

$$F = C_{n_\delta} \cdot \delta \cdot \frac{1}{2} \cdot \rho \cdot V^2 \cdot S \tag{10.8}$$

In Equation 10.8, C_{n_δ} is obtained using an XFLR5 analysis. In order to size the control surfaces, stall speed is assumed. This ensures that the surface is capable of providing enough force for the whole speed range. Comparing control surface deflection angles of different aircraft, the following maximum deflection angles were defined:

$$\delta_{elevator_{max}} = 28deg \quad \delta_{rudder_{max}} = 25deg \quad \delta_{aileron_{max}} = 30deg$$

Using these parameters, it is now possible to calculate the surface area of the different control surfaces by rearranging Equation 10.8. Now, the aileron chord is assumed to be 20% of the wing chord, elevator span to be 70% of the horizontal tailplane span, and rudder span to be 90% of the vertical tailplane span. This makes it possible to calculate the different dimensions for the surface area.

Using the dimensions of the different control surfaces, an appropriate servo has to be chosen. For this, it is necessary to calculate the torque required to maintain a the maximum certain deflection.

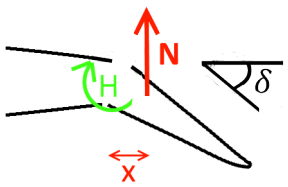

Figure 10.3: Hinge Moment Created by the Control Surface Force

As can be seen in Figure 10.3, the hinge moment created by the normal force N is dependant on the aerodynamic centre of the control surface. For calculation purposes it is assumed that the force acts halfway through the chord. The actual hinge moment will be lower as the aerodynamic centre is in general located at the quarter-point of the chord. Then for the sizing, worst case scenario is assumed, meaning flying at maximum speed of 200 km/h and deflecting the control surface to maximum deflection. The control force is then calculated using Equation 10.8, which, when multiplied by the moment arm, gives the hinge moment. The final control surface results are illustrated in Table 10.2.

Table 10.2: Control Surface Properties

	Span [cm]	Chord [cm]	Surface Area [cm^2]	Maximum Hinge Moment [Ncm]
Aileron	17.1	3.69	63.1	23
Elevator	47.2	2.89	136	36
Rudder	16.3	2.67	43.4	12

Four SAVÖX SC-0254MG servos are used for both ailerons, the elevator, and the rudder. They are able to deliver a torque of 62 Ncm at minimum power consumption[2].

[2] https://www.hacker-motor-shop.com/Servos/Savoex-Servos/Servos-Flugmodelle/Servo-SAVOeX-SC-

10.3.5 Vertical Flight Manoeuvres

During the vertical flight phase of the the UAV various manoeuvres have to be considered, namely pitch, roll, and yaw, all of which are achieved purely through varying the thrust level of the four propellers. By varying the power applied to motor couples the required moments about the axis around which the manoeuvre takes place can be produced. In this section the power required to achieve specified angular accelerations about the three axes will be characterised. However it is necessary to first define the locations of the four motors with respect to the centre of gravity. It is important to note that the conventional body axis system with its origin located at the centre of gravity is used in this section, i.e. the x-axis points in the direction of the nose, the y-axis runs along the right wing, and the z-axis completes the right hand coordinate system.

General Layout of Motors As explained in Chapter 8 the front motor-propeller combination was chosen to provide most of the thrust during the vertical flight phase whereas the aft motor-propeller combination was chosen to propel the UAV during horizontal flight. This results in the distance from the centre of gravity to the front motors being smaller than the distance from the centre of gravity to the aft motors in the longitudinal direction. For control reasons and simplicity's sake it is beneficial if the lateral and longitudinal distances between the motors are equal.

It was also important to define the direction of rotation of the propellers in order to perform calculations for the required torque about z-axis for yaw manoeuvres. The direction of rotation of the motors is chosen such that during hovering and vertical climb the total torque around the centre of gravity is zero, as well as such that yaw manoeuvres can be performed. Both conditions are satisfied when the front motors rotate in opposite directions as well as when motors diagonally opposite rotate in the same direction. The following configuration with respect to the centre of gravity is assumed for further calculations.

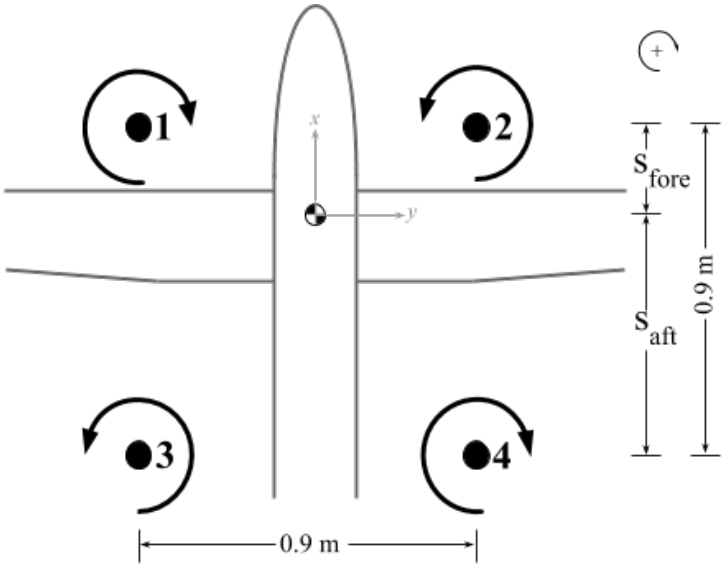

Figure 10.4: Configuration with respect to the Centre of Gravity

By equating the moment created by the front motors to the moment created by the aft motors around the y-axis, the distances from the centre of gravity to the front and aft motors can be calculated. Values for S_{fore} and S_{aft} are presented in Table 10.3 below.

0254MG.htm?SessionId=&a=article&ProdNr=80101005&p=6264, Accessed 22-06-2017

Table 10.3: Table of the Distances of the Motors from the c,g,

Distance	**from min c.g. [m]**	**from max c.g. [m]**
S_{fore}	0.23	0.39
S_{aft}	0.77	0.61

Pitch In order to perform a pitch up or down manoeuvre during vertical flight a change in moment around the y-axis has to be induced by the motors. As stipulated by requirement **SUB-PR-3.5** the propulsion subsystem shall be capable of providing an angular acceleration, $\ddot{\theta}$ about the y-axis of 0.8 rad/s^2. The moment required to deliver the stipulated angular acceleration is defined as the follows:

$$M_{pitch} = I_{yy} \cdot \ddot{\theta} \tag{10.9}$$

The required moment to deliver the angular pitching acceleration outlined by the requirement can then be translated into the change in thrust required (ΔT) of the motor-propeller couples by dividing by the moment arms presented in Table 10.3. During pitch manoeuvres it is assumed that the required moment will always be delivered by increasing the thrust of the front or aft motors-couples rather than increasing one and simultaneously decreasing the other. This is done as it is assumed that unless the UAV is in transition, the rotation of the motors will be kept to a minimum. Because of this, as the pitch motion is initiated the effective vertical force of the propellers decreases with the cosine of the angle of rotation. If the overall power was to be kept constant during pitching (by increasing either the fore or aft motors and decreasing the opposite) altitude will be lost. The loss of altitude can be mitigated by simply delivering the entire required moment with the increase of thrust of the fore **or** aft motor-propeller couples (depending on the direction of pitch required) rather than splitting the required moment over both the fore and aft motors.

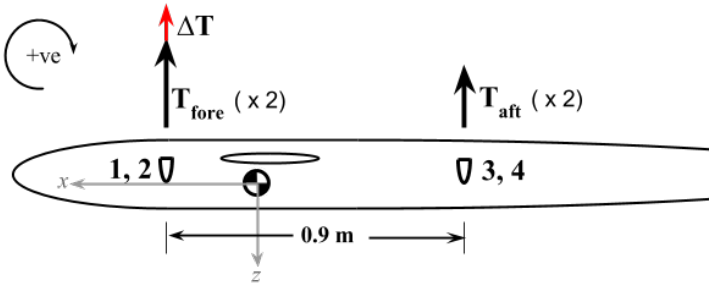

Figure 10.5: Side View Schematic of Pitch

For a pitch up manoeuvre (positive pitch) with an angular acceleration of 0.8 rad/s^2 the power required is calculated using Equation 10.10. Note that this procedure is the same for a pitch down manoeuvre apart from the fact that the aft motors will be responsible for the manoeuvre as opposed to the front motors.

$$P_{req} = \sqrt{\frac{(T_{fore} + \frac{\Delta T}{2})^3}{2 \cdot \rho \cdot A_{fore}}} \tag{10.10}$$

Where T$_{fore}$ is the thrust of the front motor-propeller couples during hovering. The change in power required in order to deliver the required moment is therefore the difference between the power required to hover and the power required calculated above in Equation 10.10.

Power can also be defined as the product of the torque delivered and the angular velocity and so by increasing the angular velocity of the propeller the power required to perform the pitch manoeuvre can be achieved. The relationship between power, torque and angular velocity is given by the following equation

$$P = \tau \cdot \omega \tag{10.11}$$

By increasing the voltage supplied to the motor (also increasing the power for a fixed current) the angular velocity can be increased since the angular velocity of the motor is proportional to the voltage.

Roll In order to perform a roll manoeuvre during vertical flight a change in moment around the x-axis has to be induced by the motors. Essentially the same procedure as laid out in the above section can be employed, however, it is slightly more complicated given the fact that the fore and aft motors are not the same.

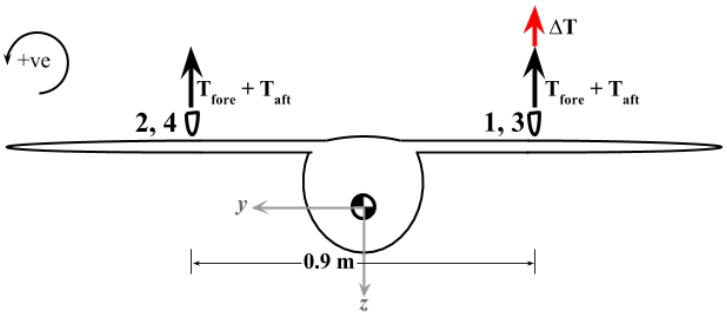

Figure 10.6: Front View Schematic of Roll

The moment required to achieve the angular acceleration stipulated by requirement **SUB-PR-3.4** is given by the equation below.

$$M_{roll} = I_{xx} \cdot \ddot{\phi} \tag{10.12}$$

By dividing the roll moment by the y-distance from the centre of gravity to the motors the combined required change in thrust (ΔT) is obtained. Because the fore and aft motors are different, in order to eliminate any pitch induced as a result of this roll manoeuvre, the same ratio as during hovering of the thrust produced by the front propeller to the thrust produced by the aft propellers must be used. Whatever yaw moment induced can be limited by increasing the voltage applied as opposed to the current delivered. By doing this the increase in power required for roll is delivered mainly by an increase in angular velocity and not an increase in torque. For a positive roll manoeuvre the power required to deliver this thrust is characterised by the following equation.

$$P_{req_1} = \sqrt{\frac{(T_{fore} + (\frac{\Delta T}{2} \cdot \frac{T_{ratio}}{T_{ratio}+1}))^3}{2 \cdot \rho \cdot A_{fore}}} \tag{10.13}$$

$$P_{req_3} = \sqrt{\frac{(T_{fore} + (\frac{\Delta T}{2} \cdot \frac{1}{T_{ratio}+1}))^3}{2 \cdot \rho \cdot A_{fore}}} \tag{10.14}$$

Where subscripts 1 & 3 represent motor 1 and 3 from Figure 10.4 respectively as those are the motors responsible for a positive roll moment. Again, the required moment is not split across the x-axis in order to mitigate altitude loss because of effective vertical thrust decreasing with the cosine of angle of rotation. The change in power required for motors 1 and 3 during a positive roll manoeuvre can be achieved by increasing the angular velocity of the motors which in turn can be done by increasing the applied voltage.

Yaw Positive or negative yaw manoeuvres during vertical flight can be performed by altering the torques of the motors. Each motor exerts a certain torque on the entire body due its rotation and this phenomenon can be exploited to perform manoeuvres. As depicted in Figure 10.4 motors 1 and 4 rotate in the same direction as do motors 2 and 3 and so during yaw manoeuvres these pairs of motors will work together to provide the required moment. As stipulated by requirement **SUB-PR-3.6** the propulsion subsystem shall be capable of providing an angular acceleration, $\ddot{\psi}$ about the z-axis of 0.1 rad/s^2. The moment required to deliver the required angular acceleration is characterised by the following equation.

$$M_{yaw} = I_{zz} \cdot \ddot{\psi} \tag{10.15}$$

This moment can be achieved by altering the torque of the motors. During hovering, the torque delivered by each motor can simply be calculated by dividing the power required to hover by the nominal angular velocity of the motors during hovering.

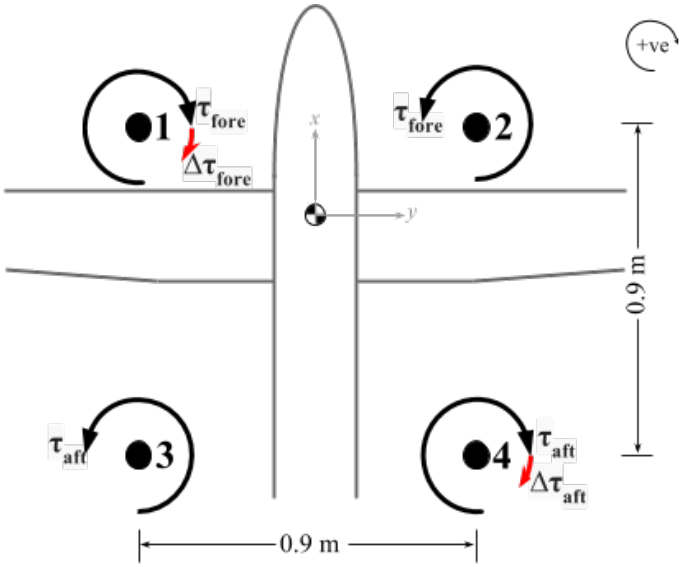

Figure 10.7: Top View Schematic of Roll

For a positive yaw manoeuvre the change in torque ($\Delta\tau$) required is split amongst motor 1 and 4 (from Figure 10.4). This torque is split up according to the ratio of the torque of motor 1 to the torque of motor 4 (please note that for a negative yaw manoeuvre the same procedure is applied except the opposite motor pairs will be increasing or decreasing power respectively). The change in power (ΔP) of the motors delivering the manoeuvre (i.e. motors 1 and 4) as a result of the increase in torque required can be calculated by multiplying the torque required of each motor with their respective angular velocities as shown in Equations 10.16 & 10.17.

$$\Delta P = \Delta\tau_1 \cdot \omega_1 \tag{10.16}$$

$$\Delta P = \Delta\tau_4 \cdot \omega_4 \tag{10.17}$$

In order to maintain altitude, this increase in power must be countered by a decrease in power from the other two motors, namely motors 2 and 3. The increase in power required of motor 1 (from Equation 10.16) needs to be subtracted from the power required of motor 2 to hover and likewise the increase in power required of motor 4 (from Equation 10.17) needs to be subtracted from the power required of motor 3 to hover. Since the moment arms perpendicular to the x-axis are the same for the front and aft motors, despite them having different thrust levels, a rolling motion will be induced. This roll moment can be corrected for with the control system by overlaying the two manoeuvres.

In order to ensure that the required torque is delivered, the positive change in power required

of motors 1 and 4 should be achieved by increasing the current delivered to the said motors as torque is proportional to current. The decrease in power of the remaining two motors can simply be achieved by decreasing the respective angular velocities by lowering the applied voltage.

Results The following tables breaks down the required power to perform the three outlined manoeuvres.

Table 10.4: Table of Power Required for Motors 1 & 2

			Motor 1		**Motor 2**	
			c.g.$_{min}$	**c.g.**$_{max}$	**c.g.**$_{min}$	**c.g.**$_{max}$
Hover		P_{req} [W]	1574	1009	1574	1009
Pitch	+ve	P_{req} [W]	1657	1049	1657	1049
	−ve	P_{req} [W]	1474	960	1474	960
Roll	+ve	P_{req} [W]	1617	1036	1533	982
	−ve	P_{req} [W]	1533	982	1617	1036
Yaw	+ve	P_{req} [W]	1925	1262	1224	755
		($\Delta\tau$, $\Delta\omega$)	(0.74 , 0.0)	(0.54 , 0.0)	(0.0 , -105)	(0.0 , -118)
	−ve	P_{req} [W]	1224	755	1925	1262
		($\Delta\tau$, $\Delta\omega$)	(0.0 , -105)	(0.0 , -118)	(-0.74 , 0.0)	(-0.54 , 0.0)

Table 10.5: Table of Power Required for Motors 3 & 4

			Motor 3		**Motor 4**	
			c.g.$_{min}$	**c.g.**$_{max}$	**c.g.**$_{min}$	**c.g.**$_{max}$
Hover		P_{req} [W]	430	1023	430	1023
Pitch	+ve	P_{req} [W]	408	983	408	983
	−ve	P_{req} [W]	458	1074	458	1074
Roll	+ve	P_{req} [W]	441	1051	418	996
	−ve	P_{req} [W]	418	996	441	1051
Yaw	+ve	P_{req} [W]	334	766	525	1281
		($\Delta\tau$, $\Delta\omega$)	(0.0 , -175)	(0.0 , -197)	(0.12 , 0.0)	(0.33 , 0.0)
	−ve	P_{req} [W]	525	1281	334	766
		($\Delta\tau$, $\Delta\omega$)	(-0.12 , 0.0)	(-0.33 , 0.0)	(0.0 , -175)	(0.0 , -197)

10.3.6 Transition

The transition phase is defined by two sequences, namely the transition from vertical flight to horizontal flight and the transition from horizontal flight to vertical flight. Each sequence requires a different set of steps in order to be carried out. Only steps required to transition from vertical flight to horizontal flight will be outlined however it is important to note that the steps required to transition from horizontal back to vertical flight are essentially the inverse.

Hovering is the least power intensive sector of the vertical flight phase (apart from descent) and therefore it is assumed that transition always starts from hovering. During hovering, moment equilibrium holds to maintain attitude and therefore in order to ensure that both altitude and attitude are conserved during transition, both the moment equilibrium about the centre of gravity as well as vertical force equilibrium need to hold.

In order to perform the transition, horizontal velocity needs to be introduced. This is done by rotating the aft motors counterclockwise from there hovering position (pointing in the positive z-direction, thrust vector pointing upward). Simultaneously the thrust level of the aft motors must be increased to counteract the vertical thrust decrease because of the rotation.

As horizontal velocity increases, lift generated by the wing increases linearly with the square of velocity (i.e. $L \propto V^2$). This means that by subtracting the lift as a function of velocity (which is therefore a function of time) the total vertical thrust required during transition will decrease.

Figure 10.8 shows the angle of rotation of the aft motor versus the horizontal velocity during the transition. It is apparent from the graph that for the most aft centre of gravity location there is no problem attaining the stall velocity of 20 m/s before the aft motors have rotated a complete 90 °. For the most forward centre of gravity location, this is not the case since once the aft motor has completely rotated additional thrust is required to gather enough velocity to generate sufficient lift from the wing. This is not a problem as the front motor, being substantially closer to the most forward centre of gravity location, can provide enough lift to maintain altitude. Whatever moment around the centre of gravity created by the front motors can now be countered with the elevator as, with a velocity of approximately 15 m/s the elevator is sufficiently affected to deliver small control moments.

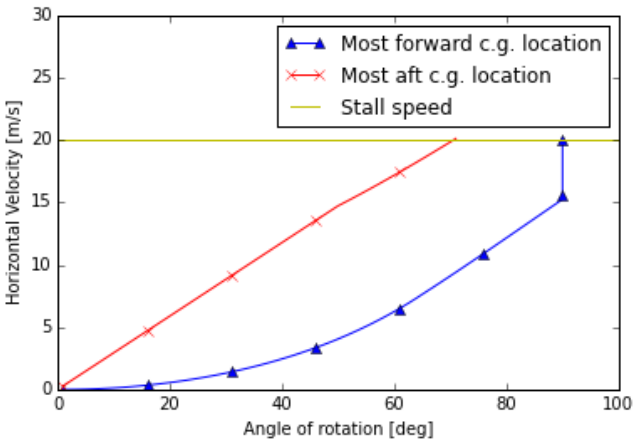

Figure 10.8: Graph of Angle of Rotation vs. Horizontal Velocity

10.4 Verification & Validation

In this section the verification and validation of the stability and control analysis and design is performed.

Tail Configuration The T-tail configuration choice can be validated by confirming that the downwash caused by the wing calculated using XFLR5 is in the order of magnitude of 0.001. Since this was one of the main reasons why the T-tail was chosen, it can be considered validated.

The incidence angle of the horizontal tailplane was checked by inspecting if the angle has a realistic value. Angles between -3 and 3 degrees are typically used [27, p. 67]. Hence, the design value of 2.6 degrees lies within realistic boundaries.

Longitudinal Stability & Control The c.g. position as a function of the leading edge calculated in the c.g. plot can be verified by calculating the actual c.g. position of the final CATIA model for the actual leading edge position and comparing it to the point on the curve. Due to time constraints, this was not possible but it can be considered as a future recommendation.

The c.g. position is now verified by making hand calculations for the minimum and maximum c.g. range for a certain leading edge position and comparing it to the value in the python code. Another way the c.g. plot was verified was to check if special inputs (e.g. all masses zero, all arms zero, all arms in the middle) also gave the required, known output (e.g. error because of dividing by zero, c.g. is zero, c.g. is in the middle). Finally, a sanity check was performed on the final c.g. range. For example: checking whether the c.g. lies inside the fuselage.

The scissor plot can be validated by checking if all the assumptions used in the model for the stability and control curve are valid. In Section 10.2, all assumptions used are explained and the effects and deviations from reality are mentioned. As can be seen, the assumptions needed for the control and stability curve deviate only slightly. The calculations are verified by checking if the input coefficients all have the correct sign and magnitude. For instance, the minimum tail lift coefficient should not exceed minus one, the lift slope coefficient should be positive and have a magnitude of one. The results of the scissor plot can be verified by performing a sanity check. Attention can be paid to the slope and the shift of the curves. For example, the neutral point should lie behind the leading edge, the slope of the control curve should be negative and the slope of the stability curve should be positive.

Lateral/Directional Stability & Control The method used to size the vertical tailplane was validated by comparing the calculated surface area with that of the surface area estimated through the statistical method outlined in literature [27, p. 112]. The method based on statistics makes use of typical vertical tail volume coefficients (c_{vt}) from which the surface area can by calculated as follows:

$$S_v = \frac{c_{vt} \cdot b_w \cdot S}{l_v} \tag{10.18}$$

It is very difficult to find typical vertical tailplane volume coefficients for UAVs however using a typical value for light aircraft, a surface area in the same order of magnitude is obtained ($S_{vertical}$ of 0.04 m^2).

Control Surfaces In order to check the control surface results, the moment generated by the control surface was calculated by hand and checked with the required moment it is supposed to generate. Also, the code was checked by putting different values for deflection angles (e.g. delta = 0 deg, delta = 30 deg) in the code and verifying if the outputs are reasonable.

The maximum hinge moment produced by the control surfaces was verified by doing the calculation by hand for the maximum deflection angle and checking whether the values comply.

Vertical Flight Manoeuvres The required power splits were calculated using a python script. This script was validated by calculating the inverse, beginning with the outputs and seeing whether the inputs were obtained as results. The inputs of the main python script were also validated with hand calculations to ensure that the script was executed using valid inputs.

Another way the the script was validated was by setting the angular accelerations for pitch, roll, and yaw ($\ddot{\theta}$, $\ddot{\phi}$ & $\ddot{\psi}$) to zero. This was done to ensure that the output of the code, given this condition, was simply the power split calculated for hovering.

11 Structural Analysis

Connecting the various components of the UAV, the structure plays an essential role in the system design effort and therefore requires a careful analysis. Due to time constraints, the focus was put on the main wing internal structure, engine-wing connection, and fuselage. The chapter presents the design approach that was used for those three components independently, followed by the main assumptions and the analysis section. The latter is divided into the analysis of manoeuvre and gust loads, wing, fuselage, and other parts such as tail and landing gear. Finally, the verification and validation procedures and an overview of the entire structure are presented.

11.1 Design Approach

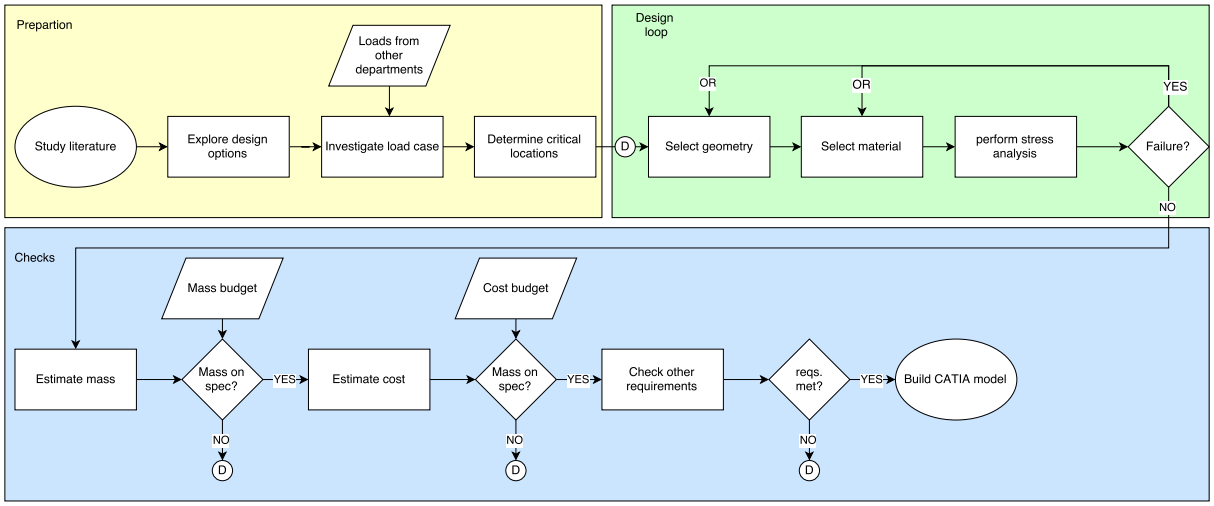

Figure 11.1: Work Flow Diagram

The design approach that was chosen for the structural analysis and design of the UAV can be split up into three different phases, which are presented in Figure 11.1. The first one is a preparation phase in which the literate study is carried out to get a grasp of possible design choices and the various loads that act on airframe structures. Gathering data such as component weights, engine thrust and aerodynamic loads from other expert departments, it is possible to determine different load cases and find the maximum values for all locations of interest. Keeping other requirements in mind, the next steps are selecting a geometry which can be expected to perform well under the given loads and a material, and then run a stress analysis. Looking at the most critical combination of stresses, the structure can be checked for failure and re-designed if necessary. This iteration loop can be executed by either selecting a different geometry, a different material or both at the same time. If the structure is able to carry all loads without failing, various checks are performed to ensure compliance with other requirements. The first one is to calculate the total mass and compare it to the allocated budget. In case it is too heavy, another design iteration loop has to be entered, which is indicated by a D in the figure. Next, a cost estimate is done to determine if the selected combination of geometry and material is producible within the budgetary constraints. Once those steps are completed, all other requirements such as environmental ones are considered and finally a CATIA model is created for verification and visualisation purposes.

11.2 Assumptions

During the design process a number of assumptions was made to simplify the analysis, while still having reasonable accuracy. The most important ones are presented below, including a short description and impact they have.

- **Maximum gust and manoeuvre loads do not occur simultaneously.** Pilots are not likely to perform high-G manoeuvres in heavy turbulence [27], therefore the load factors do not need to be added
- **There are no axial forces in wing span direction.** loads in y-direction, e.g. those induced by rolling manoeuvres, are considered negligible in comparison to lift, drag and engine thrust. This is justified by the relatively low angular acceleration values in Chapter 10
- **Stringers only carry bending and axial loads.** Their contributions to the resisting of shear and torsional loads is thus neglected in the stress and failure analyses.
- **In the structural idealisation the fuselage frames are assumed to be purely loaded in shear.** This means that the stresses in the frames that are caused by bending and axial loads are not taken into account. Also no stress criterion other than the materials ultimate shear stress is needed to determine failure of the frames.
- **The idealised fuselage skin carries only shear stresses.** In the idealised structure the boom areas have an additional area contribution to account for the load carrying capacity of the skin in bending.
- **The area moment of inertia of a stringer about its centroid is negligible compared to its Steiner term.** Since the stringers have a relatively small size compared their distance from the centroid of the entire fuselage the contribution of the parallel axes theorem dominates the MOI.

11.3 Analysis

The purpose of this section is to present the steps that were taken to design the major structural components of the wing. It therefore covers preparatory aspects such as the determination of load factors and distributions, as well as descriptions of the methodology and results. Furthermore, considerations on components that were not designed in detail are given.

11.3.1 Manoeuvre and Gust Loads

The shape and dimension of any structure depends on the loads that it is designed to withstand. In case of aircraft, loads heavily depend on the accelerations generated by manoeuvres and wind gusts, so an analysis as suggested by Raymer [27] was performed for both situations. Figure 11.2 shows the outcome, where the gust loads are indicated by solid lines and the manoeuvre loads by dotted lines. As can be seen in the figure, the gust loads are driving the design with a value of about +8.7 and -6.7 at cruise speed. These high values are mainly due to the low wing loading of 31 $\frac{kg}{m^2}$ and dwarf the manoeuvre loads of +4.4 and -1.8 found for typical general aviation utility aircraft, also in Raymer [27]. For this reason a factor of 8.7 is applied to all loads, which was also used in the load diagrams. Whenever stresses are calculated, an additional safety factor of 1.5 was taken into account. Therefore the structure was effecetively sized for a worst-case acceleration of 13 Gs at MTOW.

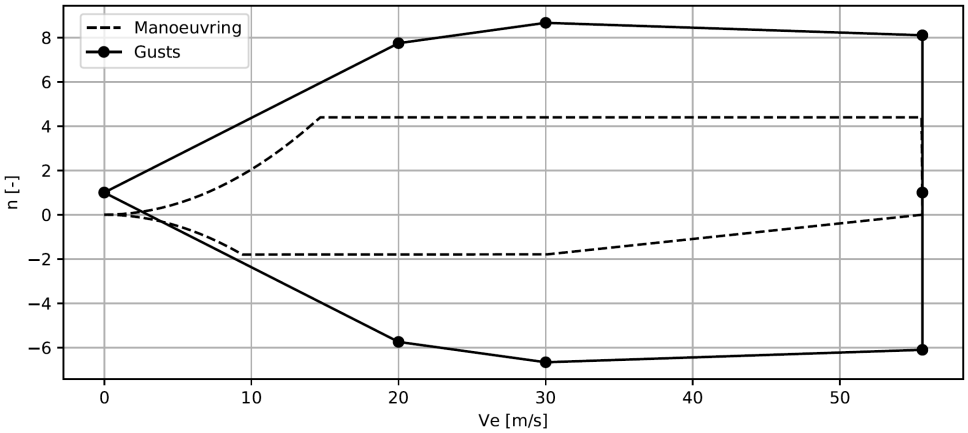

Figure 11.2: V-n Diagram

11.3.2 Main Wing

The wing design involved almost all departments, the most prominent ones being aerodynamics for skin shape and aerodynamic loads, propulsion for thrust and control & stability for engine and aileron positioning. This section deals with the load analysis, the chosen internal layout, a stress analysis including failure checks and some additional considerations which are not load-related.

Load Analysis The loads acting on the main UAV wing can be separated into three groups: aerodynamic forces in horizontal flight, vectored engine thrust and weight contributions of various components. Not all of them act at the same time and in the same direction, so a separate analysis was performed for different flight conditions, and the most critical values identified for each part of the structure. The aerodynamic loads were imported directly from XFLR5, an open-source aerodynamic analysis tool, the wing weight approximated by distributing the allocated mass budget of the wing planform and the engine and fuselage connections modelled as point forces. Figure 11.3 shows the vertical shear force and corresponding bending moment diagram for half the wing span, starting from the axis of symmetry and ending at the wing tip. The dotted vertical lines indicate sections of interest, namely, from left to right: fuselage connection, engine pylon connection, wing disassembling point, inward aileron boundary, outward aileron boundary. The three curves represent the flight situations that were analysed: clean cruise conditions, manoeuvring with maximum aileron downward deflection and vertical climb at full engine thrust. In all cases, the wing and engine weight produce a downward force and therefore a relieving bending moment, however, the lift and thrust forces are dominant. It was found that the largest maximum shear force and bending moment occurs while the UAV is manoeuvring, which is because the deflected aileron creates additional lift at a large distance from the root. On the contrary, the loads in VTOL phases are low due to the small moment arm. A similar analysis was performed in the horizontal plane, however, is not shown due to space constraints.

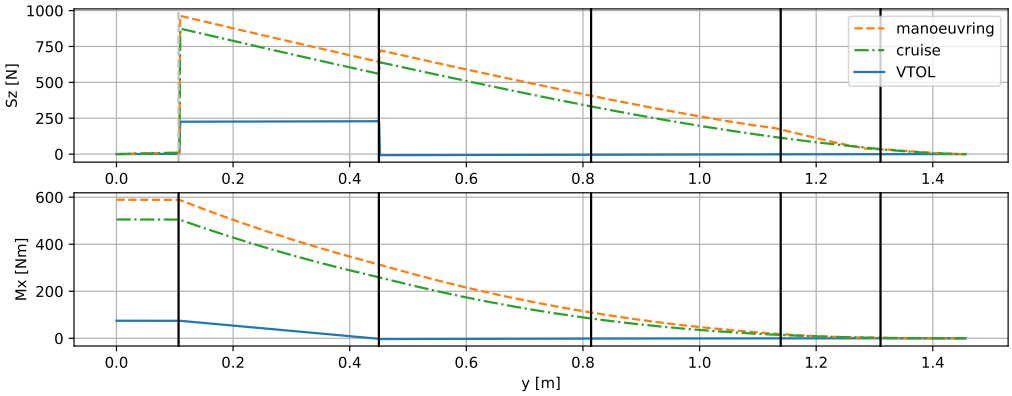

Figure 11.3: Vertical Shear Force and Bending Moment Diagram

The torque around the y-axis exerted on the wing is displayed in Figure 11.4. In this case the most critical condition is one engine being inoperative in VTOL mode, while the other one generates maximum thrust. The torques generated by the offset of the CP to the assumed shear centre of the load carrying structure is almost negligible.

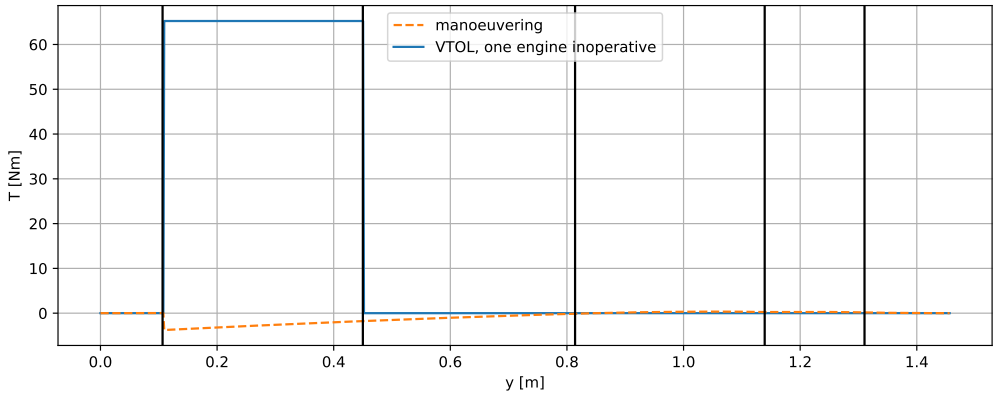

Figure 11.4: Torque Diagram

Internal Layout After determining the loads that can be expected during operations, it is possible to design a structure that is able to carry them while also meeting the remaining subsystem requirements. After performing a literature study and consulting experts from the ATMOS and 2seas UAV projects, it was decided to design a load carrying tubular structure which is connected to a thick foam skin via a limited amount of ribs. The alternative would have been a classic wing box and stressed skin including stringers, but due to time constraints choosing a proven design seemed to be the better option. Furthermore, the chosen wing planform results in a low wing loading and having internal space for systems and fuel is not necessary, so the large volume and low strength of foam structures is not problematic. Since the only requirement on the skin is to not deform under aerodynamic loads, the main focus was put on sizing the tubular structures and choosing an appropriate material. Figure 11.5 shows a rendering of the the main wing structure including the skin, the exact dimensions of the main parts can be found in Figure 11.6.

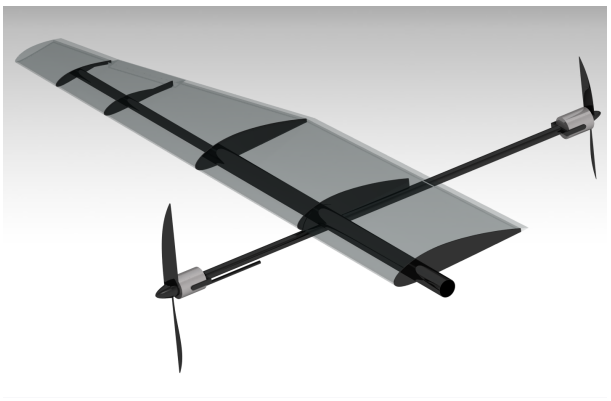

Figure 11.5: Wing Structure

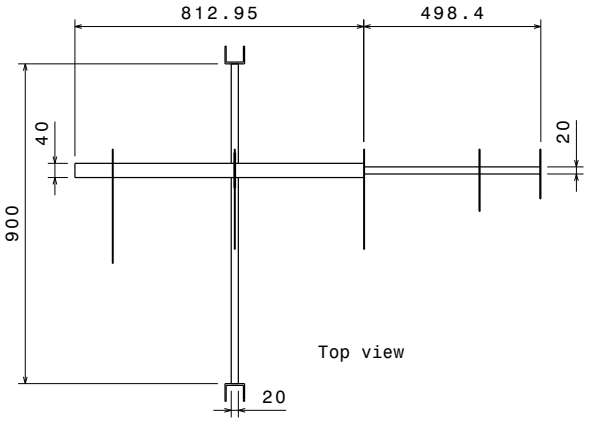

Figure 11.6: Tube Dimensions

The support structure can be broken up into three parts: the root tube, which is permanently connected to the fuselage, the detachable outer tube and the engine pylon. It was decided to use carbon fibre tubes with constant diameters because they feature a good torque resistance with minimal warping while being relatively simple to produce. The shear force and moment analysis showed that vertical loads outweigh horizontal loads, however, the weight benefit of having different MOIs per axis is not likely to justify the increase in complexity. The connection between the root tube and engine pylon is achieved via a rib attached at this position. Spanning almost the entire chord at this wing section and fully enclosing the tube it is able to efficiently transfer all loads generated by upward and forward thrust of the engines and especially the torque in One Engine Inoperative (OEI) conditions. The connection between the root and outer tube has not been designed in detail yet, but is likely to have the smaller slide into the larger to transfer shear forces and moments and include some pins to prevent twisting. Also, the requirement for quick and easy disassembly would need to be taken into account. There are other ribs placed at the location where the wing intersects the fuselage skin, the location where the wing tip is detached, the outer edges of the aileron where the actuators are attached and at the end of the outer tube. The foam skin is glued to the ribs, which are in turn connected to the tubes by a yet to be determined method. Possibilities would be using glue on low-torque sections and a clamping construction encompassing an aluminium ring within the tube, e.g. at the engine pylon mounting locations. Attached to the most outward rib is the wing tip, which fully consists of foam due to the low loads.

Material Selection Having determined the loads and selected an internal layout, the next step in the design process was to identify materials that do not fail under the applied stresses, while at the same time having low mass and cost. For the tubes in the wing, the three materials presented in Table 11.1 were considered because of their frequent application in the aerospace industry. Looking at the properties only, the uni-directional carbon-epoxy composite features superior performance in fibre direction and acceptable in the transverse, while having the lowest density of all three. For this reason it was decided to use this kind of composite, despite the very high cost per mass.

Table 11.2 shows the engineering foams considered for the wing shell, Depron and expanded polypropylene (EPP). Both are common choices in the construction of scale models, and are therefore considered suitable to carry the aerodynamic loads.

Table 11.1: Structural Materials [28]

Material	**Type**	**Density** [g/cm^3]	**E** [Gpa]	**G** [Mpa]	σ_{yield} [Mpa]	σ_u [Mpa]	τ_u [Mpa]	**cost** [EUR/kg]
Aluminium	Al 7075	2.8	71	27	103	570	330	11.6
Carbon-epoxy	T300/N5208	1.6	181	7.17	N/A	1500	68	220
Glass-epoxy	E-glass	1.8	38.6	4.14	N/A	1062	72	33

Table 11.2: Engineering Foams

	Density [**g**/cm^3]	**E** [**Gpa**]	**cost** [**EUR/kg**]
Depron	0.04	0.0144	34
EPP	0.1	0.013	17

Stress Analysis A stress and subsequent failure analysis is crucial in every structural design effort. Having determined all loads and selected a preliminary geometry it is possible to calculate stresses, check for failure and iterate if necessary. Equation 11.1 shows the formulas which were used to determine the direct stresses on each point in the tubular cross-section due to moments in the vertical and horizontal plane:

$$\sigma_{bend,x} = \frac{M \cdot x}{I} \qquad \sigma_{bend,z} = \frac{M \cdot z}{I} \tag{11.1}$$

Equation 11.2 shows the shear stresses due to the applied torque and the shear forces in x- and z-direction, where θ is defined to run counter-clockwise from the negative x-axis:

$$\tau_{torque} = \frac{T}{2At} \qquad \tau_{shear,z} = \frac{S_z}{I} tr^2 \left[\cos\theta - \cos\frac{\pi}{2}\right] \qquad \tau_{shear,x} = \frac{S_x}{I} tr^2 \left[\sin\theta\right] \tag{11.2}$$

Figure 11.7 and Figure 11.8 show the outcome of the stress analysis for the root tube-fuselage connection point, where the direct and shear stress components are superimposed separately. The maximum tensile stress is obtained at the bottom of the tube, slightly to the back. This is what can be expected due to the large aerodynamic load in combination with the forward engine thrust. Looking at the shear stress, the maxima are located at the front and the back of the tube, again due to the dominant lift forces. An analysis has been performed on the outer tube and engine pylon, resulting in very similar stress distributions.

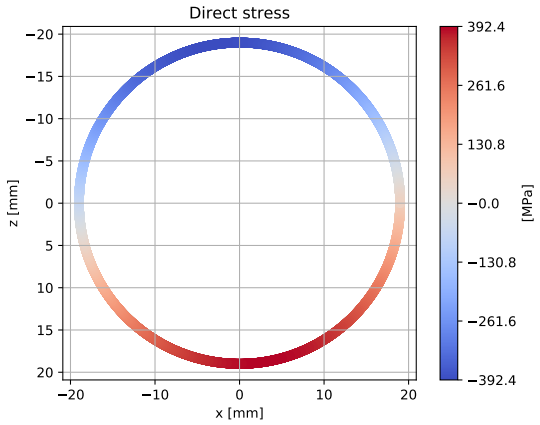

Figure 11.7: Root Direct Stresses

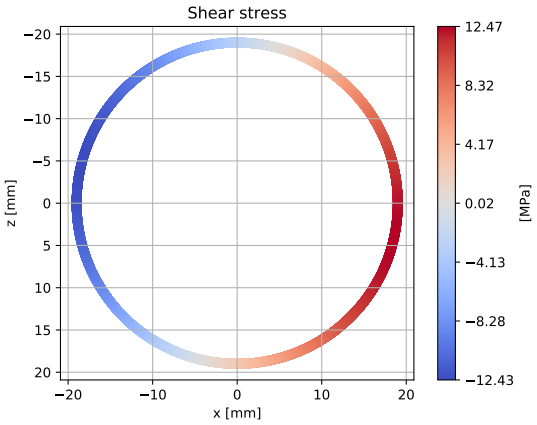

Figure 11.8: Root Shear Stresses

Failure Analysis Similar to using the von Mises yield criterion to check if a ductile material fails, failure of composites can be checked by using the Tsai-Hill criterion [29] presented in Equation 11.3. Substituting the longitudinal, transverse and shear stresses at each point in the cross-section and the material's maximum allowable values results in a distribution such as Figure 11.9. As can be seen, all values are well below 1.0, so the structure is not likely to fail in the modes considered.

Table 11.3 shows the outcome of the stress and failure analysis for all three tubes. The outer tube has a direct stress close to the ultimate, resulting in a maximum Tsai-Hill failure value of 0.732. The engine pylon appears to be over-designed since the stresses are far below the maximum allowable, however, in a pusher-prop configuration it needs to handle the compressive stresses generated by the engine and provide internal space for electric wires.

$$\left(\frac{\sigma_L}{\sigma_{Lu}}\right)^2 + \left(\frac{\sigma_T}{\sigma_{Tu}}\right)^2 - \frac{\sigma_L}{\sigma_{Lu}} \cdot \frac{\sigma_T}{\sigma_{Lu}} + \left(\frac{\tau_{LT}}{\tau_{LTu}}\right)^2 \leqslant 1 \tag{11.3}$$

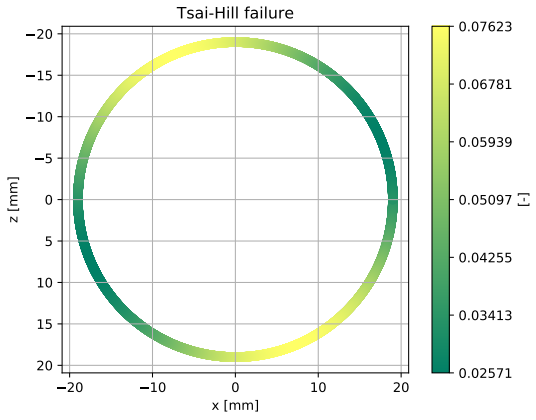

Figure 11.9: Root Tube Failure Check

Additional Considerations Due to time constraints it was not possible to cover all elements that make up a typical main wing, and the ones that had been analysed might require re-designing in light of new insights:

Table 11.3: Stress and Failure Overview

	Diameter [mm]	**Thickness** [mm]	σ_{max} [MPa]	τ_{max} [MPa]	**Tsai-Hill** [-]
Root tube	40	2	392	12.47	0.076
Outer tube	20	2	320	10.6	0.046
Engine Pylon	20	1	268	4.3	0.031

Wing tube materials: In the previous analysis it was found that a uni-directional carbon fibre material was the best option to use for the wing tubes. While this is certainly the case for pure bending and shear, there might be problems at the ribs where load introduction happens. For this reason it might be advisable to have a number of fibres in the transverse direction, to also account for those load cases. However, the decrease in longitudinal strength might lead an increase in structural weight, so an in-depth analysis is required to find an acceptable balance.

Wing skin: Foam materials are susceptible to both environmental influences and impact of foreign objects. For this reason it might be advisable to cover them with a very thin layer of fabric and resin material, which could be of the same fibre-glass type as the fuselage skin. While adding structural weight, the smooth surface increases the aerodynamic performance and, which should not be neglected, the look and feel of the UAV.

Vibrations: Vibrations induced by flutter effects and especially the engines cause additional loads, and the structure should be designed accordingly. Since they are rather difficult to predict the detailed analysis was postponed to a future design phase, however, a way to cope with them could be to apply damping at the engine hinges or adjusting natural frequencies by stiffening critical parts.

Wiring: A number of electrical components such as aileron actuators are attached to the main wing, which require wires to run throughout the structure. A natural place to put them are be the inside the carbon fibre tubes, where holes would be required to let the wires exit at the right locations. However, this measure reduces the load carrying capabilities of the tubes, so it would be beneficial to attach the wire harness to the outer side of the root and tip tubes, inside cavities of the foam structure. Because of aerodynamic reasons this is not possible for the engine pylons, but the long ribs connecting them to the root should ensure no weak points in the load introduction.

Torque reinforcements: In the design of the wing structure it was taken for granted that solid connections could be established between wing ribs and the tubes without difficulties. If the detailed design of the connectors showed that torsion is a problem which cannot be solved using the current single-tube design, additional tubes could be installed to distribute the moments more evenly. Figure 11.10 shows a possible reinforcement concept for the engine pylon connector rib, which has to bear the main share of all torsional loads. If necessary, this second rod could be extended to other ribs to enhance the torsional stiffness.

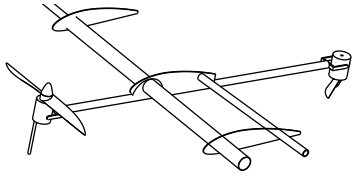

Figure 11.10: Reinforced Wing Structure

11.3.3 Fuselage

Load Analysis In the load analysis of the fuselage, the forces and moments about the aircraft's principal axes are determined for a wide range of operational situations. Out of these, the most critical ones are selected to guide the design.

The foreseeable loads to which the fuselage will be subjected during the UAV's operational life are divisible into:

- In-flight manoeuvre loads
- Gust loads
- Take-off and landing loads
- Ground handling loads

This analysis mainly focuses on the in-flight manoeuvre and gust loads. The maximum design load factors for both gust and manoeuvre loads are 8.7 and 3.0 respectively, see the V-n diagram in Figure 11.2. On top of the aforementioned load factors a safety factor of 1.5 is also included to ensure safe operations within the design limits and to have a safety margin.

The strongest bending moment about the y-axis as well as the highest vertical shear force loading are encountered during a maximum load factor pull up from a dive whilst in the fixed wing flight mode. The corresponding internal shear force and bending moment throughout the fuselage are depicted in Figure 11.11. The vertical dashed lines indicate the positions of the start of the payload bay, the fuselage mounted battery pack, the wing-fuselage connection, the end of the payload bay and the tail-fuselage connection. The maximum vertical shear force and bending moment are encountered during a maximum load factor gust. These occur at the wing fuselage intersection and are 1642 N and 606 Nm respectively. The maximum torque on the fuselage is 60.9 Nm and at full thrust the highest axial tensile load is 246 N. The strongest bending moment about the z-axis and horizontal shear load occur in the case of a one engine out scenario, in which the remaining engine is operating at full thrust. The internal bending moment M_z and the shear force S_y are 83 Nm and 81.6 N respectively in this case.

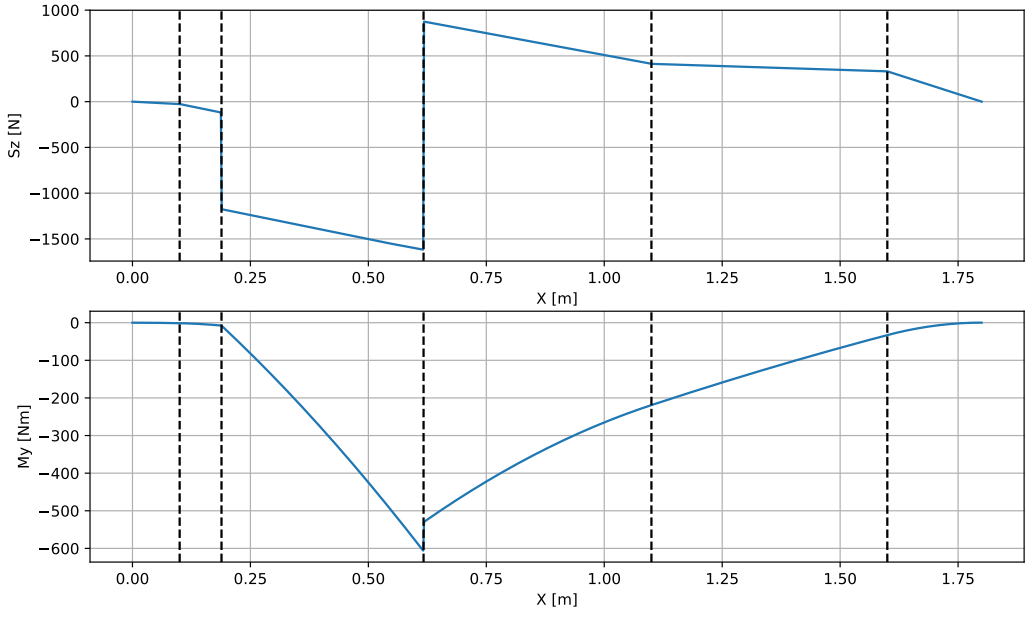

Figure 11.11: Vertical Shear Force and Bending Moment in the Fuselage

Internal Layout Figure 11.12 shows the internal layout of the vehicle. On the bottom floor of the centre section of the fuselage the payload bay is located. It is accessible from the underside and has dimensions of 0.15 x 0.15 x 1.0 m (width x height x length). In the nose section two 0.082 x 0.045 x 0.162 m battery packs are situated in front of the main avionics. The wing intersects the fuselage above the payload bay so that the internal load carrying structural elements of the wing are not interrupted. Along the length of the fuselage, seven frames are placed at the main locations of load introduction into the fuselage and to interrupt some large singular pieces of skin that would otherwise buckle under compression stresses. Frame one guides the inertial loads from the avionics and batteries into the rest of the structure. Frames two and six disperse the loads introduced by the front and rear landing skids. The loads generated by the main wing will be introduced into the fuselage via frames three and four, whilst frame seven will introduce the tail loads into the fuselage structure. The frame protects the skin in the centre part of the fuselage around the payload from buckling. Another important feature of this design is the accessibility of the payload bay from the bottom side of the fuselage. The frames in the middle section of the fuselage are essentially cut to allow the floor of the payload bay to be released. The bottom sections of the frames are part of the standard payload bay floor and thus the frames are closed in flight. Only during ground handling the frames will actually be open. On the contrary, the payload module with dropping capability will have open section frames during flight. Therefore, this payload bay has an additional reinforcing structure to support the now significantly weaker frames, mainly in torsional loads. The motivator for this choice was that no one closed frame structure could be designed within the given mass budget. And since only a small fraction of the foreseen missions for the UAV actually require dropping of the payload, it is more efficient to only let those missions cope with the associated payload weight penalty.

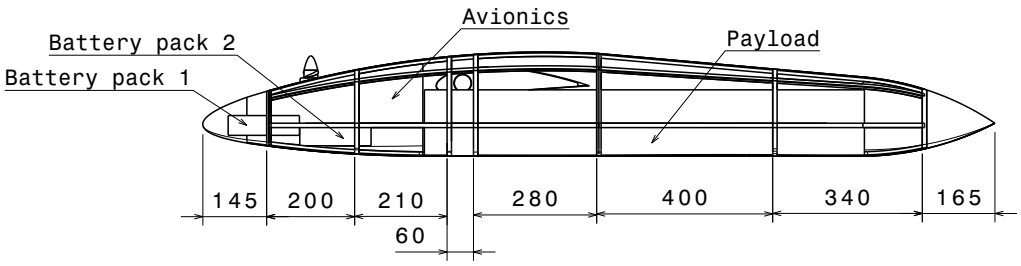

Figure 11.12: Internal Layout of the Hybrid UAV

Between the first and seventh frame a total of seven stringers run in the longitudinal direction. Their positions are shown on frame 4 in Figure 11.13. The stringers have T-shaped cross-sections with 10 by 2 mm webs and flanges. They are bent to follow the curvature of the fuselage.

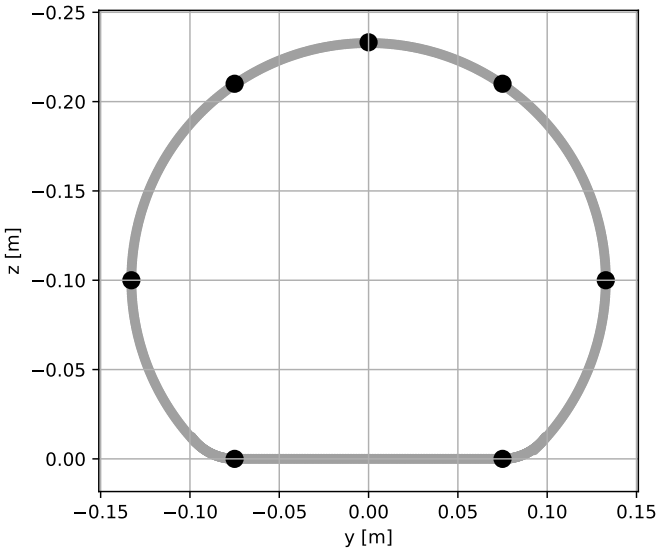

Figure 11.13: Stringer Locations on Frame 4

Stress and Failure Analysis The stresses resulting from the loads discussed before are analysed by applying the method of structural idealisation [30]. The bending moments on the fuselage which are in reality resisted by both the longitudinal stringers and the fuselage skin are assumed to be carried by a series of concentrations of area known as booms. These have a cross-sectional area that accounts for both the stringers and the skin in between a boom and its neighbouring counterparts as can be seen from Equation 11.4.

$$B_1 = B_{stringer} + \frac{tb}{6}\left(2 + \frac{\sigma_2}{\sigma_1}\right) \tag{11.4}$$

The contribution of the skin to the boom areas is based on the change in stress between the booms as to constrain equal elastic deformation in both the original and the idealised structure. The second moments of area of the idealised structure about the neutral axes are evaluated by taking only the Steiner terms of the booms. Then, the bending stress in each boom can be determined with Equation 11.1.

$$\sigma_x = \frac{T_{max}}{\sum_{r=1}^{7} B_r} \tag{11.5}$$

The highest total direct stress is acquired by adding the stresses caused by the strongest axial load, calculated with Equation 11.5. An overview of the boom stresses at the wing-fuselage connection can be found in Table 11.4. The bottom section of the fuselage which lies beneath the neutral axes of bending is loaded in compression. On the other hand, the top part of the fuselage is loaded in tension. This means that in the lower section the tensile direct stresses from the axial loads increase the total stress. Conversely, in the upper section the direct loads actually provide a small amount of stress relief.

The fuselage skin and frames are carrying the shear and torsional loads acting on the vehicle. They are analysed for shear stress at the wing fuselage intersection, where both the torque and shear loading are highest throughout the structure. In accordance with the structural idealisation method from [30], the shear flow is assumed to be constant between booms. The

Table 11.4: Fuselage Boom Stresses at x=0.617 m

Boom	$\sigma_{x_{bending}}$ **[MPa]**	$\sigma_{x_{axial}}$ **[MPa]**	σ_x **[MPa]**
B_1	21.6	0.7	22.3
B_2	1.6	0.7	2.3
B_3	-16.1	0.7	-15.4
B_4	-17.6	0.7	-16.9
B_5	-10.8	0.7	-10.1
B_6	11.1	0.7	11.8
B_7	27.0	0.7	27.7

shear flow in a piece of skin past boom n is then given by Equation 11.6

$$q_{s_n} = -\frac{S_y}{I_{zz}} \sum_{r=1}^{n} B_r y_r - \frac{S_z}{I_{yy}} \sum_{r=1}^{n} B_r z_r \tag{11.6}$$

The vertical shear force's line of action passes through the shear centre as it lies in the plane of symmetry. The horizontal shear loads do in reality induce additional shear stresses on the fuselage as both the engines and the vertical tail do not generate forces in line with the shear centre. Therefore, the horizontal shear loads are treated as a superposition of cases of pure shear and torsion. The location of the shear centre is approximated by the centroid of a circle with a radius equivalent to that of the actual fuselage. Although this introduces a small error in the model, it is only minor since the horizontal shear forces are an order of magnitude smaller than their vertical counterparts. Next, the shear flow due to a torsional load is calculated with Equation 11.7.

$$T = 2Aq \tag{11.7}$$

Now, the actual shear stresses are found by dividing the shear flow in each section by the skin thickness, which is 0.5 mm (Equation 11.8).

$$\tau = \frac{q}{t} \tag{11.8}$$

The resulting stresses are shown below in Table 11.5. Since the skin and frames are assumed

Table 11.5: Fuselage Shear Stresses

Section	τ_{S_z} **[MPa]**	τ_{S_y} **[MPa]**	τ_{M_x} **[MPa]**	τ **[MPa]**
$s_{1,2}$	-6.8	$-1.1 \cdot 10^{-1}$	1.1	-5.7
$s_{2,3}$	-7.8	$2.4 \cdot 10^{-1}$	1.1	-6.9
$s_{3,4}$	-3.6	$3.8 \cdot 10^{-1}$	1.1	-2.8
$s_{4,5}$	3.6	$3.8 \cdot 10^{-1}$	1.1	4.4
$s_{5,6}$	7.8	$2.4 \cdot 10^{-1}$	1.1	8.7
$s_{6,7}$	6.8	$-1.2 \cdot 10^{-1}$	1.1	7.8
$s_{7,1}$	$-1.2 \cdot 10^{-3}$	$-4.26 \cdot 10^{-17}$	1.1	1.1

to only carry shear stresses, whilst the stringer resist all the axial and bending loads, they can be compared directly to the materials ultimate stress. As Table 11.1 shows, Glass-epoxy is strong enough for to endure all of the stresses shown in Table 11.5 and Table 11.4.

Material Selection The stringers, fuselage frames and skin are to be made out of a glass fibre epoxy composite. This material was chosen over aluminium and carbon fibre composites because it combines low cost and high strength. As Figure 11.1 shows, the material and geometry where first selected and then the stress analyses and budget checks were performed. Every combination of geometry and aluminium considered either failed or violated the mass budget. Since the extra strength that carbon fibre offers over glass fibre was not needed according to the stress analysis, Glass fibre was chosen because it is significantly less expensive.

11.3.4 Tail

Due to limited resources it was not possible to design the vertical and horizontal tailplanes with the same level of detail as the main wing and fuselage, however, a preliminary internal structure was established to determine the expected cost and mass. For the main wing the combination of carbon fibre tubes for load transfer and engineering foam for having an aerodynamic shape proved to be beneficial, so it was decided to use a similar concept for the tail. The vertical tailplane would therefore consist of a a hollow carbon fibre tube surrounded by a solid layer of foam. Attachment of the rudder hinge and actuator would ideally be directly at the tube and not at ribs, however, those could be added if necessary. The tube supporting the horizontal tail is then fixed to the vertical one, with a similar hinge/actuator placement for the elevator.

11.3.5 Landing Gear

Since the UAV is expected to take off and land vertically, the landing gear design can be very simple and light. Two aerodynamically shaped blocks of rubber are attached to the fuselage frames number 2 and 6 in Figure 11.12 to dampen the impact loads that occur during landings. The ground clearance is very limited with this configuration, however, the sensor layout allows for scanning of downward surfaces and can therefore ensure that the ground is smooth enough for safe landings. Furthermore, the skin at the belly could be reinforced if frequent outdoor landings are required by a customer. Tipping over onto the wing tips is prevented by installing carbon fibre rods to the front engines, as shown in Figure 11.14. This configuration ensures a side tip angle of no more than 5.75 degrees and, tilting backward with the engine casing, stores in a aerodynamically favourable position without the need of extra mechanisms.

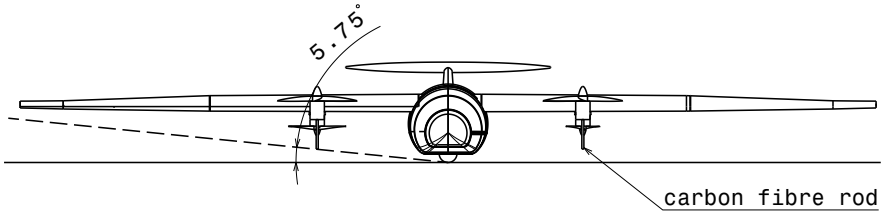

Figure 11.14: Ground Clearance

11.3.6 Integration

In the previous sections all structural components that have been designed were presented separately, however, together they form a single subsystem of the UAV. Figure 11.15 shows the complete skeleton, which comprises the main wing, engine pylons, fuselage and the preliminary tail. As previously mentioned, the wing tips can be easily removed while the rest of the wing is rigidly connected to the fuselage frames. This configuration does not lead to the smallest possible transportation size, as can be seen also in Section 14.1, however, having uninterrupted parts where the loads are highest generally allows for a lighter design. Since the tail has not been designed in detail, also the connection to the fuselage is to be determined yet. It is expected

though that the loads on the tail are introduced to the fuselage via the rearmost frame, which would need to be reinforced accordingly.

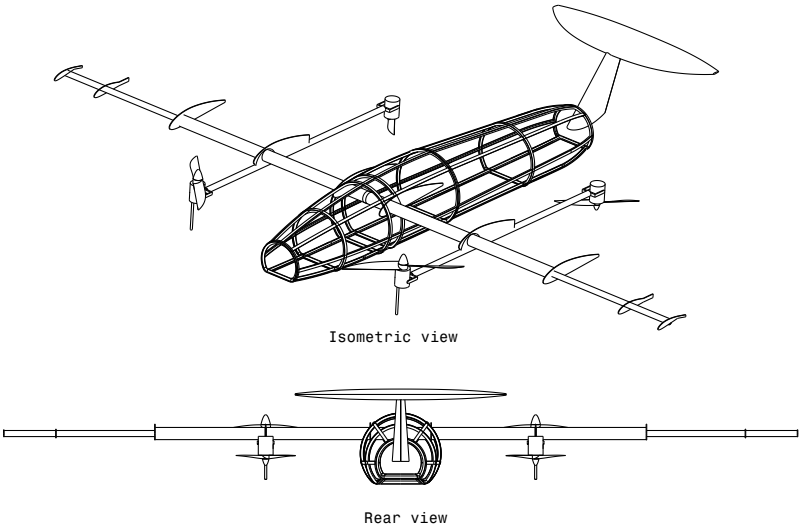

Figure 11.15: Internal structure of the UAV

11.4 Verification & Validation

Verification of the tools used and validation of the resulting outcomes are of vital importance to the credibility of any analysis. In this section the verification and validation procedures for the structural analysis are described.

Loads The loads throughout the wing and fuselage were computed with Python scripts with the data retrieved from the master document. To verify these scripts they were subjected to unit testing methods. Simple loading cases comprising combinations of 1 N forces were analysed by the script and the resulting maximum and minimum shear force and bending moments as well as their locations were compared to calculations performed by hand.

Stresses The stresses in the structural components of both the wing and fuselage were calculated using scripts written in Python. They used the loads calculated before, inputs from other subsystems and the geometry of the parts to evaluate the stresses in the structure.

The verification method for these scripts was similar to the one followed to verify the load calculations. Different loads and stringer locations were fed into the script to uncover a source of error. For a configuration in which some stringers where very close to the centroid of the cross-section erroneous boom areas resulted. This could be traced to a limitation of Equation 11.4, where the boom area will approach infinity as the distance of a given boom approaches the neutral axis.

For the fuselage the results from the stress analysis were compared to the those from a calculation performed by hand. For this calculation the fuselage was simplified as a thin-walled tube with an equivalent diameter and was put under the same loads. This was not accurate enough to fully validate the results from the stress analysis. However, a more elaborate validation procedure was not possible within the given time constraints. Furthermore, the order of magnitude of the results was proven to be the same. In the future, an improved validation could be performed with a finite element method stress analysis on the CATIA model.

12 Command & Data Handling

In this chapter the command and data handling subsystem is designed. This includes all UAV avionics and the general design of the ground station. First the design approach is illustrated in Section 12.1 using a flow chart. Then in Section 12.2 the avionics of the UAV are designed. In Section 12.3 the ground station is explained together with different payload modules. Finally, sections 12.4 to 12.7 show the communication flow diagram, data handling block diagram, hardware diagram, software diagram, and the electrical block diagram.

12.1 Design Approach

In Figure 12.1 the design approach is visualised. In order to start the design of the command and data handling subsystem, first the a literature study on the different required modules in order to sustain autonomous flight has been performed. Here, it was found out that the most important part in the subsystem design the flight controller is. After having chosen an adequate flight controller, the next steps were to take a look into suitable required sensors and a telemetry system. Using software, hardware, data flow and communication flow diagram, the final choices were checked for their feasibility. This means the data rate was compared to the actual sampling rate of the sensors and cost, mass and power budgets were analysed.

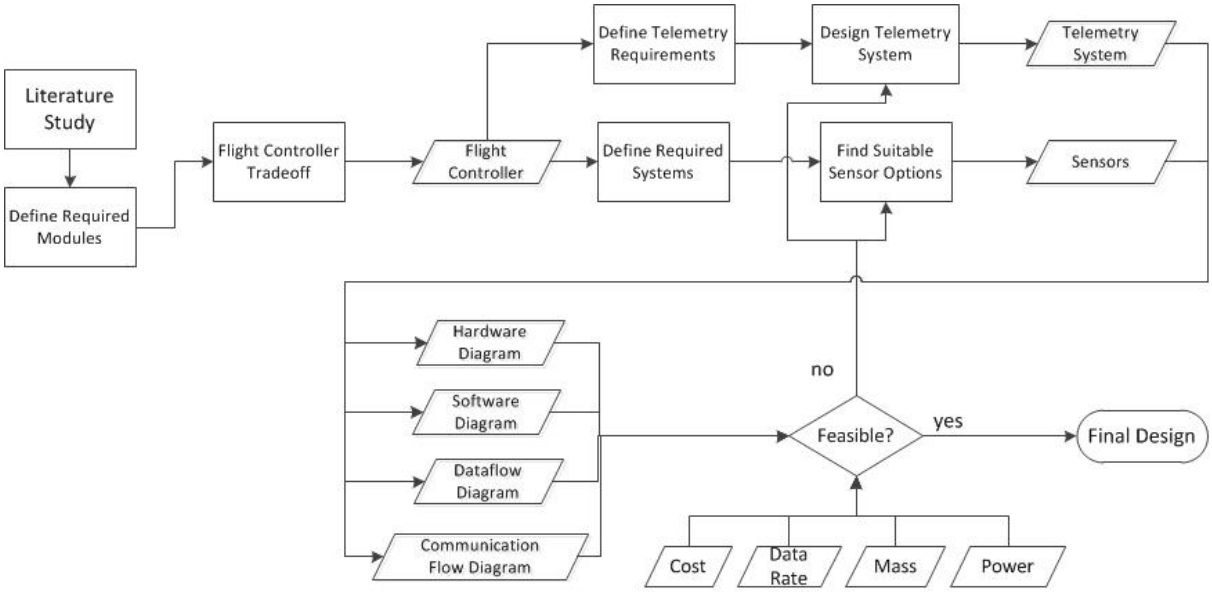

Figure 12.1: Command and Data Handling Work Flow Diagram

12.2 Avionics

In this section, all avionics used in the preliminary design will be explained. In order to cut down on cost as batch size increases, in future design stages some of the selected systems will be replaced by in-house designed systems. However, that would mean requirement SYS-OP-2.3 (electrical components used should be off-the-shelf parts) has to be discarded.

An overview of the systems that were selected can be found in Table 12.1. This was done based on the requirements in the SYS-OP category and on extensive online research. Further specifications on the selected systems can also be found here. In Section 12.2.1 a comparison is made between different available systems. The design of the telemetry system is discussed in Section 12.2.2. Finally, in Section 12.2.3 a secure communication protocol is established.

Table 12.1: List of Avionics Subsystem Components

System type	Selected system	Price	System specifications
Flight control module	Pixhawk 2.1[1]	175 EUR	Isolated IMU (3x accelerometer, 3x gyroscope, 3x magnetometer, 2x barometer), flight controller board, multiple input ports, micro SD card for internal memory. Estimated size 10x5x2 cm, estimated weight 200 g.
Software	Paparazzi[2]	0 EUR	Open-source, easy implementation of different functionalities
Ground avoidance system	SF30-C Laser Rangefinder[3]	620 EUR	Range 100 m, accuracy ±0.1 m, weight 35 g, dimensions 30 x 55 x 50 mm
Object avoidance system	Jenoptik DLEM 20[4]	Estimated at 1000,- EUR	Sensor uses flight control module for avoidance of obstacles. Dimensions 50 mm x 22 mm x 34 mm, weight 33 g, range 5 km, accuracy 0.5 m.
GPS	Here GNSS for Pixhawk[5]	43 EUR	Concurrent reception of up to three GNSS, -167 dBm navigation sensitivity, weight 49 g, dimensions 8x8x2 cm.
2x Airdata sensors	Digital Airspeed sensor[6]	115 EUR	0.84 Pa resolution, Kit dimension 24x17x10 mm. Mounted at both wingtips.
Radio Control	Frsky V8FR-II receiver[7]	14 EUR	2.4 GHz, Weight 39g, dimensions 34x19x8 mm.
	FrSky 2.4GHz Accst Taranis X9D PLUS[8]	160 EUR	RC Transmitter for the ground station.
Telemetry	u-Blox TOBY L2-series [9]	60 EUR	Weight 4.8g, dimensions 25x36x3 mm.
Payload link	USB or other cable	Estimated at 10 EUR	Pixhawk module has multiple extra ports for both power and camera modules.
	Estimated total:	EUR 2200,-	Estimated total size: 400 cm^3, 400g.

12.2.1 Trade-off

In this section, different options for the flight control and positioning systems are discussed. The systems need to be able to measure axial and angular accelerations, orientation, attitude, altitude, distance to the ground, distance to obstacles, and determine its global position. The communication system will be discussed in Section 12.2.2.

In Table 12.2, an overview of (combinations of) systems is given. These can determine all

[1] `http://www.robotshop.com/en/pixhawk-21-standard-set.html`, Accessed on 12-06-2017

[2] `http://wiki.paparazziuav.org/wiki/Pixhawk`, Accessed on 22-06-2017

[3] `http://www.robotshop.com/en/sf30-c-laser-rangefinder-100m.html`, Accessed on 13-06-2017

[4] `https://www.jenoptik.com/products/defense-and-security/laser-rangefinders/oem-modules-system-integration/dlem`, Accessed on 13-06-2017

[5] `http://store.jdrones.com/digital_airspeed_sensor_p/senair02kit.htm`, Accessed on 21-06-2017

[6] `https://www.unmannedtechshop.co.uk/here-gnss-module-for-pixhawk-2/`, Accessed on 22-06-2017

[7] `https://hobbyking.com/en_us/frsky-v8fr-ii-2-4ghz-8ch-receiver-hv.html`, Accessed on 20-06-2017

[8] `https://hobbyking.com/en_us/frsky-2-4ghz-accst-taranis-x9d-plus-digital-telemetry-radio-system-mode-2.html`, Accessed on 22-06-2017

[9] `https://www.u-blox.com/en/product/toby-l2-series`, Accessed on 19-06-2017

previously mentioned flight parameters and are able to process some data from for example monitoring equipment. For some of the systems the exact size or weight is not known. In these cases, sizes are estimated based on reviews and images. When this was deemed too inaccurate, no size has been given. This overview is then used to perform a trade-off between the different system layouts. First, weights were determined. The CPU has been assigned with the greatest weight factor, since it is the driving factor in a lot of missions. Size, including weight and dimensions, modularity, defined as the amount of available connections, and accuracy have been given equal weights. They are considered very important, however not as significant as the CPU. Size can make it very hard to carry the module and could pose some severe constraints on the structure. Modularity is essential to the connection of different controllers and monitors, yet for most boards it is possible to overcome this by installing intermediate connectors. Accuracy is essential to the control of the UAV. Then cost, GPS, and software were assigned with the smallest weight. The cost of all of the systems was found to be within the budget limits, a separate GPS system could be added in case the current system is not accurate enough, and software modules could also be changed. Then each of the concepts has been graded per criterion, where '- -' means that performance is extremely poor, '0' means average and '+ +' means very beneficial to the design or system. Then based on these weights and scores, the systems have been assigned with a grade that was found by adding or subtracting the weight factors as the scores stated it, then dividing by two and adding 40. That means scores between -15 and 105 are theoretically possible.The range was made larger (than from 0 to 100) to make different scores more outspoken.

Table 12.2: Overview of Flight Control Systems

System(s)	**Specifications**	**Price, Size**
Navio2 Autopilot, Raspberry Pi 3	GNSS receiver, extension ports, includes power module, dual IMU, 10 cm resolution barometer, 14 PWM servo outputs, 1.2GHz 64-bit quad-core ARM Cortex-A53 CPU, Integrated 802.11n wireless LAN and Bluetooth 4.1, software still required.	232 EUR, 2x 55x65x15 mm, 68g
Radiolink PixHawk 1	32bit STM32F427 Cortex M4 core with FPU, 256KB RAM, 3-axis IMU, 16 bit gyroscope, 14 bit accelerometer and magnetometer. Size estimated.	129 EUR, 100x40x20 mm, 100g
Lynxmotion Quadrino	Nano Drone/UAV Flight Controller, Software included, IMU, Expansion ports, ATmega 2560 (256Kb flash @ 16MHz) Processor.	137 EUR, 53x53x17 mm
MWC MultiWii	2 Servo output for camera (only available when using 4 motors or less), Separate 3.3V and 5V LDO voltage regulators.	21 EUR, 36x36x2 mm
AfroFlight Naze32 Rev6	Up to 8 ch RC input, 32-bit processor running at 3.3V/72MHz. BMP280 barometer.	20 EUR, 36x36 mm, 7.3g
DJI Naza-M V2	Software included, Intelligent Orientation Control, PPM, S-BUS & Ordinary Receiver Supported, Built-in Gimbal Stabilisation Function, Remote Gain Adjustment, Hovering Accuracy (GPS Mode) Vertical:±0.8m, Horizontal:±2.5m .	146 EUR, 4x 45x45x10 mm, 95 g
Pixhawk 2.1, Here+ GNSS	Modular design for flexibility, Triple Redundant IMU system, Modular cube. All inputs/outputs in one single DF17 connector, Concurrent reception of up to three GNSS, -167 dBm navigation sensitivity.	225 EUR, GPS 79x82x17 mm, 49g
Paparazzi	Open source software and hardware, all required components can be installed, manuals available. Hardware cost and size estimated.	92 EUR, 50x50x10 mm, 50g

Table 12.3: Flight Control Trade-Off

Concept \ Criterion	Size	Cost	CPU	Modularity	GPS	Accuracy	Software	Result
Navio2	-	-	++	++	+	+	-	**78**
Pixhawk 1	0	0	+	++	+	+	+	**70**
Lynxmotion	+	0	0	+	+	++	+	**65**
MultiWii	++	++	- -	- -	-	0	++	**28**
Afroflight	++	++	- -	-	-	0	-	**25**
DJI Naza M	- -	0	+	+	++	- -	+	**43**
Pixhawk 2.1	0	-	++	++	++	+	+	**80**
Paparazzi	+	0	++	++	++	++	++	**95**
Weight	10	5	20	10	5	10	5	

From Table 12.3 it can be seen that the MultiWii and AfroFlight system are not suitable for this UAV. The DJI Naza M also underperforms, however, not as much as the other two. On the other hand, the Pixhawk 2.1 and the Paparazzi system are the winners of this trade-off, closely followed by the Navio2 system. Solely based on the trade-off, the most logical option to choose the Paparazzi system. However, this system also has no ready to go hardware, which means it still needs to be built. Requirement SYS-OP-2.3 states that all electrical components should be off-the-shelf. The Paparazzi system is not qualified as such, and therefore the hardware used will be the Pixhawk 2.1. Since the Paparazzi software does allow for easy adaption as it is open-source, this will be used instead of the Pixhawk software. Paparazzi software is easily implemented on the Pixhawk module[10].

Object Avoidance The object avoidance system was selected after the flight control module. Initially, a trade-off is performed on these as well. Both a ground sensor as well as a sensor that functions as the 'eyes' of the UAV need to be selected. For these sensors, different options are available. Some options and their (dis)advantages can be seen in Table 12.4. Based on this comparison and the need for a sensor that can detect objects located up to 3 km away (Requirement SUB-AV-3.2), laser rangefinders were found to be the most suitable option. Some research was done on suitable laser rangefinders, and it was found that especially for the object avoidance, not a lot of options were present. The selected ground detection system was the cheapest one within acceptable sizes and acceptable detection range (Requirement SUB-AV-3.3). The selected object detection system was the only one that was within acceptable size limits while being able to detect objects very far away (Requirement SUB-AV-3.2). The specifications of these systems can be found in Table 12.1.

[10] See footnote 2.
[11] `https://www.intorobotics.com/types-sensors-target-detection-tracking/`, Accessed 20-06-2017
[12] `https://www.rli.com/resources/articles/classification.aspx`, Accessed 20-06-2017

Table 12.4: Object Avoidance Sensor Types[11]

Type	Advantages	Disadvantages
Laser rangefinder	Ranges varying from 10 cm to up to 25 km. Laser has to return, yet does this at the speed of light making it very fast.	Accuracy comes at high cost. Eye-safety must be taken into account meaning not all lasers can be used (only class 1 and 2)[12]
LIDAR	Very accurate.	Complete 3D surfaces can be mapped, which means more CPU is used than required for the purpose, expensive, large, heavy.
Infrared	Cheap, direct response, can also be used at night.	Very sensitive to sunlight.
Doppler radar	Used more often in aviation.	Measures relative velocity, not distance; signal needs to bounce back.
SONAR	Can also detect very small objects.	Very expensive, large.

12.2.2 Telemetry System

In this section, the Radio Control (RC) system used for Visual Line of Sight (VLOS) is discussed. Then, different possible telemetry systems for Beyond Visual Line of Sight (BVLOS) communication are introduced and a final system is chosen.

VLOS In order to control the UAV in VLOS, an RC receiver is added to the telemetry system of the UAV. The main purpose of this receiver is to obtain flight commands sent by the operator while in VLOS. These flight commands are sent directly to the UAV and are used in order to change thrust and provide control over the different control surfaces. It means that the operator can control the deflection angles and magnitude of thrust directly via the controller.

Although the long range telemetry system described in the next section could also be used for this purpose, an RC transmitter is preferred in close range due to the lower latency as a direct link is established between an operator and the UAV. Also the reliability of an RC link is higher as the package loss is decreased due to the closer range.

One disadvantage of the RC link is that it is only used as a one-way link. Measurements of the different sensors are not sent towards the ground station, hence it is only used for VLOS control. Data gathered on-board the UAV is sent using the cellular link or has to be stored on the internal memory in case the cellular link is broken or unavailable.

The most common RC link uses frequency of 2.4 GHz. Comparing different 2.4 GHz receivers, it was concluded that a Frsky V8FR-II receiver will be used[13]. It uses eight channels, four used to simultaneously control rudder (change in yaw angle), elevator (change in pitch angle), throttle (change in thrust) and ailerons (change in roll angle). One remaining channel is then used for the tilting mechanisms of the motors, making it possible to manually perform a transition from vertical to horizontal flight. The last three channels can be used for different payload modules which might require separate control, such as opening and closing the payload bay, rotating cameras or dropping the payload. In case none of these are necessary, it can be decided that the three remaining channels are coupled to the 4 engine tilting mechanisms separately. This makes it possible to control the rotation of a single engine and can be used for control in vertical flight for example.

[13] `https://hobbyking.com/en_us/frsky-v8fr-ii-2-4ghz-8ch-receiver-hv.html`, Accessed on 19-06-2017

BVLOS The main requirement set for the BVLOS telemetry system is given by requirement SYS-PF-1.3, stating that the UAV, shall be capable of achieving a range of 200 km. As radio frequency communication can not reach these ranges, two alternatives are presented in this section:

1. **Satellite Modem**

   In order to increase the range, a satellite modem could be used. This first sends the data towards a satellite which in turn redirects it towards the drone. The main advantage is that most areas of the Earth are covered and BVLOS operation is thus possible. While using a satellite modem, there are no range limitations. A major disadvantage is the higher latency, as propagation and processing delays can be up to one second for a geostationary satellite connection. Furthermore, costs for using a satellite link are expensive and data rate dependant. Comparing only the data flow of the sensors, a constant flow of up to 65 kbps can be necessary (see Section 12.5). Using the Iridium satellite network, this results in a cost of around 6 euro per second transmitting all the relevant data, which does not include yet live video feeds or other data consuming devices mounted in the payload[14].

2. **GSM/LTE Modem**

   Global System for Mobile Communications (GSM) and Long Term Evolution (LTE) modems make use of mobile cellular networks for the data transfer. As mobile telecommunications are widely available nowadays, using a GSM/LTE modem greatly increases the range compared to a radio modem. On top of that, data rates of up to 50 Mbps can be achieved in good conditions[15]. Although this makes it possible to perform BVLOS operation, cellular networks are less developed in developing countries and do not cover oceans at all. This reduces the possible operational areas significantly compared to satellite networks. The cost of data services is relatively low compared to satellite links. Several distributors in the Netherlands provide 10 GB of data transfer for approximately 30 EUR per month[16].

Although the higher coverage of satellite communication is preferred for save and rescue missions, the cost is limited and high data transfer is required in order to obtain a reliable video feed for monitoring. Furthermore, satellite communications require bigger antennas in order to achieve a safe and reliable data connection. Another major advantage of using cellular networks is the fact that the packages are sent using conventional networking technologies and hence also routed this way. This makes it easier to securely deliver the messages, which is in more detail explained in Section 12.2.3. For these reasons, a GSM/LTE modem is used as the large-range telemetry system. This then also comes with the advantage that in order to control and monitor the drone only an internet connection is necessary.

The chosen GSM/LTE modem is a u-Blox TOBY L2-series LTE Modem. It can be connected directly to the Pixhawk Flight Controller via UART. Care should be taken that the correct module is chosen depending on the geographical location where the drone is operating.

Final Layout Finally, the UAV uses a cellular network connection as the main telemetry system. Via an internet connected device, way points can be sent to the telemetry module for navigation. The flight controller then chooses the best control inputs to perform the mission. Furthermore, higher data rates are supported using this connection, hence also attitude data and monitoring data is sent on this channel.

[14] `http://www.rock7mobile.com/products-rockblock`, Accessed on 19-6-2017

[15] `https://www.u-blox.com/sites/default/files/TOBY-L2_DataSheet_%28UBX-13004573%29.pdf`, Accessed on 12-06-2017

[16] `https://www.kpn.com/mobiel/mobiel-internet/simkaart/mobiel-internet-standaard/1-jaar`, Accessed on 19-06-2017

A second, more reliable link is created using the RC connection. This connection can only be used for lower ranges (up to 2 km) and hence it is only used for VLOS operation. Using the RC channel, the operator can control the thrust as well as pitch, yaw, and roll angles. Transitioning from vertical to horizontal flight will also be possible using the controller. RC communication is thus preferred in case a higher precision is required, as position determination is otherwise dependant on GPS accuracy.

In case the flight controller receives messages from both links, the newest messages are preferred and performed. Furthermore, in case the main cellular link breaks, the flight controller tries to establish a connection with the RC transmitter. If no link is available within 10 seconds, a *return to take-off location* procedure is performed during which the UAV aborts its mission and returns to its starting point.

12.2.3 Encryption

The UAV market is increasing significantly without a major consideration in the safety of the exchanged messages. This comes with the problem that an adversary can control the UAV without major troubles.

A secure communication should be confidential (only the receiver can read the message), authenticated (the receiver is sure about who sent the message), and integrous (nobody can change the message). However, for the flight control communications of the UAV, it is of no relevance whether an adversary knows that the UAV is going to perform a certain action, this section only focuses on authentication and integrity. In case data has to be confidential, it is recommended to look into different encryption techniques using less processing power.

The protocol used for flight control message exchange is the Micro Air Vehicle Communication (MAVLink) protocol. It is used for internal communication between the different sensors and the flight controller as well as to transmit useful information as attitude, speed, and battery status of the vehicle and to send new waypoints for control of the drone. Although the integrity of the messages is already ensured by the checksum, it only has a length of 2 bytes (16 bits). A checksum is a set of bits dependant on the message. Each message obtains a different checksum, however as only 2 bytes are used, this checksum can be guessed easily by current computers and hence the scheme is not secure. Integrity and authentication are obtained using a Message Authentication Code (MAC). Before the MAVLink data is sent to the cellular network, a Hash-based message authentication code (HMAC) is attached to it. In order to prevent replay attacks, the current time and date will also be added to the message before calculating the MAC. The HMAC uses the same principles as the checksum explained before, however, it can only be calculated knowing a symmetric key, stored at both the internal memory of the ground station and the UAV. Furthermore, the length of the checksum is equal to 16 bits, a HMAC however can have a length of 128 bits, making it more secure. This scheme is only secure if no third party is able to access either the UAV or the ground station. Regular exchange of the key improves the security of the system.

The preceding encryption algorithm makes sure that the UAV does not accept any commands sent by an unauthenticated device. Furthermore, random noise errors and messages that have been interfered with are also discarded. The final message sent over the cellular network is depicted in Figure 12.2. Due to the fact that the cellular network is used to transmit the message, an IP header is added in front of the MAVLink message, which includes routing information. Its size can range from 20-60 bytes depending on the optional fields. The MAC is added at the end of the message and is calculated using only the orange fields (as seen in Figure 12.2), the MAVLink Frame, and the Time and Date (T/D).

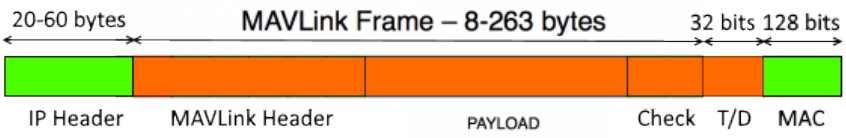

Figure 12.2: Final Message Layout

12.3 Ground Handling and Payload

In this section, some relevant aspects related to the ground handling are discussed as following: a payload mounting mechanism, possible payload modules and the ground station layout.

12.3.1 Ground Station Layout

In this section, the different options for the ground station are discussed, after which a layout for the system is chosen. Before selecting a layout, the functionalities of the ground station are defined. This is done based on different aspects of the UAV missions.

Automated flight control The location of the UAV shall be displayed, as well as its velocity, heading, and altitude. It shall also be possible to see the flight plan. Besides that, waypoints can be added and the destination can be changed. The battery percentage shall also be shown.

Manual flight control Since the UAV is in VLOS operation, showing its location is redundant here. However, battery, attitude, heading, and velocity are useful parameters and shall therefore be shown. It shall be possible to give directional inputs, that cause accelerations.

Mission specific capacities When a camera module is present in the payload, the recorded video shall be visible through the ground station. The payload status shall also be visible, showing whether a payload is present or not. In the case of a disposable payload, the payload bay closing mechanism must be operated. Therefore, in that case the status of the mechanism shall be shown, and it shall be possible to open or close it from the ground station.

The two categories to choose between are a large ground station with a case, displays and controls, or just software that can be installed on any tablet or laptop with an internet connection. It was decided that using software is preferred, since it allows for more flexibility in interfaces, which is beneficial for the variation of mission types. Also, a tablet is easier to transport. Furthermore, as cellular technology is used for communication, only an internet connection is required for control. The only disadvantage is that the UAV will have to rely more on the autopilot, because the inputs given on a tablet will not be control inputs, but waypoints. After some research on world network coverage, it was decided that using just software and a tablet is a viable option[17]. However, to have manual control in VLOS, an RC controller is used. This will be incorporated in the system.

It was decided to choose a system that is compatible with the Pixhawk system that was selected in Section 12.2. Therefore, Paparazzi software will be used[18]. It is compatible with the Pixhawk, all sensors and equipment connected to it can be incorporated into the program because of the open-source character of the software.

Then, in order to use the more reliable RC Link, as explained in Section 12.2.2, an RC transmitter is needed. A FrSky ACCST TARANIS X9D PLUS Digital Telemetry Radio System[19]is used for this, since it is recommended to use with the Pixhawk module and its pricing fits within

[17] `http://data.worldbank.org/indicator/IT.CEL.SETS.P2?view=map`, Accessed on 12-06-2017
[18] See footnote 2.

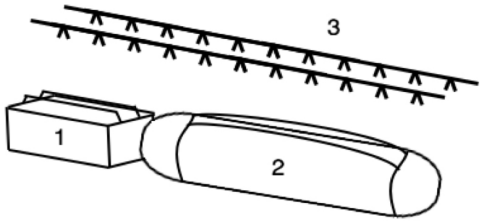

Figure 12.3: Schematic Example of Payload Mounting System

the avionics and ground station budget. It supports at least 8 channels and can hence be used for direct control of the aircraft.

12.3.2 Payload Mounting

In this section, the payload mounting mechanism will be explained. For the closing mechanism of the fuselage, please refer to Section 12.3.3.

Since some missions require a deployable payload module, the mounting mechanism should allow for this. There are also cases when it would be beneficial to only drop a part of the payload, making it possible to take extra batteries or camera equipment. This means two things:

Modular payload In order to enable for part of the payload to be dropped, it should be possible to put in different pieces of the payload as long as they have widths and heights of 15 cm with varying lengths, and the total length of the payload modules does not exceed 1 m. In order to keep fragile payloads from shaking, magnets will be used.

Releasable payload The payload will be mounted using a clipping system. Each module will have rigid bars, disposable ropes or something else that allows the module to be held. This is then clipped to a system that works similar to nippers. The 'claws' are mounted to two parallel bars, as shown in Figure 12.3.(3), and can be operated individually by the CPU.

12.3.3 Payload Bay Closing System

In this section, the closing mechanism of the payload bay is explained. In the midterm report, no intentions of incorporating such a system were expressed [2]. However, since for some missions (part of) the payload will be released from the fuselage, it needs to be possible to close the fuselage to prevent excessive drag. The possibility of closing the fuselage also allows for different payload shapes to be transported without extra packaging.

To determine how the system would look, first some brainstorming was done. Different options were swinging doors, sliding doors, a mechanism in which the door would be positioned above the payload, and a roller system. Each of these systems has advantages and disadvantages. In Table 12.5, some of these are listed.

It was decided that the most important aspect in the design of the closing was the ability to help the rest of the fuselage sustain stresses. This is because if the bottom of the fuselage can not transfer any stresses, the whole design needs to be a lot stronger. Based on this, the decision was made to make a distinction between constant and in-flight removed payload.

[19] `https://hobbyking.com/en_us/frsky-2-4ghz-accst-taranis-x9d-plus-digital-telemetry-radio-system-mode-2.html`, Accessed on 19-06-2017

Table 12.5: Comparison of Different Fuselage Closing Mechanisms

System	Negatives	Positives
Swinging doors	Difficult to transfer stresses, extra connecting mechanism is required. Heavy. Large.	Closes automatically as payload is dropped.
Sliding doors	Difficult to transfer stresses, extra connecting mechanism is required. Heavy. Large.	Closes automatically as payload is dropped.
Fall-down door	Heavy. Large.	Can transfer stresses. Closes automatically as payload is dropped.
Roller system	Requires an additional rolling system.	Can include bars to transfer stresses. Light as it can be partially made out of fabric. Compact.
Discard entire module	Very unsustainable. Only closes the fuselage before release; this is actually not a closing mechanism.	Can transfer and sustain stresses considerably better than the other systems.

Stationary payload This is a payload module that is not dropped. A complete payload module can sustain a lot more stresses than a separate closing mechanism, as the walls of such a module also carry loads, in the missions that do not require dropping the payload, a closed box is used, as shown in Figure 12.3.

Deployable payload In the case of a payload that needs to be delivered in-flight, a separate small payload module is installed that closes the fuselage after payload release. This module will be installed next to the payload that is dropped, so that it only covers that part of the fuselage that needs to be closed. It will consist of a small box with dimensions 15x15 cm times the diameter of the rolled-up closing sheet. This shall be a roller system which consists of fabric to reduce the drag and bars to carry strength. Within the closing module, a small motor is present that operates the unwinding of the sheet. The module shall be connected to the CPU so that it closes the fuselage right after the payload is dropped.

12.3.4 Payload Modules

In this section, a short discussion will be given about suggested payload modules for the different mission profiles. The payload modules *will not* be designed into full detail, however, components such as cameras are preferably chosen such that they are easily compatible with the Pixhawk flight control system. A modular clicking system will be installed, so that it is possible to drop (part of) the payload.

1. **Search and rescue and support to disaster relief operations.** This requires a module that is able to locate the person(s) in need, and drop a help module. The difficulty in this module is that it will be dropped, so if an extra camera or battery is needed, those should be put in a separate module. As the object avoidance system that was chosen in Table 12.1 only shows presence without being specific, some camera should be taken or dropping location would be based on GPS. The payload then only contains a care package or buoy. Velocity and range are most important here, but a mission specific trade-off should be made between that performance and payload capacity.
2. **Precision agriculture by monitoring cattle and crops.** For this type of mission, high-quality camera equipment is required. Endurance is the most important feature for

this mission type, so an extra battery will also be installed. A camera that takes images at a high frequency should be selected, so that it is possible to take pictures at a high flight speeds and generate lift using the wings only.

3. **Transportation of parcels at sea and on land.** This type of mission requires large range. Therefore it will probably make use of a separate battery payload module and parcel module, where maximum battery size is dependent on payload size.
4. **Inspection of extensive industrial assets and infrastructure such as railways, high-tension power lines, pipelines, wind farms, etc.** This type of mission requires similar equipment as mission 2. The difference is that this mission type documents long-range objects, while the agricultural one should cover large areas. Therefore, range is very important in this mission type. It will also make use of high-quality camera equipment and if possible an extra battery module.
5. **Transportation of organs for transplants.** In the case of transporting organs, high velocity is very important. The payload should be well-protected, which means it will probably be light, yet large. Some room might be available for extra batteries. The payload will not be dropped, but the UAV will land for unloading, so a cooling case could be designed for this purpose.

12.4 Communication Flow Diagram

In this section, the communication flow diagram is illustrated in Figure 12.4. It illustrates the flow to and from the UAV system to the environment.

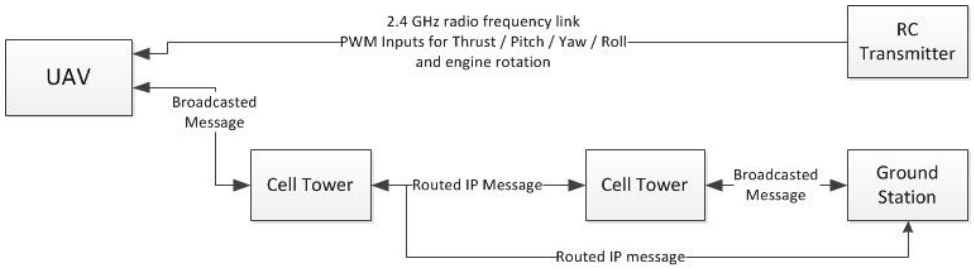

Figure 12.4: Communication Flow Block Diagram

As explained in Section 12.2.2, the telemetry system consists of two different links, a direct link between the UAV and the control station using radio frequency, and an indirect link using cellular technology. The radio frequency link is a one-way link to only send control commands to the flight controller. These commands are sent using Pulse Width Modulation (PWM) techniques. As seen in Figure 12.4, data sent using the mobile network is first broadcast through the air until it reaches a cell tower. Using the routing information on the IP packet, the data is either routed directly towards the ground station (in case it is connected to the internet) or to the closest cell tower from the ground station (in case it is connected via the mobile network). In the latter case, the cell tower broadcasts the message and the ground station can receive it. The data sent via the mobile network ranges from monitoring data to new waypoint or commands sent to the drone to change its flight path.

12.5 Data Handling Block Diagram

In this section, the data handling block diagram is depicted in Figure 12.5. The main purpose of this diagram is to illustrate the different data flows across the system. Furthermore it depicts the sample rates and processing speeds.

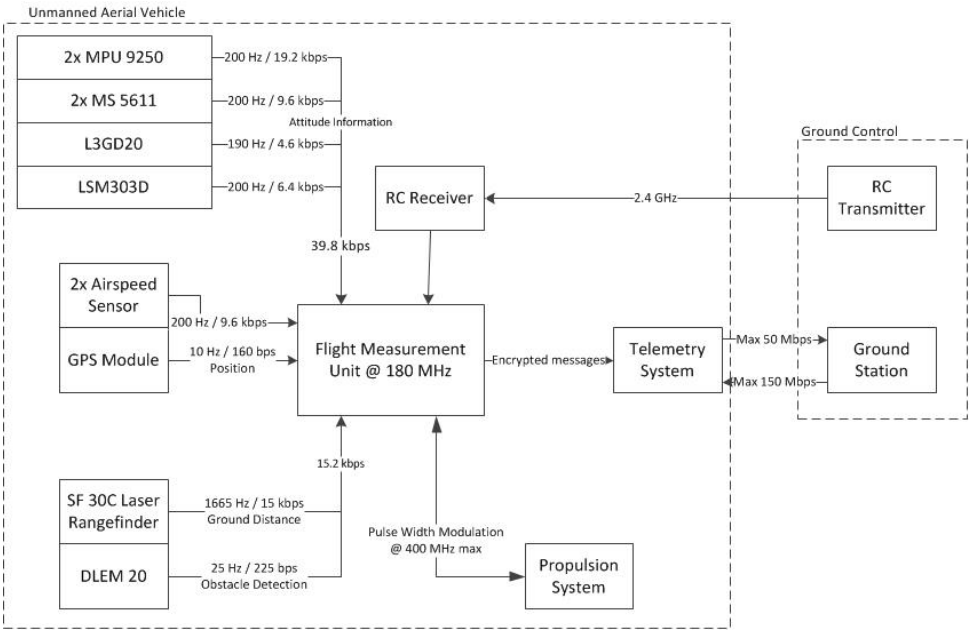

Figure 12.5: Data Handling Block Diagram

The attitude sensors can sample the information at different rates, however more sampling results in a larger data flow and higher required processing power. It was assumed that sampling attitude information at a frequency of 200 Hz results in a good overview of the UAV attitude. The sampling rates for the object avoidance, ground distance, and GPS measurements are set to their maximum sampling rates. As no specifications have been obtained until now considering the sampling rate of the airspeed sensor, it is also assumed to sample at 200 Hz. The frequency at which commands can be sent to the propulsion system is limited by the physical link, in this case 400 MHz, which can however never be achieved due to the bottleneck set by the flight measurement unit of 180 MHz. The down- and uplink speeds of the telemetry system are their maxima and only achievable if the network is not congested.

All sensors (position, attitude, and object/ground avoidance) have a total data rate of 65 kbps. Some minor headers are added to the packages after processing due to the message authentication code and routing information, however, the end data rate is orders of magnitude lower than the total achievable rate of 50 Mbps. This means enough margin is provided for the payload data rate and minor network congestion.

12.6 H/W & S/W Block Diagrams

In this section, the hardware and software diagrams are represented in Figures 12.6 and 12.7. As can be seen, they are are closely related. The hardware diagram focuses on the different physical interfaces used in the UAV and shows the different types of link between each interface. The software diagram illustrates the software that processes the data of each interface.

As seen in both diagrams, the central part of the system is the flight management unit. It is the processor used for autonomous flight control and to handle the data inside the system. With the exception of the propulsion and control system, all internal interfaces are connected to it and powered by it. Power related aspects are managed by the power brick. It regulates the voltage and current in order to prevent damage such as burnout. It also monitors the power consumption and sends battery specific data to the flight management unit. -The propulsion and control system in turn is powered by the battery itself. Each engine, however, has a separate buck converter (a DC-DC step-down converter) in order to reduce the battery voltage to its

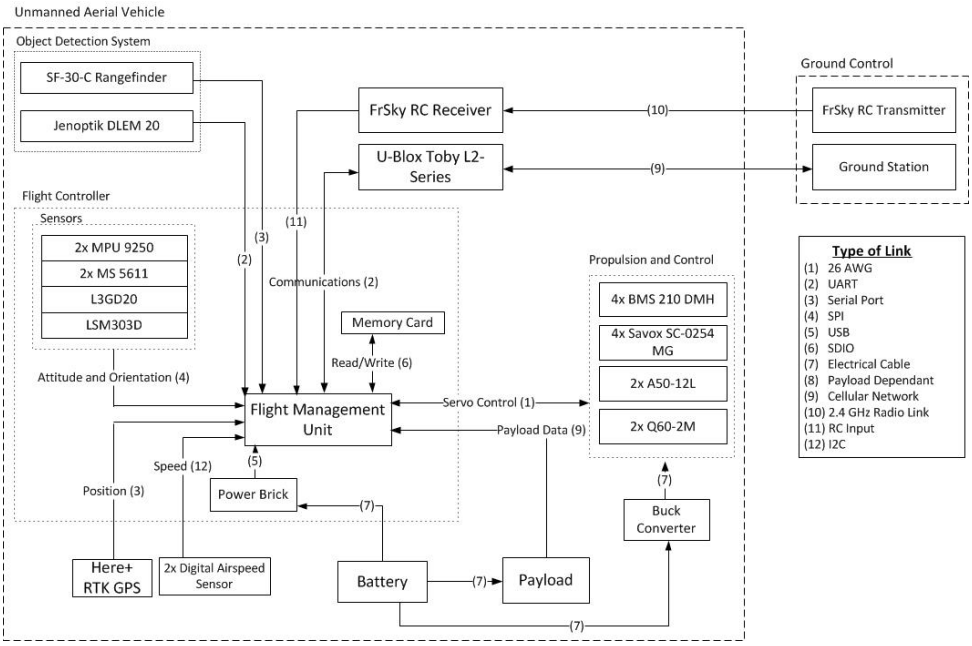

Figure 12.6: Hardware Block Diagram

operational voltage. The figures show that the engines, actuators, and servos used for propulsion and control use a 26 AWG link with PWM technique. The pixhawk 2.1 flight controller has 14 different PWM outputs, eight of them directly controllable by the R/C without need of the flight measurement unit. These will be the four engines used for thrust and the 4 servos used for control. The four tilting actuators are connected via the flight measurement unit. Finally, two more outputs are available in case the payload module with the possibility of drop-off is connected for example.

12.7 Electrical Block Diagram

Figure 12.8 shows the electrical block diagram of the UAV system. It includes the different batteries used for power provision, buck converters to regulate the voltage, and the different power receivers. Also the cable connectors required for disassembly and assembly are illustrated. As can be seen, the flight controller is just represented as one entity. More information regarding the internal structure can be found in the hardware diagram (Figure 12.6) or the pixhawk 2.1 data sheet [20]. It was also decided to add two lights to the wing tips in order to make the drone visible in bad weather conditions. These will adhere to the conventional aircraft colours and hence use a red light on the left wing, and a green on the right wing in order to make it possible to directly recognise the drone's flying direction.

Considering the cabling of the system, there are several things that have to be considered during mounting. Firstly, the GPS module is located above the payload in order to receive the strongest satellite signal. Also, the RC receiver and the LTE module will be located here. The flight controller and the other avionics are located in the nose of the fuselage, cabling to this part of the avionics will be minimal in order to avoid electromagnetic interference with the attitude sensors. The connections to the wing tips are needed for aileron control, lights, and the speed sensor. The fuselage has an empty section above the payload department, through which cables can be routed. Furthermore, cables can be routed through the shallow carbon tube within the wing.

[20] `http://www.unmannedtech.co.uk/uploads/6/7/0/2/6702064/pixhawk_2_25th_july_2016__2_.pdf`, Accessed on 21-06-2017

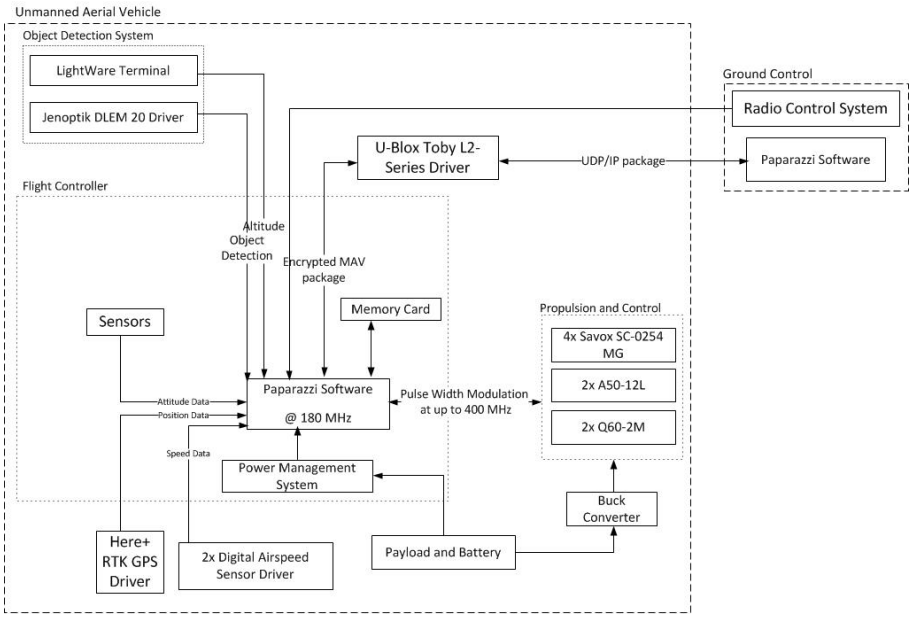

Figure 12.7: Software Block Diagram

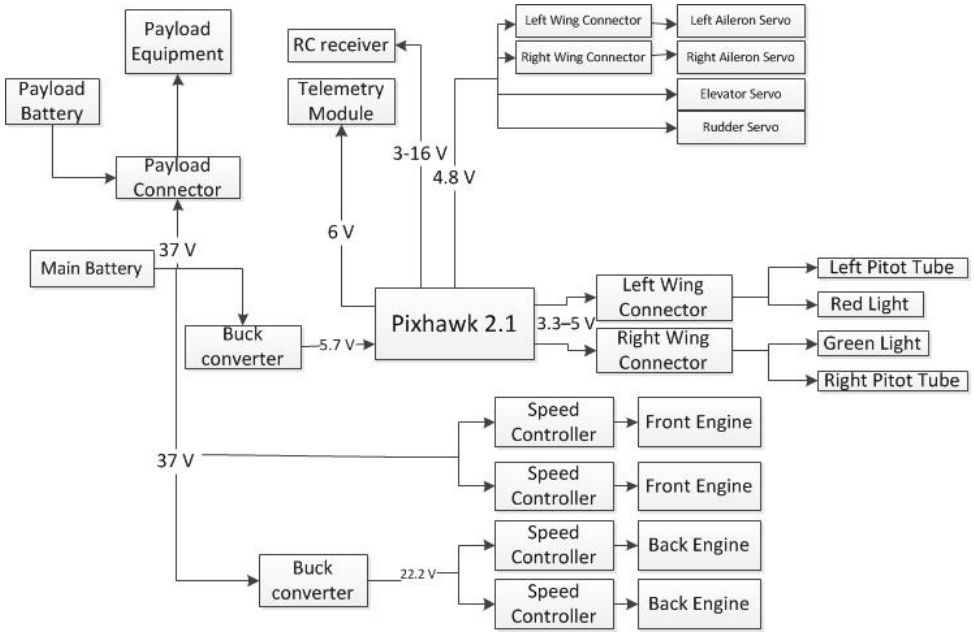

Figure 12.8: Electrical Block Diagram

13 Design Specifications

The design specifications will be presented in this chapter. First of all, the mass, cost and power breakdown of the final design is presented. Next, the compliance matrix of the system- and subsystem requirements is shown. Finally, the final design parameters are presented.

13.1 Mass, Cost & Power Breakdown

The mass, cost and power breakdown are presented in this section. The breakdown resembles the actual values of the design. For mass and cost, the breakdown is compared to the budgeted mass and cost. The margin between the budget and the actual value is also presented and explained. The power was not budgeted in the preliminary design phase. However, the breakdown of the power is presented in this chapter.

Mass Breakdown

The mass breakdown can be found in Table 13.1. As one can see, some more mass has been added to the payload subsystem since the other subsystem in general turned out to be lighter than estimated. The MTOW of the system is now equal to 23.38 kg. When entering the detailed design phase, the contingencies can be dropped and an iteration can be made in order to reach the final MTOW and mass breakdown.

Table 13.1: Mass Breakdown Compared to the Mass Budget

Subsystem	**Budgeted Mass [kg]**	**Contigency [%]**	**Target Mass [kg]**	**Actual Mass [kg]**	**Margin [kg]**
Power	8	5	7.6	7.01	0.59
Propulsion	4	5	3.8	2.39	1.41
Avionics	1	5	0.95	0.4	0.55
Wing	3.5	10	3.15	2.5	0.65
Tail	1.5	10	1.35	1.35	0.00
Fuselage	2.5	10	2.25	2.30	-0.05
Payload	4.5	5	4.28	7.43	-3.15
MTOW	25	-	23.38	23.38	0.00
Ground Station	-	-	7.5	7.5	-

Cost Breakdown

The cost breakdown can be found in Table 13.2. The total costs presented are the production cost excluding manufacturing cost. The total cost stays within the budgeted cost. However, some subsystem cost differ substantially from the budget. For example, the fuselage cost are 640 euros less than budgeted. The budgeted cost was estimated to be equal to the cost of the wing. Since for the fuselage glass fibre is used instead of carbon fibre, as for the wing, the material cost is substantially less. Also other subsystems turn out to be much cheaper then the budget. This is because manufacturing cost is not taken into account. Therefore, the excess of money can be used in order to support potential extra manufacturing costs.

Table 13.2: Cost Breakdown Compared to the Cost Budget

Subsystem	**Budgeted Cost [€]**	**Contingency [%]**	**Target Cost[€]**	**Actual Cost [€]**	**Margin [€]**
Power	800	5	760	860	-100.00
Propulsion	2200	10	1980	1950	30.00
Avionics	2200	10	1980	2200	-220
Wing	800	10	720	753	-33.00
Tail	400	10	360	210	150.00
Fuselage	800	10	720	78.40	641.60
Payload	300	5	285	200	85.00
Total	7500	-	6805	6251.40	553.60
Ground Station	-	-	-	160	-

Power Breakdown

The power breakdown can be found in Table 13.3. As can be seen, there is a difference in maximum required power depending on whether the drone is in horizontal or vertical flight. In horizontal flight, the maximum power is obtained using maximum speed. Furthermore, worst case scenario is assumed, meaning that all control surfaces on wing and tail are being deflected.

Considering the vertical flight, it can be seen that most power is drawn from the propulsion subsystem. This is due to the fact that in vertical climb, a lot of power is needed. No more control is necessary for wing and tail actuators and hence no power is drawn from these subsystems. The avionics subsystem needs to handle the data in both cases and hence uses the same amount of power.

As can be seen in the table, the margin is higher in case of horizontal flight. However, as both phases need to be considered in each mission, the maximum power margin obtained is equal to 862 W. Although this power is not used during normal mission phases, some of it will be used for the payload depending on the equipment used in it.

Table 13.3: Power Breakdown for the Final System

Subsystem	**Power required [W]**	
	Horizontal Flight	**Vertical Flight**
Propulsion	2762	4500
Avionics	3	3
Wing	7	0
Tail	7	0
Fuselage	0	0
Payload	*	*
Available Power	5365	5365
Margin	2586	862

13.2 Compliance Matrix

The compliance matrix shows which requirements are met with the current design. To show which requirements are met, the check mark is used (✓). Requirements which have not yet been analysed are noted with a circle (○). Requirements that have no been met are marked with a cross (✗), the reasoning behind the requirements not being met is explained after the compliance matrix. The compliance matrix is shown in Table 13.4.

Table 13.4: Compliance Matrix

Requirement	Compliance	Requirement	Compliance	Requirement	Compliance
System requirements					
SYS-C-1	✓	SYS-C-2	✓	SYS-S-2	✓
SYS-L-2	✓	SYS-L-3	✓	SYS-R-1	✓
SYS-ENV-1.4	○	SYS-ENV-1.5	○	SYS-ENV-1.6	✓
SYS-ENV-2.1	✓	SYS-ENV-2.2	○	SYS-ENV-2.5	✓
SYS-PH-1.1	✓	SYS-PH-2	✓	SYS-PH-4.3	○
SYS-PH-4.4	✓	SYS-OP-1.1	✓	SYS-OP-1.5	✓
SYS-OP-1.7	✓	SYS-OP-2.1	○	SYS-OP-2.2	○
SYS-OP-2.3	✓	SYS-OP-2.4	✓	SYS-OP-2.5.3	✓
SYS-OP-2.5.4	○	SYS-OP-2.5.5	✓	SYS-OP-2.7	✓
SYS-OP-2.8.2	○	SYS-OP-2.8.6	✓	SYS-OP-2.8.7	✓
SYS-OP-2.8.8	○	SYS-OP-2.9.2	✓	SYS-OP-2.9.3	✓
SYS-OP-2.9.4	✓	SYS-PF-1.1	✓	SYS-PF-1.2	✓
SYS-PF-1.3	✗	SYS-PF-1.4	✗	SYS-PF-2.1	✓
SYS-PF-2.2	✓	SYS-PF-2.3	✓	SYS-PF-2.4	✓
SYS-PF-3	✓	SYS-PF-4	✓	SYS-VS-1.1	✓
SYS-VS-1.2.1	✓	SYS-VS-1.2.2	✓	SYS-VS-1.2.3	✓
SYS-VS-1.2.4	✓	SYS-VS-2.1	✓	SYS-VS-2.2	✗
SYS-VS-2.3	✓	SYS-VS-3	✓		
Avionics requirements					
SUB-AV-1.1	✓	SUB-AV-1.2	✓	SUB-AV-2.1	✓
SUB-AV-2.2	✓	SUB-AV-2.2	✓	SUB-AV-2.3	✓
SUB-AV-2.4	✓	SUB-AV-2.5	✓	SUB-AV-2.8	✓
SUB-AV-2.10	✓	SUB-AV-2.11	✓	SUB-AV-3.1	✓
SUB-AV-3.2	✓	SUB-AV-3.3	✓	SUB-AV-4.1	✓
SUB-AV-4.2	✓	SUB-AV-4.3	✓	SUB-AV-4.4	✓
SUB-AV-5.2	✓	SUB-AV-6.1	✓	SUB-AV-7.1	✓
SUB-AV-8.2	✓	SUB-AV-8.3	✓	SUB-AV-8.4	✓
SUB-AV-9.1	✓	SUB-AV-9.2	✓		
Propulsion requirements					
SUB-PR-2.2	✓	SUB-PR-2.3	✓	SUB-PR-2.4	✓

SUB-PR-3.4	✓	SUB-PR-3.5	✓	SUB-PR-3.6	✓
SUB-PR-5.1	○				
Power requirements					
SUB-PW-1.1	✓	SUB-PW-1.2	✓	SUB-PW-1.3	✓
SUB-PW-1.4	✓				
Wing requirements					
SUB-W-2.1	✓	SUB-W-2.2	✓	SUB-W-2.3	✓
SUB-W-2.4	✓	SUB-W-2.5	✓	SUB-W-3.1	✓
SUB-W-3.2	✓	SUB-W-3.4	✓	SUB-W-3.5	✓
SUB-W-3.9	○	SUB-W-3.10	○	SUB-W-3.11	✓
SUB-W-3.14	○	SUB-W-3.16	○	SUB-W-5.6	○
SUB-W-7.2	✓	SUB-W-7.3	✓		
Tail requirements					
SUB-T-1.1	✓	SUB-T-1.2	✓	SUB-T-2.1	✓
SUB-T-2.2	✓	SUB-T-2.3	✓	SUB-T-3.1	✓
SUB-T-3.2	✓	SUB-T-3.3	✓	SUB-T-3.4	✓
SUB-T-3.5	✓	SUB-T-4.1	✓	SUB-T-4.2	✓
SUB-T-5.1	✓				
Fuselage requirements					
SUB-F-1.1	✓	SUB-F-1.2	✓	SUB-F-2.1	✓
SUB-F-2.2	✓	SUB-F-2.3	✓	SUB-F-2.4	✓
SUB-F-3.1	✓	SUB-F-4.1	✓		
Payload requirements					
SUB-P-2.1	✓	SUB-P-2.2	○	SUB-P-3.3	✓
SUB-P-3.4	✓				
Ground station requirements					
SUB-GS-2.1	✓	SUB-GS-3.2	✓	SUB-GS-4.1	✓
SUB-GS-4.2	✓	SUB-GS-4.3	✓	SUB-GS-4.7	✓
SUB-GS-5.1	✓	SUB-GS-5.2	✓	SUB-GS-5.3	✓
SUB-GS-6.2	✓	SUB-GS-6.3	✓	SUB-GS-6.4	✓
SUB-GS-7.1	✓	SUB-GS-7.2	✓		

- SYS-PF-1.3: The UAV will not have a range of 200 km with a payload of 10 kg. With 10 kg the UAV will have a range of 40 km. Decreasing the weight of the payload and replacing it with batteries will increase the range linearly to a maximum of 600 km.
- SYS-PF-1.4: The UAV will not have an endurance of 1 hour with a payload of 10kg. To achieve an endurance of one hour, some payload needs to be replaced with extra batteries.
- SYS-VS-2.2: The UAV can not communicate with other air vehicles.

13.3 Final Results

In this section, the final design results are presented. In Table 13.11, an overview of the subsystems mass and positions is given. The performance parameters can be found in Table 13.12. Tables 13.5 to 13.10 give an overview of the subsystem design parameters. A CATIA drawing of the final design can be found in Figure C.1.

Table 13.5: Final Parameters of the Wing

Geometric Parameters					
Parameter	**Value**	**Unit**	**Parameter**	**Value**	**Unit**
c_{t_w}	118	mm	c_{r_w}	348	mm
b_w	2920	mm	AR_w	10	-
λ_{tip}	0.39	-	λ_{root}	0.8	-
l_{twist}	146	mm	$l_{taperchange}$	642	mm
$\Delta\alpha_{tip}$	5	deg	S	0.80	m^2
Airfoil	NACA 4417	-	x_{LE}	0.53	m
$S_{aileron}$	63.1	cm^2	$c_{aileron}$	3.69	m
Aerodynamic Parameters					
Parameter	**Value**	**Unit**	**Parameter**	**Value**	**Unit**
$(C_l/C_d)_{Cl,cruise}$	57.6	-	α_{max}	14	deg
$(C_l^{1.5}/C_d)_{Cl,cruise}$	41.4	-	α_{cruise}	1	deg
$C_{L,cr}$	0.622	-	L_{cr}	274.3	N
$C_{D,cr}$	0.02	-	D_{cr}	8.82	N
$C_{M,ac}$	-0.137	-	$C_{l,max}$	1.53	-
Structural Parameters					
Parameter	**Value**	**Unit**	**Parameter**	**Value**	**Unit**
Thickness root tube	1	mm	Diameter root tube	40	mm
Thickness outer tube	2	mm	Diameter outer tube	20	mm
Thickness engine pylon	1	mm	Diameter engine pylon	20	mm
Skin material	Depron	-	Structural material	Carbon-epoxy	-

Table 13.6: Final Parameters of the Tail

Geometric Parameters					
Horizontal Tail			**Vertical Tail**		
Parameter	**Value**	**Unit**	**Parameter**	**Value**	**Unit**
c_{r_h}	196	mm	c_{r_v}	181	mm
c_{t_h}	0	mm	c_{t_v}	82	mm
b_h	694	mm	b_v	220	mm
AR_h	4.5	-	AR_v	3.35	-
S_h	0.11	m^2	S_v	0.03	m^2
i_h	2.6	deg	i_v	0	deg
$S_{elevator}$	136	cm^2	S_{rudder}	43.4	cm^2
$c_{elevator}$	2.89	cm	c_{rudder}	2.67	cm
Aerodynamic Parameters					
Horizontal Tail			**Vertical Tail**		
Parameter	**Value**	**Unit**	**Parameter**	**Value**	**Unit**
$C_{D,0_h}$	0.0013	-	$C_{D,0_v}$	0.0002	-
C_{D,cr_h}	0.0016	-	C_{D,cr_v}	0.0003	-
$C_{L_{\alpha_h}}$	0.1	$\frac{1}{deg}$	$C_{L_{\alpha_v}}$	-	-
Airfoil	NACA 0018	-	Airfoil	NACA 0012	-
Structural Parameters					
Horizontal Tail			**Vertical Tail**		
Parameter	**Value**	**Unit**	**Parameter**	**Value**	**Unit**
Structural material	Carbon-epoxy	-	Structural material	Carbon-epoxy	-
Skin material	Depron	-	Skin material	Depron	-

Table 13.7: Final Parameters of the Fuselage

Geometric Parameters					
Parameter	**Value**	**Unit**	**Parameter**	**Value**	**Unit**
L_{fus}	1.8	m	h_{fus}	0.18	m
x_{LE}	0.53	m	w_{fus}	0.15	m
x_{ac_h}	1.68	m			
Aerodynamic Parameters					
Parameter	**Value**	**Unit**	**Parameter**	**Value**	**Unit**
$C_{D,0_{fus}}$	0.0050	-	$C_{D,cr_{fus}}$	0.0050	-
$C_{L,cr_{fus}}$	0.0002	-	$A_{frontal}$	0.053	m^2
Structural Parameters					
Parameter	**Value**	**Unit**	**Parameter**	**Value**	**Unit**
Structural material	Glass fibre epoxy	-	Skin material	Glass fibre epoxy	-

Table 13.8: Avionics Parameters

Function	**Description**
Flight Controller	Pixhawk 2.1 using paparazzi software.
Avoidance system	Horizontal laser for object avoidance, vertical laser for ground avoidance.
Attitude & position	3x accelerometer, 3x gyroscope, 3x magnetometer, 2x barometer, GPS module, 2x airdata sensor.
Data transfer	Principal cellular network link with direct radio control link for redundancy.
Security	Message Authentication Code to ensure integrity and authentication.

Table 13.9: Power Parameters

Component	**Product Name**	**Q.**
DC - DC Converter	LM2596 DC 3.2-40V to 1.25-37V	2
Rotating Mechanism	Tricopter Tilt Mechanism	4
Servo	BMS-210DMH	4
Servo wire	DITEX Servowire Extension	4
Battery	Zippy Compact 5800mAh 10S Lipo	5
Power cabling	Turnigy HQ 8 AWG Silicon wire	4

Table 13.10: Final Parameters of the Propulsion Subsystem

Geometric Parameters					
Parameter	**Value**	**Unit**	**Parameter**	**Value**	**Unit**
$d_{front_{engine}}$	0.3	m	$d_{back_{engine}}$	0.6	m
D_{pylon}	0.02	m	$D_{prop_{front}}$	0.4	m
$D_{prop_{back}}$	0.275	m			
Aerodynamic Parameters					
Parameter	**Value**	**Unit**	**Parameter**	**Value**	**Unit**
$C_{D,0_{pylon}}$	0.0005	-	$C_{D,cr_{pylon}}$	0.0005	-
$T_{req_{vertical}}$	124	N	$T_{req_{horizontal}}$	12	N
Structural Parameters					
Parameter	**Value**	**Unit**	**Parameter**	**Value**	**Unit**
Pylon material	Carbon-epoxy	-			
Power Parameters					
Parameter	**Value**	**Unit**	**Parameter**	**Value**	**Unit**
$P_{eng_{front_{max}}}$	2800	W	$P_{eng_{back_{max}}}$	2009	W
$P_{req_{speed}}$	1381	W	$P_{req_{range}}$	314	W
$P_{req_{endurance}}$	260	W			

Table 13.11: Subsystems Mass & Locations

Subsystem	**Mass [kg]**	**Minimum c.g. Location [m]**	**Maximum c.g. Location [m]**
Wing	2.5	0.60	0.60
Tail	1.35	1.68	1.68
Battery 1	2.8	0.19	0.19
Battery 2	5.4	0.35	0.35
Payload	6.2	0.4	0.8
Fuselage	2.30	0.9	0.9
Avionics	0.4	0.3	0.3
Propulsion	2.39	0.79	0.79
Total	23.38	0.55	0.74

Table 13.12: Final Performance Parameters

Parameter	**Value**	**Unit**	**Parameter**	**Value**	**Unit**
Range full payload	40	km	Range no payload	600	km
Payload at 1h endurance	6.2	kg	V_{stall}	20	$\frac{m}{s}$
V_{cruise}	30	$\frac{m}{s}$	V_{range}	29	$\frac{m}{s}$
$V_{endurace}$	24	$\frac{m}{s}$	$V_{maxspeed}$	55.6	$\frac{m}{s}$
Max. hover time	5	min	Max. VTOL time	1	min

14 Operations & Logistics

This chapter will elaborate on the operations & logistics concept description and the RAMS characteristics of the system.

14.1 Operations & Logistics Concept Description

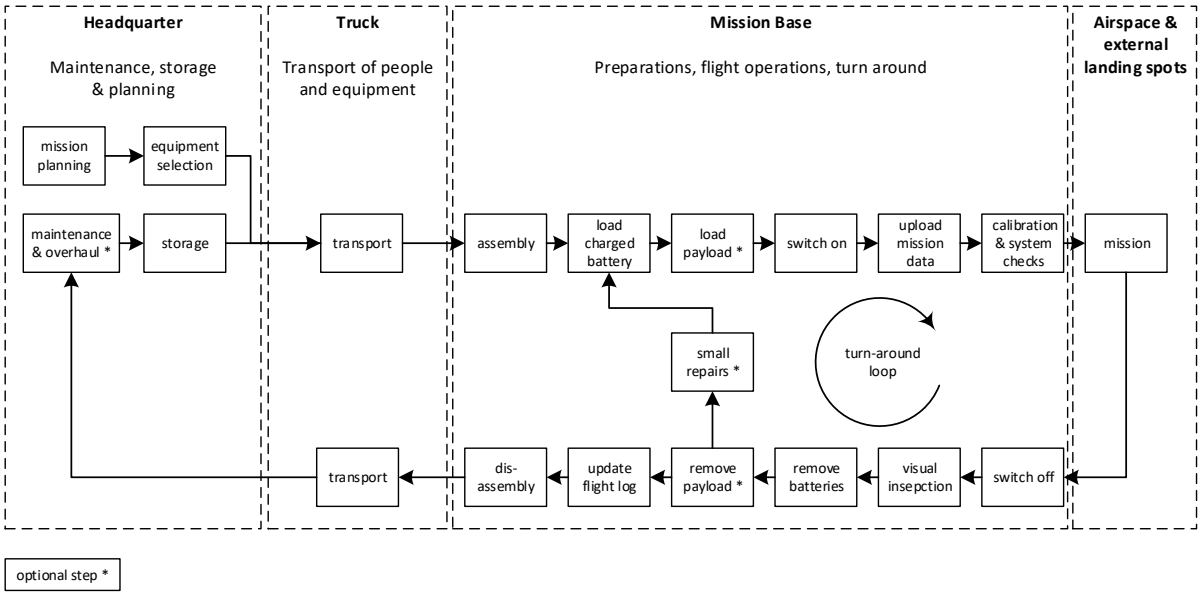

Figure 14.1: Operations & Logistics Flow Diagram

Figure 14.1 shows the the operations and logistics flow diagram for what this group expects to be typical operating conditions. It is assumed that the UAV operator has a main facility, from which the UAV, staff and mission relevant equipment are transported to a mission base at which flight operations take place. Naturally, variations to this scheme are possible, e.g. a parcel company may exclusively operate from its main facility, or long-range missions require a turn-around at a remote location, but for the sake of brevity only the most general case is presented. The starting and end point of each mission is the so-called headquarters, the place where maintenance and storage takes place. Based on customer input a mission plan is set up, which determines the kind of resources that are required. Next to one or more UAVs, this includes staff on site, equipment such as the ground station, spare parts, additional batteries and a transport vehicle. Once the preparation is done, everything is loaded into a vehicle and transported to the location where the UAV is intended to take off and land. Figure 14.2 shows the UAV body in disassembled state within a standard size van, where the remaining space can be filled with support equipment. Once on site, the equipment needs to be unloaded and the UAV assembled into its operational form. A charged battery is then loaded, followed by the payload, which can also consist of another set of batteries. The system is switched on, the mission relevant data is uploaded to the on-board computer and an automated instrument calibration and readiness check performed. The UAV is now ready to fly and carry out its mission. After its return, the system is switched off for safety reasons, visually inspected and stripped off its batteries. The next steps depend on the kind of mission in question. If another flight is scheduled, the payload can be replaced and minor repairs taken out, e.g. replacing a damaged propeller blade. Once the battery is recharged or replaced by a full one, a new flight cycle can start. In case the mission does not comprise a turn-around or substantial damage was detected, the digital flight log is updated and the UAV disassembled. After loading all equipment

the transport back to the headquarter takes place, where scheduled maintenance and all levels of repairs are carried out. Once the work is documented and approved, the equipment is stored and ready for the next mission.

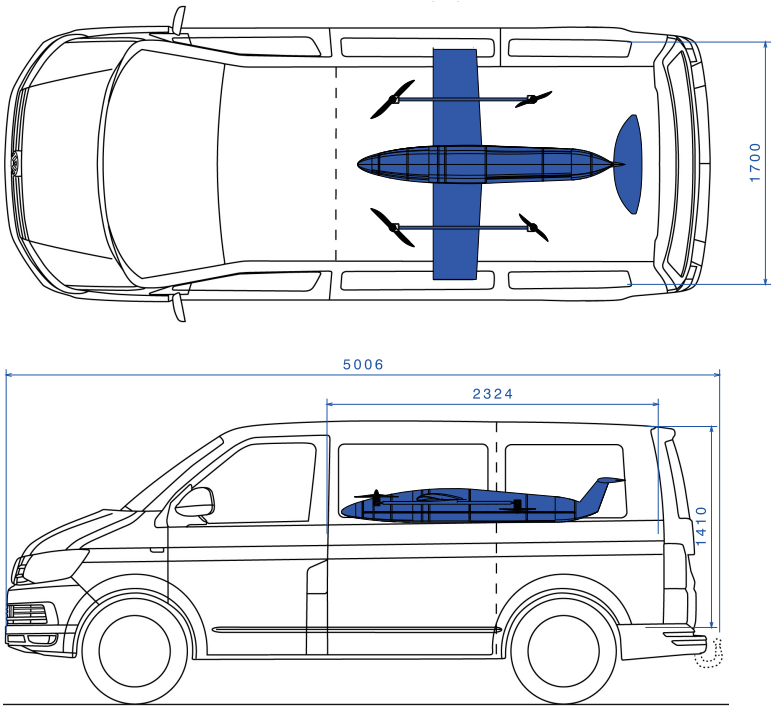

Figure 14.2: UAV Van Transport

14.2 RAMS Characteristics

In this section, the reliability, availability, maintainability and safety (RAMS) characteristics are presented. First, different safety critical functions are presented together with procedures to be carried out in their respective case. These procedures might include making use of a redundant system or emergency procedures to be carried out. The section concludes with a list of different maintenance activities.

14.2.1 Reliability and availability

As explained in Chapter 12, the UAV is highly dependant on the autopilot. Only for control in close range manual control is possible and even then the reliability of the flight controller, in order to manage the data flow, is of major importance. For this reason, the most critical functions are the ones needed for autonomous flight. The following paragraphs will explain one by one the failure of the different UAV components.

First, the flight controller bases all of its decision on the data it receives by the sensors. Wrongly assumed attitude or airspeed result in wrong actions and might in worst case lead to crashes. In order to prevent this from happening, redundancy is provided for the critical sensors. At least two accelerometers, barometers, magnetometer, gyroscopes and airspeed sensors are used in order to calculate attitude. The probability that all of them fail during a single mission can be assumed negligible. In case of object avoidance or ground distance sensor failure, the UAV will still be able to perform its mission, however the probability of crashing into an obstacle increases significantly and thus an emergency landing is performed. GPS data, with the help of

pressure sensors will be used in order to determine a ground distance estimate during landing. GPS failure will result in the inability to determine the position and hence in mission failure. In this case also an emergency landing will be performed and a notification including last known position and failure reason will be send to the ground station.

Another flight controller failure comes from the power source. Battery failure includes an empty battery, burnout or overvoltage. Empty battery will result in total failure, burnout and overvoltage can result in damaged hardware. In order to prevent this, the flight controller uses a power brick to manage the power supply. It sends useful information as battery status and battery level to the flight controller. This reduces the chances of wrong voltage distribution and makes it possible for the flight controller to perform a return to base procedure in case the energy level drops below a certain threshold. Regular inspection and replacement of the battery will also reduce the probability of battery failure.

Then, servos are used throughout the system for either engine tilting mechanisms or control surface deflection. In the former, either one or more engines are stuck in horizontal or vertical position. In case only one or two engines are stuck, the remaining ones can be used to fly the drone to a safe location and perform a landing. If stuck in horizontal mode however, a safe vertical landing will not be possible anymore and a horizontal landing has to be performed. The impact of tilting actuator failure is minimal, as horizontal flight is still possible using only one engine. If actuators are stuck in vertical mode, a safe vertical landing can be performed. A more critical case is failure of a control surface. Aileron failure results in an inability to perform rolling action. This can be counteracted by the rudder and slight tilting of the engines. Rudder failure is counteracted using different thrust at each side and elevator failure is compensated for by tilting the front or back engines. Although redundancy is provided for control surface failure, a return to base procedure will be carried out in such a case to diminish the risk of further damage.

After that, engine failure is a critical risk that has to be considered. One engine failure can be compensated by the rudder in horizontal flight, however vertical flight will not be possible anymore. In this case, also the forward propellers are used in order to generate enough thrust to perform a return to base procedure. Then in case of more engine failures, horizontal flight will be performed using the remaining engines and depending on the distance towards the base a new landing location might have to be chosen. In case the engines fail during vertical flight, no other option but to perform a emergency landing. This will not be possible in all cases but the flight controller will try to minimise the landing impact.

The last failure to be considered is the failure of the telemetry link and the RC link. In this former case, no more waypoints can be send to the drone and the drone can not send updates regarding its flight conditions. If both links become unavailable, the drone will perform a return to base action resulting in mission failure. In order to minimise the risk of telemetry failure, missions always have to be planned and configured before UAV take-off. This makes it possible for the drone to perform its initial planned mission in case something goes wrong with the return procedure during link failure.

In conclusion, all the critical systems used in the UAV system either have redundancy in case of failure or a safe procedure that can be performed limiting the damage. The most critical failure is an engine failure during vertical flight. Here no other option can be performed but landing the drone vertically while trying to minimise the impact. The reliability of the chosen engines however is high as explained in Chapter 8. As on top of that, the drone spends most of its mission time in horizontal flight, the probability of this event to occur is minimal. The modular design of the UAV ensures the availability of the drone, as in case of a failure, only the specific parts have to be exchanged. This can be performed without major complications.

14.2.2 Maintenance

Next to the reliability aspect, availability and safety aspects strongly depend on the necessary maintenance procedures for the UAV. Extra maintenance will results in better safety aspects, however, the availability will decrease. In case no maintenance is performed, the safety of the UAV can not be ensured anymore and if there is an unexpected failure the UAV will be unavailable for a longer period. The following shows different maintainability procedures depending on how often they have to be carried out.

Start of mission

1. Check previous error log for previous mission problems and ensure that they have been fixed.
2. Make sure that the battery is disconnected.
3. Assemble the wing to the fuselage.
4. Inspect all connectors, propeller blades and wings for cracks. If cracks are present they have to be reported and maintenance might be necessary depending on the crack length and thickness.
5. Mount the payload and connect a full battery.
6. Establish a cellular connection between the UAV and the ground station.
7. Configure all the waypoints needed for the mission.
8. Control correct functioning of servos and engines using RC link. If an error occurs in the functioning it has to be reported and the mission will be aborted.
9. Check for correct calibration of sensors.

End of mission

1. Check internal error log for probable errors. If errors are present report them.
2. Disconnect the battery and connect it to the charger.
3. Quick inspection on damages that might have occurred during the mission.
4. Disassemble the wing from the fuselage and clean the different parts.

Monthly Basis

1. Check all internal software for system updates and update them if necessary.
2. Full external inspection for cracks.
3. Recalibration of all the sensors.

15 Production Plan

In case the finalised concept will be produced in series, a production plan will prove to be useful to show the required activities to build the Hybrid UAV. The production plan shows which steps need to be taken successively when building the aircraft, and which steps can be done concurrently. This production plan is created for a series production of 500 units. Figure 15.1 shows the top level production plan for The Winged Quadcopter.

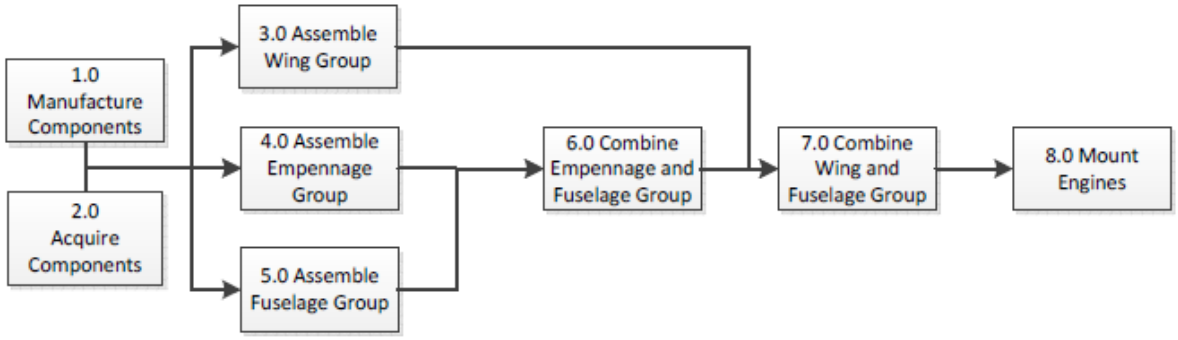

Figure 15.1: Top Level Production Flow Diagram

Looking at the top level, all of the required parts are acquired or manufactured first. Next, the three main groups of the aircraft can be constructed simultaneously, namely the fuselage, empennage and wing. Once these are constructed the assembly can begin, starting with the attachment of the empennage to the fuselage. This is followed by the attachment of the wing to the fuselage. This order has been chosen because the wings will complicate the process by taking up a lot of space. The engines are mounted last in order to minimise the risk of damaging them or the UAV during production.

The part manufacture is seen in Figure 15.2. There are three different materials that need to be manufactured. The first branch is the branch for the manufacturing of glass fibre parts. These parts will be used for the construction of the fuselage. The three separate parts will all need to be laminated, using moulds that need to be made beforehand. Once the glass fibre has been laminated, rough edges need to be sanded off for a better finish. To make sure the parts are good enough, a final flaw detection needs to be done to find imperfections. The second branch is for the manufacturing of foam parts for the wing. The foam will be bought in blocks, and these blocks will be cut into sections corresponding to the distances between ribs. When the blocks are the correct length, the inner side of the wing skin will be cut. Finally, the outer side will be wire cut as well, showing a skin in the shape of a wing. The last branch is for the manufacturing of the carbon parts. The only carbon parts needed to be manufactured are the ribs. To make the ribs, they will be cut out of plates of carbon. After the cutting, these ribs also have to be sanded to have a smooth finish.

The wing assembly is shown in Figure 15.3. Here, the wing structure is constructed by creating a spar and rib base for all other components to be fixed to. This includes attaching the foam skin to the structure, preserving the possibility to access the inside to mount components. The detailed base construction process is seen in Figure 15.4. It should be noted that this exact process is repeated for the construction of the vertical and horizontal tail bases. Next, parts such as control surfaces or engine mounts are constructed and mounted onto the base. Finally, an outer paint layer is added to the foam skin to ensure a smooth surface and protection against the environment.

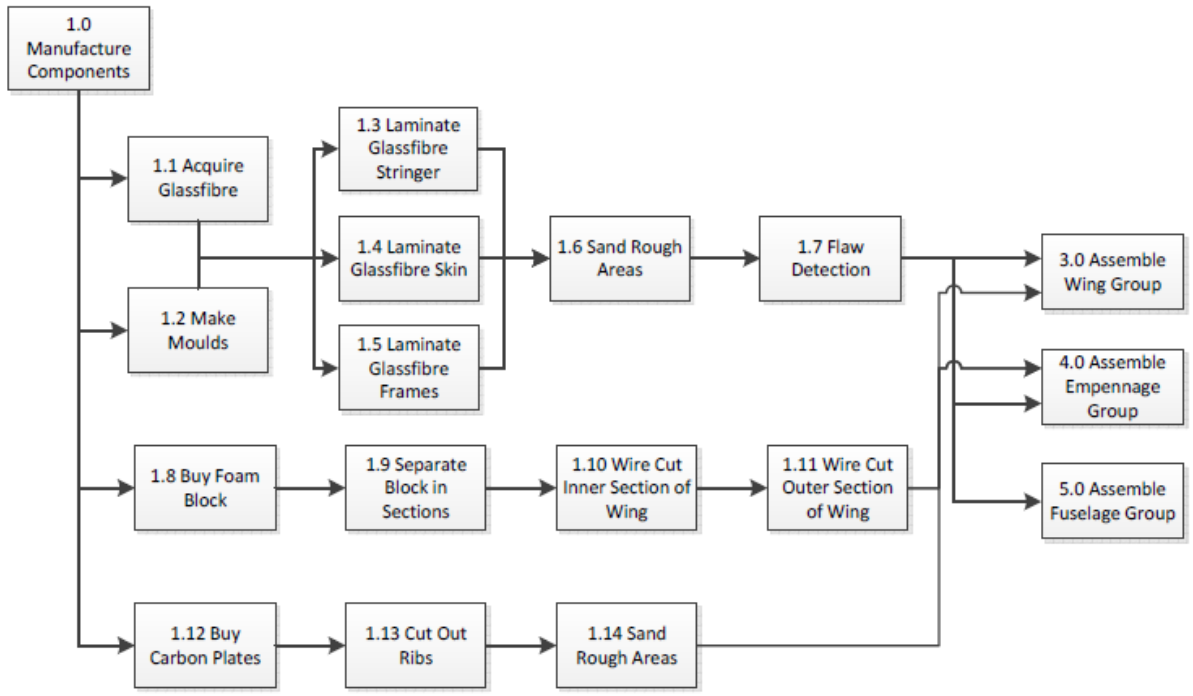

Figure 15.2: Top Level Production Flow Diagram

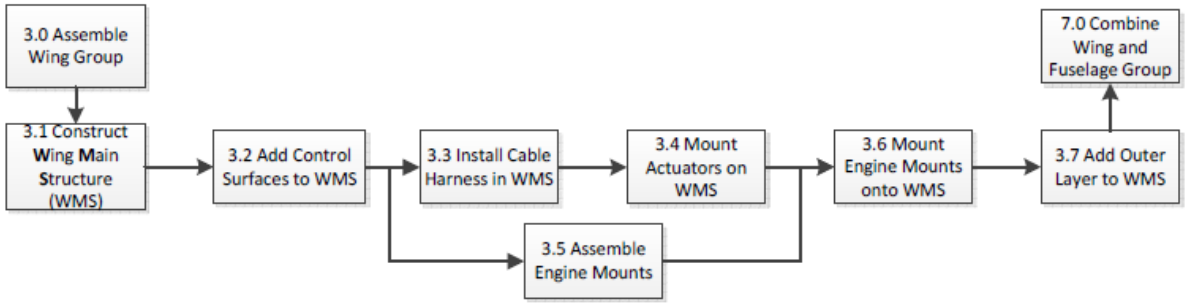

Figure 15.3: Wing Assembly Flow Diagram

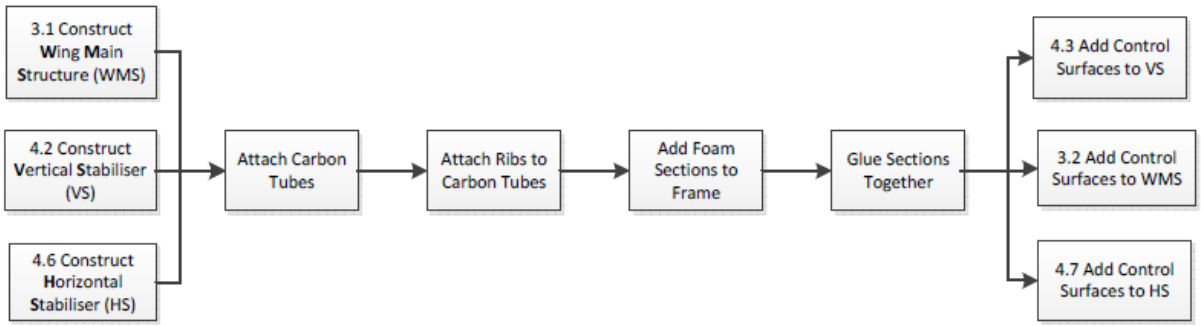

Figure 15.4: Main Structure Assembly Process

The detailed empennage assembly is shown in Figure 15.5. This production stage comprises three parallel processes, namely the construction of the vertical and horizontal stabilisers, as well as of the empennage base. These are then assembled together, after which the actuators are mounted onto the base and connected to the control surfaces. The stage ends with the addition

of an outer paint layer to the entire empennage.

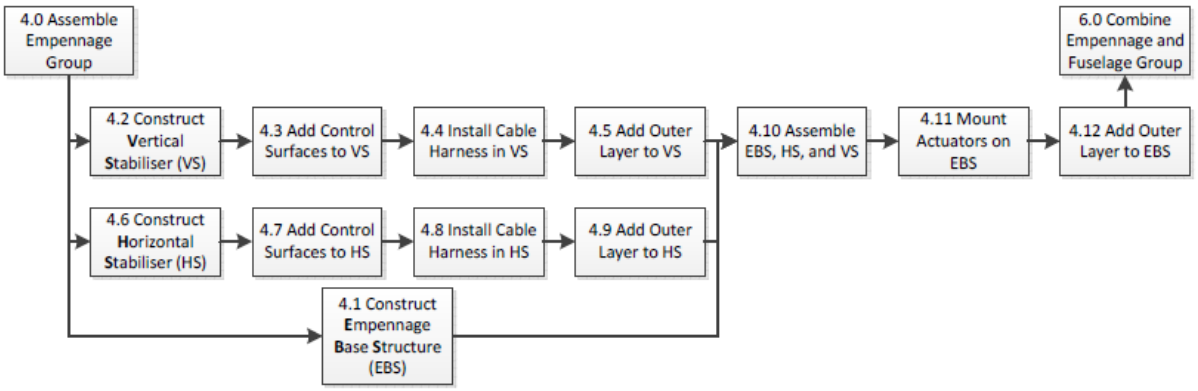

Figure 15.5: Empennage Assembly Flow Diagram

The fuselage structural assembly is described in a general manner in Figure 15.6. A detailed description of the installation of the electronics in the fuselage is shown in Figure 15.7. The structural assembly consists of constructing the fuselage base and payload bay in parallel, and then assembling them together. The rubber landing gear is mounted afterwards making it easier to assemble the payload bay beforehand. With the undercarriage installed, from this stage on the UAV will not require any additional structural supports during production. Finally the skin is attached to the fuselage structure.

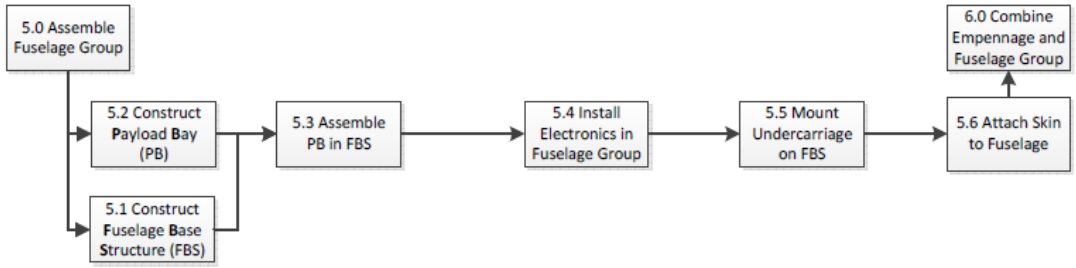

Figure 15.6: Fuselage Structure Assembly Flow Diagram

The installation of the electronics consists of installing the cabling and the control computer first. The control computer will make it possible to test all the electrical components on the UAV, such as the actuators or motors. Performing these tests immediately after the installation of each electrical component will make it easier to fix or replace them if needed. Next the sensors and communication system are mounted on the fuselage.

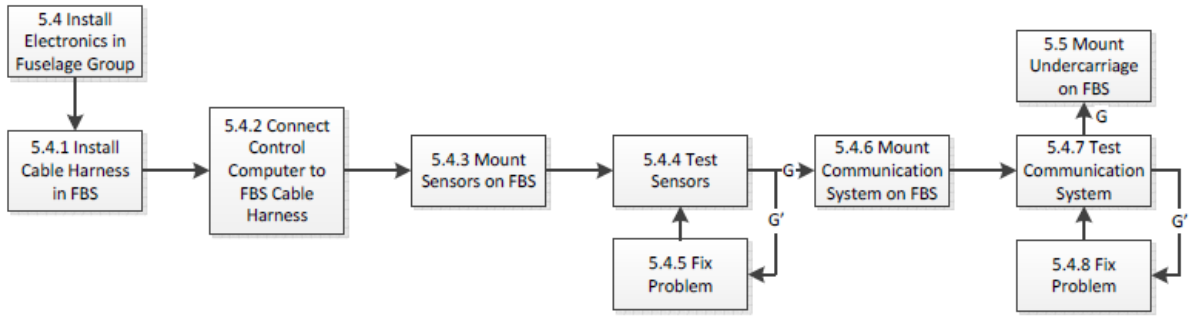

Figure 15.7: Fuselage Electronics Assembly Flow Diagram

Next, the empennage is assembled with the fuselage first (Figure 15.8), followed by the assembly of the fuselage with the wings(Figure 15.9). Both these processes consist of joining the structures, connecting the cable harnesses, and testing all the connections and actuators.

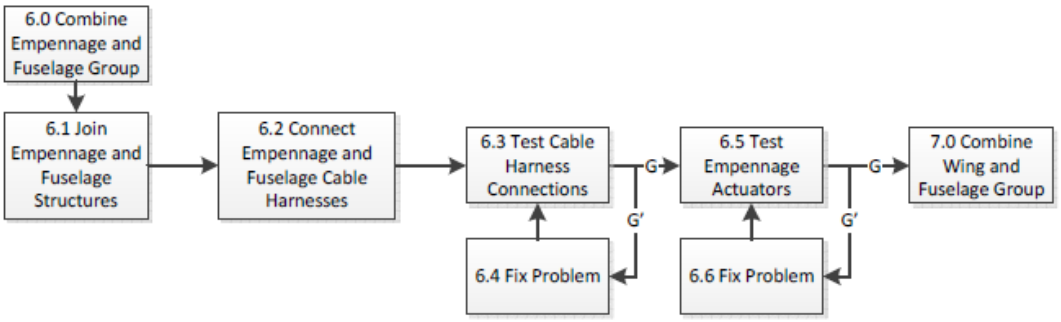

Figure 15.8: Fuselage and Empennage Joining Flow Diagram

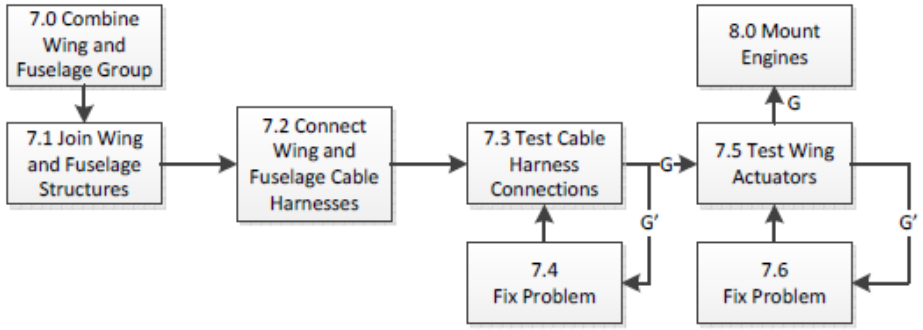

Figure 15.9: Fuselage and Wing Joining Flow Diagram

The last step (Figure 15.10) involves mounting the engines to the engine mounts on the wings. The engines are heavy, hence attaching them last will make it easier to handle the product during the preceding production stages. In addition, there will be a lesser risk of damaging the UAV or the engines themselves in case of improper handling.

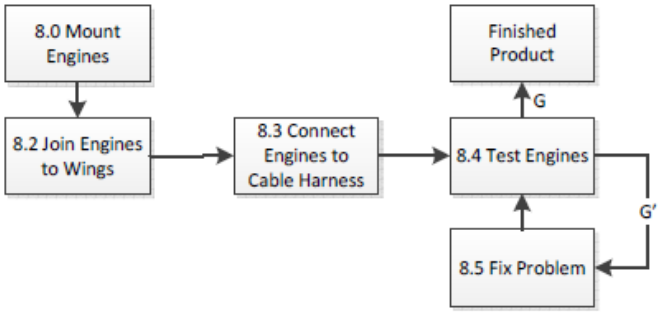

Figure 15.10: Engine Mounting Flow Diagram

16 Life Cycle Assessment

Sustainability is an import aspect of a design, as its principle of using minimal amount of material and energy is beneficial economically. This chapter elaborates on how sustainable development is incorporated in the design, followed by its LCA to see environmental impacts of the Hybrid UAV.

16.1 Sustainable Development

Sustainability was mainly considered as a trade-off criterion in the midterm phase, however, its impact on design choices in the final phase is minimal due to high performance requirements as well as VTOL capabilities.

16.2 Life Cycle Assessment

The technical framework for LCA can be seen in Figure 16.1. It starts with the central block, 'Goal and Scope', then flows into Impact Assessment, Improvement Assessment and Inventory Analysis [31].

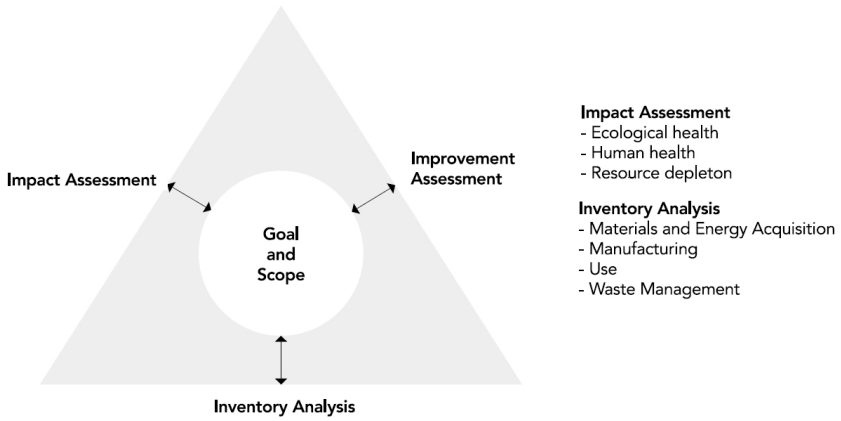

Figure 16.1: Technical Framework for Life Cycle Assessment

16.2.1 Goal and Scope

The goal and scope definitions need to be determined as a first process of a LCA. The following paragraphs elaborate on details of each aspect of the first process.

Goal The MNS can be used to define the goal. The MNS states, 'Carry out both supervised and autonomous monitoring and transport missions, comprising vertical take-off and landing, and high-velocity in horizontal flight.'

Scope In order to define the assessment methods, a system to be studied and system boundaries need to be determined. Functions of the system have been identified based on a functional breakdown structure in the baseline report [1], and can be summarised into three categories as following:

- Perform air transport
- Perform various missions
- Perform missions under various conditions

Functional Unit A main purpose for a functional unit is to set a normalised basis of comparison. For a consistent analysis, it is decided that further quantitative comparison will have a normalised scale from 0 to 100.

System Boundaries System boundaries are defined based on requirements, which can be found in Chapter 7.

Data Quality Data quality in LCA is reflected in the final LCA. At this point of the stage, it is not possible to come up with a consistent and traceable data quality, such as time-related coverage, geographical coverage and technological coverage [31]. It will be established in the next phase of the project.

Critical Review Process Critical review process is not applicable, since the process is mainly for certification of a system or product and publication of the project in terms of environmental standards.

16.2.2 Inventory Analysis

Inventory analysis is carried out after defining goal and scope definition. The online U.S. Life Cycle Inventory Database[1] and the offline version [32] are used to determine specifications of three different phases that are shown in Figure 16.2 as following: product manufacturing, use, end of life. The analysed items adhere to the production plan, which can be found in Chapter 15. Each Life Cycle Inventory (LCI) data is directly taken from the U.S Life Cycle Inventory Database. The inventory analysis primarily uses CO_2 footprint and Cumulative Energy Demand (CED).

Assumptions There are several assumptions used for LCI.

- For E-glass composites, the ratio of E-glass and high density polyethylene resin is 1:1.
- Carbon fibre composites are mainly made from acrylonitrile copolymer.
- Possible choices for different production methods are eliminated and assume that environmental impacts of all manufactured components do not differ in terms of different production methods.
- Batteries are recharged by a natural gas powerplant in the Netherlands.

Materials & Energy Acquisition and Manufacturing Phase This section analyses CO_2 footprint and CED for manufactured components, as purchased components are not considered for materials & energy acquisition and manufacturing phase.
For the fuselage, E-glass and high density polyethylene resin are used. To produce the fuselage, 3.633 kg of CO_2 is emitted and 201.9 MJ of CED is needed, which can be seen in Table 16.1

Table 16.1: Fuselage Production LCI

Material per kilogram	CO_2 footprint [kg]	CED [MJ]
E-glass	0.141	4.572
High density polyethylene resin	1.312	76.20
Fuselage total (2.5 kg)	**3.633**	**201.9**

[1] `https://uslci.lcacommons.gov/uslci/search`

Figure 16.2: Life Cycle Assessment Wheel

A carbon fibre rod and Expanded Polypropylene (EPP) foam are used to produce the wing. Most carbon fibre composites are made from polyacrylonitrile as their base[2]. The LCI of the wing can be seen in Table 16.2. In order to produce the wing, 5.642 kg of CO_2 is emitted and 217.8 MJ of CED is needed.

Table 16.2: Wing Production LCI

Material per kilogram	CO_2 footprint [kg]	CED [MJ]
Acrylonitrile copolymer	3.134	105.3
Polypropylene resin for EPP	1.216	75.20
Carbon fibre rod (0.588 kg)	1.843	61.92
Carbon fibre ribs (0.893 kg)	2.799	94.03
EPP foam (0.822 kg)	1.000	61.81
Wing total (2.500 kg)	**5.646**	**217.8**

For painting the UAV, a method of simple top coat is chosen. Per square meter of surface area, 0.731 kg of CO_2 is emitted and CED of 10.24 MJ is required. The total surface area of the UAV and corresponding CO_2 & CED values can be seen in Table 16.3. The surface area of the wing, the horizontal stabiliser and the vertical tail are multiplied by 2, as both sides of each component have to be painted. 3.056 kg of CO_2 is emitted and 31.29 MJ of CED is required in order to paint the UAV.

[2] `http://www.compositesworld.com/blog/post/the-making-of-carbon-fiber`, Acessed on 26-06-2017

Table 16.3: UAV Painting LCI

	Surface area [m^2]	CO_2 footprint [kg]	CED [MJ]
Automotive painting (top coat)	1	0.7310	10.24
Fuselage	1.184	0.8655	12.12
Wing	$0.8010 \cdot 2$	1.171	16.40
Horizontal stabiliser	$0.1062 \cdot 2$	0.1553	2.175
Vertical tail	$0.02893 \cdot 2$	0.04230	0.5925
UAV total	**3.056**	**2.234**	**31.29**

For transporting manufactured parts, a diesel-powered combination truck is used. Per km of transport, the truck emits 0.0799 kg of CO_2. However, distance between a factory and an assembly facility is not defined, thus the transport CO_2 footprint will not be considered for analysis.

Use Phase During the use phase, batteries have to be charged per mission. Per GJ of heat generated by a natural gas powerplant, it emits 56 kg of CO_2 [32]. In order to transfer the heat to electricity, an efficiency of 39 % is taken [33]. Thus, 56 kg of CO_2 is emitted from generating 0.39 GJ of electricity. Using the battery capacity of 24190 mAh as the most extreme flight scenario, required power can be found to be 467 W, based on Equation 8.5 and P = I*V. Defining that the flight time for the most extreme flight scenario is 115 minutes according to Table 8.6. By multiplying the required power with time, which is $467 \cdot 115 \cdot 60$, the required energy is 3.222 MJ per the most extreme flight scenario mission. The requirement SYS-OP-2.1 states that the UAV shall have an operational life of at least 1500 flying hours. By dividing 1500 flying hours with 115 minutes of each mission, 783 missions can be launched. Thus, $3.222 \cdot 783$ MJ of energy is needed to recharge batteries for 783 missions, which translates to 2.523 GJ of electricity. By dividing the required electricity with the unit electricity of 0.39 GJ and multiplying it by the unit CO_2 footprint of 56 kg, 362.3 kg of CO_2 is emitted for 1500 flying hours.

Waste Management EPP can be fully recycled into new wing parts, while carbon fibre rods and ribs cannot be recycled into new parts due to undesirable reduction in mechanical properties. Thus, the carbon fibre parts are considered as waste to be left in deposit containers at collection points. CO_2 footprint of the disposal method is 0.040 kg and CED of 0.55 MJ is required.
Disposal of lipo batteries is landfill safe, if they are processed with a salt water method, which discharges the batteries slowly and completely as well as neutralises the lithium. Thus, no carbon footprint and CED are considered for disposing lipo batteries.
Raw materials such as gold, silver, palladium and platinum are first extracted from circuit boards then metal parts such as steel and aluminium are removed. Then the plain circuit boards are chopped and recycled into different products or new circuit boards. Thus, no carbon footprint and CED are considered here.

16.2.3 Impact Analysis

Impact analysis is left for future as data regarding the following cannot be found without a proper license to access to detailed online database: abiotic resources, biotic resources, land use, global warming, stratospheric ozone depletion, ecotoxicological impacts, human toxicological impacts, photochemical oxidant formation, acidifitcation, eutrophication and work environment.

16.2.4 Interpretation

With the complete inventory analysis, it is possible to identity hot-spots of the UAV in terms of CO_2 footprint and CED. Table 16.4 shows carbon footprint and CED for different elements analysed for LCI. Recharging batteries for 1500 flight hours emits the most CO_2 of 362.3 kg and requires the highest CED of 2523 MJ. Thus, recharging batteries during the use phase is the hot-spot.

Table 16.4: Hot-Spot Identification for LCI

	CO_2 emission [kg]	CED [MJ]
Fuselage production	3.633	201.9
Wing production	5.646	217.8
UAV painting	2.234	31.29
Battery recharge (1500 flight hours)	362.3	2523
Part disposal	0.040	0.550

As a recommendation, different types of propulsion systems should be considered for future, such as a hybrid propulsion, an internal combustion propulsion or electric propulsion powered by renewable energy.

17 Conclusion & Recommendations

The aim of this report is to document the continuation of the design process and to justify the choices that were made in the preliminary design phase. The concept used, the Winged Quadcopter, was determined in the midterm phase [2]. It was considered best after a trade-off between five options, as brought forward in the baseline report [1]. The goal of the final design is to adhere to the mission need statement:

> *'Carry out both remotely controlled and supervised autonomous monitoring and transport missions, comprising vertical take-off and landing, and sustained high-velocity horizontal flight.'*

The design was carried out by five specialist teams, resulting in a concurrent engineering structure where design parameters are constantly updated after each design stage. These teams are aerodynamics, structure, command and data handling, power & propulsion and stability & control. Each had their corresponding tasks.

The most important performance requirements were a top speed of 200 km/h, range of 200 km, 60 minutes endurance and 10 kg payload capacity. However, during the process the team realised that it was only possible to meet these requirements simulaneously when exceeding the EASA class 3 UAV limitation of 25 kg MTOW. In order to resolve the issue, a modular payload is used such that batteries can replace a portion of payload if necessary. To prevent exceeding limits on mass, cost, and power, budgets have been implemented for each subsystem. To have an allowable margin of freedom, contingencies have been added to each budget. Subsystems were not allowed to exceed these budgets, if this was the case, changes had to be made to the design or budget.

The final outcome resulted in a design that even exceeds some of the requirements. The aircraft is able to fly 40 km with a full payload, while being able to fly up to a maximum of 600 km by replacing all payload weight with extra batteries. The requirement of having an endurance of an hour has been met, but only when flying with limited payload capacity. The structure of the aircraft will be built with lightweight materials such as glass fibre and carbon fibre to ensure the mass of the aircraft will not exceed 25 kg. To conclude, the design meets the requirements using a modular payload, while staying within the budgets assigned to the subsystems. The mission need is also answered by the design, as it is able to perform VTOL, and is able to reach a speed of 200 km/h in level flight.

Recommendations With the preliminary design, the overall layout and approximate parameters are known. For future design stages, the team has suggestions on aspects that can be improved. These are stated below.

For aerodynamics, the fuselage can be made shorter, decreasing drag. Also, a more extensive CFD analysis should be done to enhance the aerodynamic design. For general performance, modularity can also be applied to the wings, props and engines to optimise per mission. More into detail, experimental data on motor efficiencies should be obtained. Regarding the structure, a finite element method analysis of the applied forces should be made. For stability, a more thorough analysis should me made, which includes dynamic stability. Finally, considering the cost of avionics, the components that are currently off-the-shelf can be replaced by in-house designed ones.

For power & propulsion related recommendations, alternative propulsion type can be considered, such as internal combustion or hybrid propulsion. Also the propeller design might be optimised, especially the aft propeller when operating in vertical flight. Finally, motor-propeller efficiency should be obtained by means of an experimental setup; theoretical efficiency is often not accurate.

References

[1] de Jong et al. *Baseline Report*. Tech. rep. TU Delft, May 2017.

[2] de Jong et al. *Midterm Report*. Tech. rep. TU Delft, May 2017.

[3] *Systems Engineering & Technical management techniques Lecture Notes part 1*. Sept. 2006.

[4] James B. Forman and Richard Discenza. *Got Stake?* Vancouver, BC: Project Management Institute, 2012.

[5] de Jong et al. *Project Plan Report*. Tech. rep. TU Delft, Apr. 2017.

[6] Jacob Markish. "Valuation Techniques for Commercial Aircraft Program Design". MA thesis. Massachusetts Institute of Technology, June 2002.

[7] *How to use the Setup-Finder*. PDF Format - `http://www.hacker-motor.com/daten/anleitungen/hacker_antriebstabellen_2.pdf`. Hacker Motor. Schinderstrassl 32 D 84030 Ergolding.

[8] Peter Williams. "Advantages of Brushless vs Brushed Motor Technology". In: (Mar. 2013).

[9] Inc Dynamic Air Engineering. "Brush versus brushless D/C motors". In: 2 (Feb. 2011).

[10] Hyeonsoo Yeo and Wayne Johnson. *Performance and Design Investigation of Heavy Lift Tiltrotor with Aerodynamic Interference Effects*. Tech. rep. NASA, 2007.

[11] Jr. John D. Anderson. *Fundamentals of Aerodynamics*. 5th ed. New York, NY 10020: McGraw-Hill, 2011. ISBN: 978-0-07-339810-5.

[12] Itiro Tani. *Revised Fluid Mechanics*. 1969.

[13] Thomas Knauff. *The Glider Flying Handbook*. An optional note. 2013. ISBN: 978-1-62488-139-8.

[14] *The NACA Airfoil Series*. PDF format - `http://people.clarkson.edu/~pmarzocc/AE429/The%20NACA%20airfoil%20series.pdf`.

[15] *Range and Endurance Performance*. PDF format - http://www.dept.aoe.vt.edu/ lutze/AOE3104/range&endurance.pdf.

[16] *XFLR5 documentation*. PDF format - `https://engineering.purdue.edu/$\thicksim$aerodyn/AAE333/FALL10/HOMEWORKS/HW13/XFLR5_v6.01_Beta_Win32%282%29/Release/Guidelines.pdf`.

[17] *CFD Meshing with ANSYS Workbench*. PDF format - `https://caeai.com/sites/default/files/CFD_Meshing_CAEA.pdf`.

[18] Mehfooz ur Rehman. "Fast Iterative Methods for the Incompressible Navier-Stokes Equations". MA thesis. Master of Science (M.Sc.) Systems Engineering, Pakistan Institute of Engineering and Applied Sciences, Quaid-i-Azam University Islamabad, Pakistan, 2009.

[19] Ger J.J. Ruijgrok. *Elements of airplane performance*. 2nd ed. Leeghwaterstraat 42, 2628 Ca Delft, The Netherlands: Delft Academic Press, 2013. ISBN: 978-9065622327.

[20] A. P. Hettema. "Vertical Tail Desgin". MA thesis. TU Delft, May 2015.

[21] *Subsonic Aerodynamics ofAirfoils and Wings*. PDF format - `http://www.dept.aoe.vt.edu/~mason/Mason_f/ConfigAeroSubFoilWing.pdf`.

[22] Jan Roskam. *Airplane Design - Part VI: Preliminary Calculation of Aerodynamic, Thrust and Power Characteristics*. Ottawa. Kansas, 66067: Roskam Aviation and Engineering Corporation, 1987.

[23] *XFOIL: An Analysis and Design System for Low Reynolds Number Airfoils*. PDF format - http://web.mit.edu/drela/Public/papers/xfoil_sv.pdf.

[24] G. La Rocca. *Systems Engineering & Aerospace Design Lecture 5 - Design for AC longitudinal control*. TU Delft. 2017.

[25] G. La Rocca. *Systems Engineering & Aerospace Design Lecture 4 - Design for AC longitudinal stability*. TU Delft. 2017.

[26] Brian Roth. *Control Power Design Requirements for Aircraft Flying Qualities*. Apr. 2009.

[27] Daniel P. Raymer. *Aircraft Design: A Conceptual Approach*. AIAA, Jan. 10, 2013. ISBN: 1600869114. URL: http://www.ebook.de/de/product/19757236/daniel_p_raymer_aircraft_design_a_conceptual_approach.html.

[28] William D. Callister. *Materials Science and Engineering: An Introduction*. Wiley, 2006. ISBN: 978-0-471-73696-7.

[29] Christos Kassapoglou. *Design and Analysis of Composite Structures: With Applications to Aerospace Structures*. JOHN WILEY & SONS INC, Nov. 11, 2010. 300 pp. ISBN: 0470972637. URL: http://www.ebook.de/de/product/12149189/christos_kassapoglou_design_and_analysis_of_composite_structures_with_applications_to_aerospace_structures.html.

[30] T. H. G. Megson. *Aircraft Structures for Engineering Students (Elsevier Aerospace Engineering)*. Butterworth-Heinemann, 2012. ISBN: 978-0-08-096905-3.

[31] Allan Astrup Jensen, Leif Hoffman Birgitte, and T. Møller Anders Schmidt. *Life Cycle Assessment*. 6th ed. European Environment Agency. dk-TEKNIK Energy & Environment. Denmark, Aug. 1997.

[32] Peter Isley. *The US Life Cycle Inventory Database*. Excel sheet. This is an excel sheet. 2013.

[33] EURELECTRIC "Preservation of Resources" Working Group's "Upstream" Sub-Group in collaboration with VGB. *Efficiency in electricity generation*. Tech. rep. Boulevard de l'Impératrice, 66 – B-1000 Brussels: EURELECTRIC, July 2003.

A Gantt Chart

ID	Task Name	Start	Finish
1	~~Final Design~~	~~Fri 2-6-17~~	~~Fri 23-6-17~~
2	~~System Description~~	~~Fri 2-6-17~~	~~Tue 6-6-17~~
12	~~Design and Analysis~~	~~Wed 7-6-17~~	~~Fri 16-6-17~~
53	~~Final Deliverabes~~	~~Mon 19-6-17~~	~~Thu 22-6-17~~
68	~~Project Closing~~	~~Fri 23-6-17~~	~~Fri 23-6-17~~
73	~~Final Report Deadline~~	~~Fri 23-6-17~~	~~Fri 23-6-17~~
74	**Further Analysis and Improvements**	**Mon 10-7-17**	**Fri 21-7-17**
75	Vibrational analysis	Mon 10-7-17	Fri 14-7-17
76	Improvements in data handling	Mon 10-7-17	Wed 12-7-17
77	Improvements in encryption	Thu 13-7-17	Fri 14-7-17
78	Dynamic stability analysis	Mon 10-7-17	Wed 12-7-17
79	Improvements in transition phase	Thu 13-7-17	Fri 14-7-17
80	Analysis on other power types	Mon 10-7-17	Wed 12-7-17
81	Analysis on other propulsion types	Thu 13-7-17	Fri 14-7-17
82	Skin design	Mon 10-7-17	Tue 11-7-17
83	FEM validation	Wed 12-7-17	Fri 14-7-17
84	Improve wing fuselage modularity	Mon 17-7-17	Mon 17-7-17
85	Design of connectors	Tue 18-7-17	Tue 18-7-17
86	Design of fairing for engine pylons	Mon 17-7-17	Tue 18-7-17
87	Improved tail design	Mon 17-7-17	Tue 18-7-17
88	Drag improvements on fuselage	Mon 17-7-17	Tue 18-7-17
89	Final design of wiring	Mon 17-7-17	Tue 18-7-17
90	Final design iterations	Wed 19-7-17	Fri 21-7-17
91	**Prototype**	**Mon 21-8-17**	**Fri 22-9-17**
92	Order/buy off the shelf components	Mon 21-8-17	Mon 21-8-17
93	Build fuselage prototype	Tue 22-8-17	Fri 25-8-17
94	Build tail prototype	Tue 22-8-17	Fri 25-8-17
95	Build wing prototype	Tue 22-8-17	Fri 25-8-17
96	Build command and data handling prototype	Tue 22-8-17	Fri 25-8-17
97	Individual prototype testing	Tue 22-8-17	Fri 25-8-17
98	Assemble final prototype	Mon 28-8-17	Wed 30-8-17
99	Final prototype testing	Thu 31-8-17	Fri 8-9-17

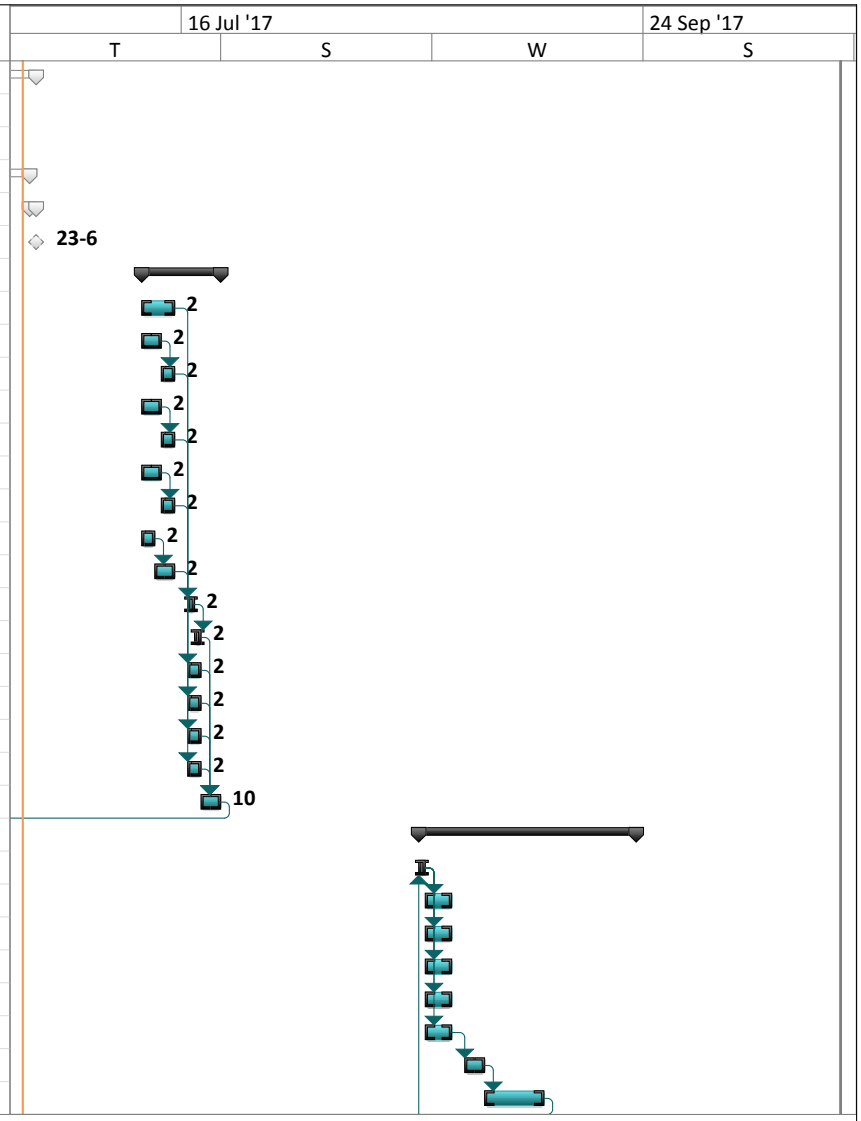

ID	Task Name	Start	Finish
100	Test Analysis	Mon 11-9-17	Fri 15-9-17
101	Final changes	Mon 18-9-17	Fri 22-9-17
102	**Market Plan**	**Mon 24-7-17**	**Fri 4-8-17**
103	Assign marketing manager	Mon 24-7-17	Mon 24-7-17
104	Discuss customer target	Tue 25-7-17	Tue 25-7-17
105	Establish unique selling proposition	Wed 26-7-17	Wed 26-7-17
106	Create final cost analysis	Thu 27-7-17	Thu 27-7-17
107	Organise distribution plan	Fri 28-7-17	Fri 28-7-17
108	Create website	Mon 31-7-17	Wed 2-8-17
109	Publish customer support	Thu 3-8-17	Thu 3-8-17
110	Start advertisement	Mon 31-7-17	Fri 4-8-17
111	**Funding**	**Mon 7-8-17**	**Mon 21-8-17**
112	Find suitable sponsors	Mon 7-8-17	Fri 11-8-17
113	Sell design to interested sponsors	Mon 14-8-17	Fri 18-8-17
114	Receive funding	Mon 21-8-17	Mon 21-8-17
115	**Final Product**	**Mon 7-8-17**	**Mon 23-10-17**
116	First buying order	Mon 7-8-17	Mon 7-8-17
117	Detailed production plan	Mon 25-9-17	Tue 26-9-17
118	Manufacturing process	Wed 27-9-17	Fri 13-10-17
119	Create maintainability support	Mon 16-10-17	Fri 20-10-17
120	First sold UAV	Mon 23-10-17	Mon 23-10-17

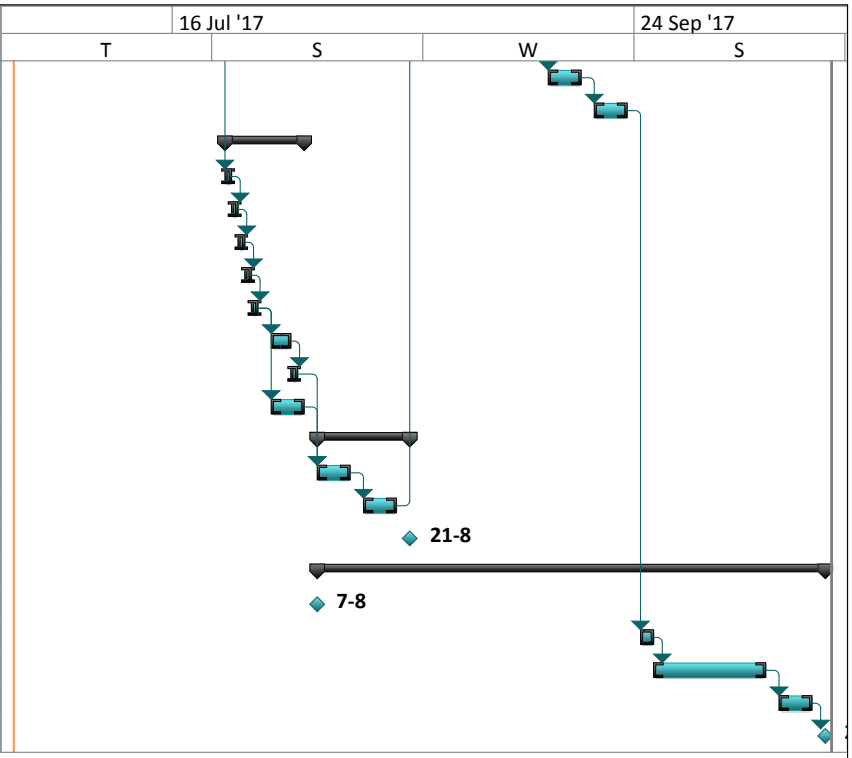

B Input Parameters

Table B.1: Input Values Used in Chapter 10

Parameter	Value	Unit	Parameter	Value	Unit
$C_{L_{cruise}}$	0.56	-	C_D	0.029	-
$\frac{S}{S_h}$	7.54	-	ρ	1.225	kg/m^3
$x_{a.c._w}$	0.60	m	V_{range}	26.7	m/s
$x_{a.c._h}$	1.67	m	S	0.801	m^2
$x_{c.g.}$	0.65	m	y_{engine}	0.45	m
$C_{L_{\alpha_h}}$	0.1	1/deg	M_{yaw}	4.61	Nm
$C_{L_{\alpha_{A-h}}}$	0.093	1/deg	l_v	0.94	m
$\frac{d\epsilon}{d\alpha}$	0	-	C_{L_v}	0.55	-
$\frac{V_h}{V}$	1	-	λ_v	0.53	rad
l_h	1.08	m	I_{xx}	3.96	kg· m^2
$\bar{c}$	0.291	m	I_{yy}	4.91	kg· m^2
SM	0.05	-	I_{zz}	8.66	kg· m^2
$C_{M_{a.c.}}$	-0.157	-	V_{stall}	20	m/s
$C_{L_{A-h}}$	1.3	-	C_{n_δ}	80.2	1/deg
C_{L_h}	-0.8	-	$T_{fore_{c.g.,min}}$	92.4	N
$T_{fore_{c.g.,max}}$	68.6	N	$T_{aft_{c.g.,min}}$	30.3	N
$T_{aft_{c.g.,min}}$	54.0	N	A_{fore}	0.13	m^2
A_{aft}	0.061	m^2	b_w	2.92	m
c_{vt}	0.02	-			

C Design Overview

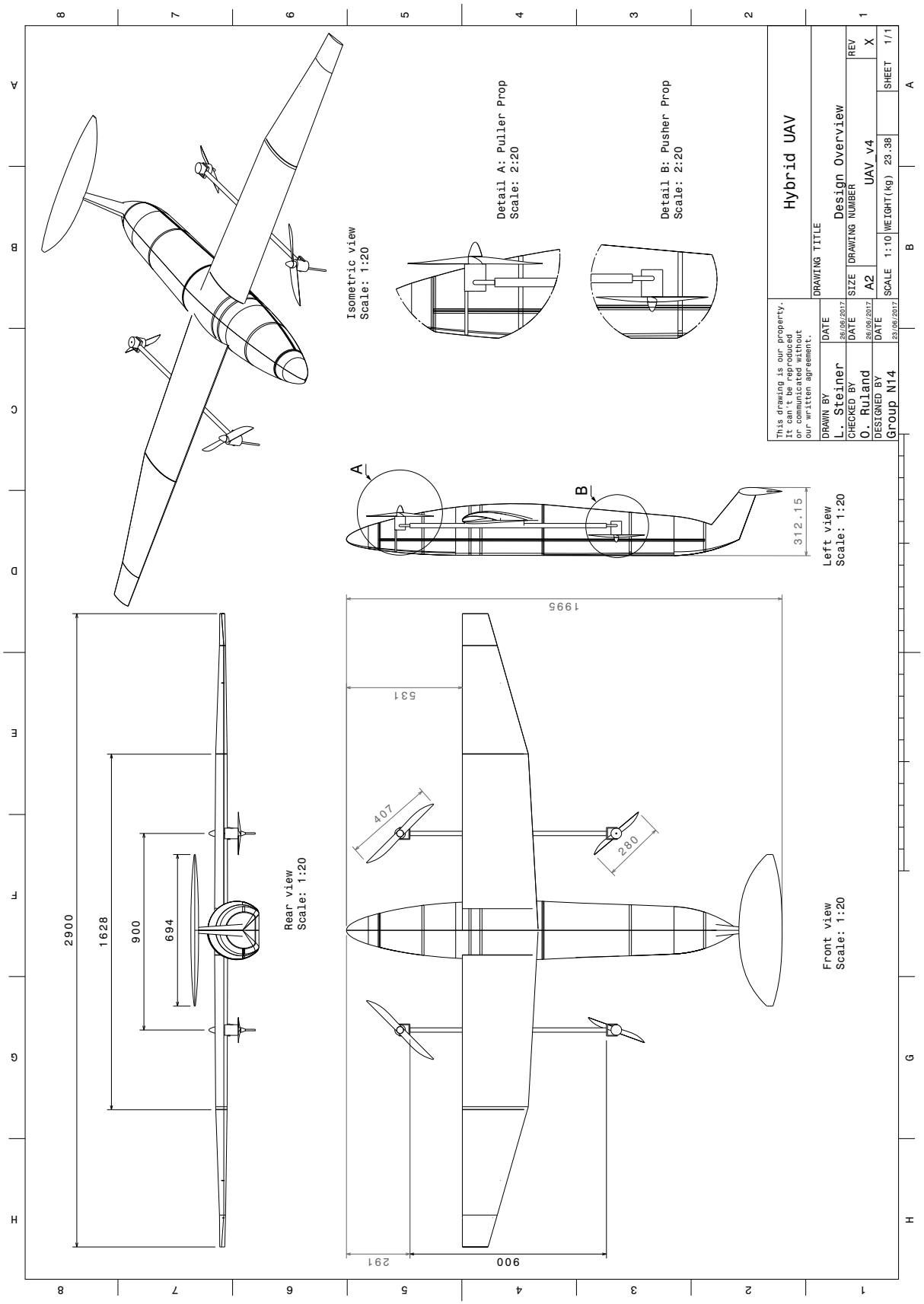

Figure C.1: Overview of the Final Design

D Task Division Tool

GENERAL

Deadline	Task	Sub-division	Name	Name	Name	Responsible	Progress
wo 07-06	**Task Division**		Lotte	Kelbey	-	Lotte	Done
vr 23-06	**System Description**	Define Subsystems	Stephanie	Piotr	Gervase	Joël	Done
		Define Interrelations	Joël	Piotr	Bryan	Joël	Done
		The Design Approach	Oscar	Lukas		Oscar	Done
		Establish Budgets (Mass, Power, Cost) & Contingencies	Chris	Gervase	Lotte	Chris	Done
		Define Subsystem Requirements	Oscar	Gervase	Chris	Lukas	In Progress
		Analyse & Rank Requirements	-	-	-		Not Started
vr 16-06	**Design**	Aerodynamics	Piotr	Kelbey			Done
		Command&DH	Stephanie	Chris			Done
		Power&Prop	Joël	Bryan			Done
		S&C	Lotte	Gervase	Chris		Done
		Structures	Lukas	Oscar			Done
vr 23-06	**Writing**	Report	-				In Progress
wo 05-07		Executive Summary					Not Started
do 29-06		Poster	-				Not Started
vr 23-06		Jury Summary					Not Started
		Project Logboek	Lukas			Lukas	In Progress
ADD ROW	ADD ROW	ADD ROW					Done

Figure D.1: Task Division Tool, General Tab

Aerodynamics

Deadline	Task	Sub-division	Name	Name	Name	Responsible	Progress
	Propulsion	Pylon	Piotr	-	-	-	Done
		Engine mounting	Kelbey	Piotr			Done
	Wing	Airfoil	Kelbey	-			Done
		Shape & size	Kelbey	-			Done
		Wing-Fuselage Integration	Kelbey	Piotr			Done
		Wing-Prop Integration	Kelbey	Piotr			Done
		High Lift Devices	Kelbey	Piotr			Done
		Wingtip device	Kelbey	Piotr			Done
	Tail	Shape & size	Kelbey	Piotr			Done
	Fuselage	Shape	Piotr	-			Done
ADD ROW	ADD ROW	ADD ROW					Done

Figure D.2: Task Division Tool, Department Tab

Writing

Page limit	Deadline	Task	Sub-division	Wrote & Responsible	Contributed To	QC1	QC2	Progress
1 p	vr 23-06	**Front Page**		Bryan				In Progress
1 p	vr 23-06	**Inner Cover**		Bryan				In Progress
1 p	vr 23-06	**Preface**		Stephanie				Done
1 p	vr 23-06	**Summary**		Stephanie				In Progress
3 p	vr 23-06	**Table of Contents**		Bryan				In Progress
2 p	vr 23-06	**List of Symbols**		Bryan				In Progress
1 p	vr 23-06	**Introduction**						Not Started
4 p	vr 16-06	**Project Description**	Mission Description	Lotte				Done
	vr 16-06		Functional Flow	Lotte				Done
	vr 16-06		Functional Breakdown	Lotte				Done
5 p	vr 16-06	**Project Approach**	Design/Iteration Process + Allocation of Departments to Subsystems	Kelbey				In Progress
	vr 16-06		V&V Procedures	Lotte				Done
	vr 16-06		Sustainable Development Strategy	Bryan				Done
4 p	vr 16-06	**Market & Stakeholder Analysis**	Market Analysis	Stephanie	-			In Progress
	vr 16-06		Stakeholder Analysis	Gervase				Done
3 p	vr 16-06	**System Requirements**		Piotr	Joël			In Progress
7 p	vr 16-06	**Concepts & Trade-off**	Concept Generation	Stephanie				Not Started
	vr 16-06		Concept Analysis: Technical Risk Assesment	Stephanie				Not Started
	vr 16-06		Trade-off&Sensitivity	Kelbey		Lotte		Done

Figure D.3: Task Division Tool, Part of Writing Tab

E Master Set Tool

Parameter	Value	Unit	Editing rights	Description	
g	9.81	m/s^2	O,G	Gravitational constant	Geometric parameters
n_max	8.7		W,G	maximum load factor	
n_min	-1		W,G	minimum load factor	
V_stall	20	m/s	K,P	Stall speed	Weight parameters
V_a	25	m/s	W,G	Maneuvre speed	Coefficients
V_b	20	m/s	K,P	Max. turbulence speed REVISE	
V_c	30	m/s	K,P	Cruise speed	
V_d	55.6	m/s	K,P	200 km/h	
rho	1.225	[kg/m^3]		ISA sea level air density	Ratios & fractions
Airfoil	NACA 441	-		Main wing airfoil	
V_range	26.65	m/s	G,C	optimal velocity for maximum range	
n_safety	1.5	-	O,L	Structural safety factor	Constants & properties
b	2.9127	m	O,G	Wing span	
b_h	0.7866	m	K,P	Horizontal stabiliser span	
c_r	0.347577	m	O,G	Root chord	Others
c_t	0.118176	m	O,G	Tip chord	
c_bar	0.291	m	O,G,K,P	MAC	
c_twist	0.159	m		root chord of twist section	
c_tapercrook	0.302	m		root chord of section with different twist	
c_ail	0.036868	m		aileron root	
S	0.801	m^2	O,G,K,P	Wing area	
tapercrook	0.6424	m		location of taper discontinuity from tip chord	
twist	0.146	m		distance to twist kink from tip chord	
twistangle	-5	deg		twist angle at wing tip	
S_h	0.106254	m^2	G, W	horizontal stabiliser area	
i_w	2.5	deg	K,P	wing incidence angle	
i_h	2.6	deg		incidence angle of the tail	
S_v	0.028931	m^2	G, W	vertical stabiliser area	
w_fuselage	0.15	m	O	fuselage width (top view)	
L_fuselage	1.8	m		fuselage length (1.7 max)	
h_fuselage_back	0.18	m	O	fuselage heigth at back	
X_CG_pl_min	0.4	m		minimum payload CG distance from A/C nose including battery	
X_CG_pl_max	0.8	m		maximum payload CG distance from A/C nose including battery	
X_LE	0.5301	m	G, W	wing leading edge distance from A/C nose	
X_CG_av	0.3	m	G,W	cg location of avionics from A/C nose	
X_CG_fus	0.8772	m	O	cg location of the fuselage structure from A/C nose	
X_CG_bat_1	0.1887	m		battery 1 CG distance from A/C nose	

Figure E.1: Portion of the Master Set